Hydrogeological conceptualization and numerical modeling of groundwater resources in the Zamra catchment, Northern Ethiopia

AYISHESHUM WALLE MIHIRET
August 2022

SUPERVISORS:
Dr. Ir. Maciek W. Lubczynski
Dr. Yijian Zeng

ADVISOR:
Mewcha Amha Gebremedhin (PhD Candidate)
Mostafa Gomma Daoud (PhD Candidate)

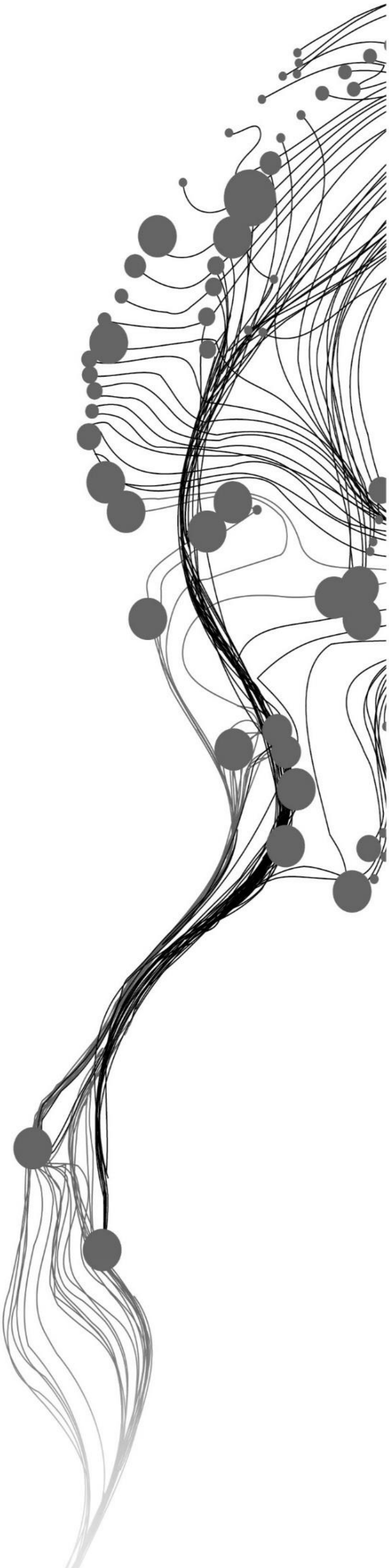

Hydrogeological conceptualization and numerical modeling of groundwater in the Zamra Catchment, Northern Ethiopia

AYISHESHUM WALLE MIHIRET
Enschede, The Netherlands, August 2022

Thesis submitted to the Faculty of Geo-Information Science and Earth Observation of the University of Twente in partial fulfilment of the requirements for the degree of Master of Science in Geo-information Science and Earth Observation.
Specialization: [Water Resources and Environmental Management]

SUPERVISORS:
Dr. Maciek W. Lubczynski
Dr. Yijian Zeng

THESIS ASSESSMENT BOARD:
Dr. Tom H.M. Rientjes (Chair)
Dr. Jacek Gurwin (External Examiner, University of Wroclaw, Poland)

ABSTRACT

Due to the short rainy season and high rainfall variability, water scarcity remains a significant issue in the semi-arid region of Ethiopia, including the Zamra catchment (ZC). Groundwater evaluation and management are the most crucial aspects of groundwater in the areas where groundwater is the primary source of potable water. Groundwater resources can be successfully evaluated by applying a numerical model. A reliability of such models primarily depends on the adequately built hydrological conceptual model (HCM).

The study's main aim was to build a realistic HCM by integrating numerous datasets and converting it to a steady-state numerical model. To create HCM of the ZC, the hydrologic system's lithology, stratigraphy, hydrostratigraphy had to be well understood. This was done through development (applying Rockworks 3D modelling software) of the 3D hydrostratigraphic model presented through a series of cross-sections. In that model, the sequence of seven hydrostratigraphic units (layers, none of them fully covering the whole ZC) consisted of (from top to bottom): 1) unconsolidated sediment, 0–27 m thick; 2) flood basalt, 0–69 m thick; 3) Agulae shale, 0–76 m thick; 4) Antalo limestone, 0–76 m thick; 5) Adigrat sandstone, 0–49 m thick; 6) Enticho sandstone, 0–45 m thick; and 7) metavolcanic, 0-45.5m thick.

The groundwater flow pattern and direction were defined by interpolation of the available hydraulic head records. As the first aquifer was unconfined and the topography of the study area complex, the interpolation was carried out using regression kriging accounting for topographical relief variability. The obtained head pattern: i) showed eastward groundwater flow direction aligned with the main river course; ii) defined catchment no-flow boundaries along groundwater divides; and iii) allowed to roughly quantify groundwater flow rate.

Based on HCM, a steady state numerical model was developed using MODFLOW 6 code, applying unstructured grid (originally 500x500 m), densified around streams and head observations. The numerical model consisted of five spatially discontinuous layers, obtained from seven hydrostratigraphic units, merging the two sandstone layers, Adigrat and Enticho into one sandstone layer and the Agulae shale and Antalo limestone into one limestone-shale layer.

The steady-state ZC model was calibrated using hydraulic heads as a target parameter. The water budget showed the annual mean *ET* (38.65% of *P)*, annual mean total stream discharge q (61.20% of *P)* and a very small amount of lateral groundwater outflow q_g (0.16 %of *P*). There is mean gross recharge of 517.54 mm year^{-1} (78.38 % of *P*) and a net recharge of 33.90 mm year^{-1} (5.47% of P_e) with a substantial amount of groundwater exfiltration and groundwater evapotranspiration. The total groundwater exfiltration (66.78% of q) and the rejected infiltration (25.09% of q) were routed to the stream using the water mover (MVR) package and contributed a significant value to the total river discharge (q). This q (61.19% of P) covers the most significant value of the catchment outflow.

Key words: Rockworks**;** 3D lithological model; 3D hydrostratigraphic model; regression kriging; HCM; MODFLOW 6; Steady state.

ACKNOWLEDGEMENTS

First and foremost, I want to thank the omnipotent God who gave me the strength to finish my studies. I want to express my gratitude to the University of Twente, the Orange Knowledge Program (OKP), and the Dutch government for providing me with the funding and opportunity to pursue my master's in science degree.

Without the assistance of helpful people nearby, I could not have finished and prepared this thesis. I want to convey my sincere gratitude to Dr. Ir. Maciek W. Lubczynski, who served as my first supervisor, for providing the necessary direction, support, encouragement, and generosity during the research. I would also like to thank Dr. Yijian Zeng, my second supervisor.

I wish to express my appreciation to Mr. Arno Van Lieshout for his assistance throughout the entirety of the studies at ITC.

My advisor, Mewcha Amha, and the very helpful person, Mostafa Gomma Daoud, deserve a particular appreciation. Your assistance with all technical issues and conversations has been greatly appreciated. Best wishes to both of you as you continue your PhD journeys.

I would like to express my gratitude to the entire WREM department team at ITC as well as to my fellow students for making my time in school memorable. I want to thank all the other ITC academic and support staff for their assistance. At ITC, I gained much knowledge about geoinformation and water resources, theoretically and practically.

I would like to thank Dr. Richard Winston for his assistance and support in resolving issues while running the steady-state model using the USGS software (MODFLOW 6).

In the end, I want to thank and love my mother, brothers, sisters, and friends back home for their help and support as I worked toward getting my MSc.

LIST OF FIGURES

LIST OF ABBREVIATIONS

A	Area of the flow in the drain
ALOS PALSAR	Advanced Land Observation Satellite Phased Array L-Band Synthetic Aperture Radar
BCF	Block-cantered flow
C_d	Drain conductance
CHIRPS	Climate Hazards Group Infrared Rainfall with Stations
DEM	Digital elevation model
d_{ext}	Specific extinction depth
DISV	Discretization by vertices
DRN	Drain package
d_{surf}	Surface depression depth
E_I	Canopy interception
ET_g	Groundwater evapotranspiration
ET_o	Reference evapotranspiration
ET_u	Unsaturated zone evapotranspiration
Exf_{gw}^{s}	Groundwater exfiltration routed to stream
FAO	Food and agricultural organization of the United Nations
GHB	General head boundary package
GNC	Ghost-node package
GWR	Geographically weighted regression
h	Piezometer head
H_{obs}	Observation head
H_s	Simulated head
I	Interception rate
i_{ET}	Unsaturated evaporation rate per unit depth
IHM	Integrated hydrological model
K	Hydraulic conductivity
$K(\theta)$	Vertical hydraulic conductivity as a function of water content
Kb	Stream bed conductivity
K_c	Crop coefficient
K_h	Horizontal hydraulic conductivity
K_v	Vertical hydraulic conductivity
LAK	Lake Package
LPF	Layer property flow
MAE	Mean absolute error
MAW	Multi-Aquifer Well package
ME	Mean error
MPEG	Multi-Sensor Precipitation Estimate-Geostationary satellite
MVR	Water mover package
P	Precipitation
p_e	Effective precipitation
PET	Potential evapotranspiration
q	Total stream discharge at the catchment outlet
q_a	Specific infiltration rate
q_B	Base flow
q_g	Groundwater lateral flow
q_{gs}	Groundwater leakage to stream

Q_{out}	Flow to out of the system
Q_p	Flow rate at the provider
Q_r	Flow rate at the receiver
q_{sg}	Stream leakage to groundwater
rbth	Stream bed thickness
R_g	Gross groundwater recharge
rgrd	Stream gradient
RI^s	Rejected infiltration routed to stream
RIV	River package
rlen	Stream reach length
RMSE	Root mean squared error
R_n	Net groundwater recharge
rwid	Stream reach width
SAGA	System for Automated Geoscience Analysis
SFR	Streamflow routing package
stp	Stream top
t	Time
Td	Drian bed thickness
UPW	Upstream weighting package
UTB	Upper Tekeze basin
UZF	Unsaturated zone flow package
UZT	Unsaturated zone thickness
W	Source or sink
WaPOR	FAO Water Productivity Open-access portal
WEL	Well package
z	Vertical distance
ZC	Zamra catchment
a	The variable that transforms the supplier flow rate to the receiver flow rate
ε	Brooks Corey epsilon
θ	Volumetric water content in vadose zone
θ_i	Initial water content
θ_{qa}	Water content corresponds to a specific infiltration rate
θ_{resid}	Residual water content
θ_{sat}	Saturated water content

1. INTRODUCTION

1.1. General background

Groundwater represents the world's largest source of available drinking water, and, as a result, it's one of the most vital resources for people (Dassargues, 2019). Nowadays, groundwater is one of the most critical natural resources globally, with several advantages compared with surface water (Everett, 2006). Groundwater makes up around 30% of freshwater globally (Figuères et al., 2012). Freshwater demand is rapidly increasing due to urbanization, population growth, intensive agricultural activities, and industries (Aghazadeh et al., 2017). Climate change and anthropogenic activities mainly threaten groundwater resources (Boukhemacha et al., 2015). Groundwater has better protection, is highly spread in a large domain, and is significantly less subjected to perennial and seasonal variation than surface water like rivers and lakes (Everett, 2006). In arid and semi-arid locations, particularly in Africa, groundwater is the main source of safe drinking water(Lekula et al., 2018). Ethiopia is one of those countries in the arid regions of Africa. In the areas with no optional water source, it is used not only for drinking but also for irrigation, industries, cattle, and others. In such an environment, groundwater becomes highly susceptible to depletion and pollution.

Successful groundwater management and evaluation are currently done using distributed numerical modeling (Lekula and Lubczynski, 2019). Numerical models are primarily dependent on the conceptual hydrological models. Developing a representative conceptual model is one of the most important aspects of any successful modeling project (Karlovi and Markovi, 2021). Hydrogeological conceptual models would be one of the most significant sources of uncertainty in groundwater flow and transport modeling if they were not adequately developed. The level of detail of every conceptual model varies depending on the data availability, purposes, and model complexity. Using an inadequate conceptual model when estimating parameters through calibration could result in biased model parameters (Enemark et al., 2019).

It is a summation of different hypotheses that describe the groundwater system (Enemark et al., 2019). Groundwater modeling is considered a preferred tool for coordinating many groundwater problems (Anderson and Woessner, 1992). According to Anderson et al. (2015), the conceptual hydrological model contains the hydrological system characterization and the hydrogeological identification of the study area. It is a quantitative characterization of aquifer systems that complies with the hydrogeological principle. A hydrogeological conceptual model is primarily based on subsurface hydrological, hydrogeochemical, geological, geophysical, and other significant surface and subsurface data (Lekula et al., 2018).

According to Anderson et al. (2015), most models' conceptual model design contains the flow boundary, flow direction, recharge sources, hydrogeologic and hydrostratigraphic properties, and groundwater budget estimate of the model domain. If all parameters are designed in the conceptual model, it is recommended to transition from the conceptual model to a numerical model at a selected model domain. 3-D geological modeling has recently become a popular method for realistically depicting subsurface lithologies and structures. The 3-D geological and hydrogeological models investigate the aquifer's geometry and volume and examine the impact of faulting and other geological structures on the aquifer system (Hassen et al., 2016). In addition, it is used to estimate the aquifer's potential and safety.

The schematization of the subsurface geological data like lithology and stratigraphy is difficult due to geological heterogeneity and subsurface data limitations. In addition, Lekula et al.(2018) stated that converting stratigraphic and lithological units into hydro-stratigraphic units is challenging due to the lack of a defined transition between formations and groups. However, 3-D geological modeling is the only solution for solving such a problem and is the basis for the hydrogeological conceptual model in groundwater studies (Royse, 2010). Several types of research have been done on groundwater resource management and evaluation, including the hydrogeological conceptual modeling of groundwater.

The conceptual model can be represented by fence diagrams, cross-sections, and tables that show the distribution of boundary conditions hydrostratigraphic units, flow direction, and groundwater budget components of the study area. The final output must be smoothly transitioned to a numerical model (Diana et al., 2007). The hydrogeological conceptual model of the study area will be a crucial result in a detailed analysis of groundwater resource management, especially to emphasize the aquifer's future condition and guide the water resource management decision. The modeler can confirm the groundwater resources' sustainability and improve the local water management mechanisms. Geologists will also use the conceptual and 3-D geological models for primary input resources. It is also applicable to petroleum geologists and other professions depending on the area's geology (i.e., sedimentary area for potential assessment of hydrocarbons).

The governing equation of a steady-state model ($\frac{\partial h}{\partial t}$) is zero, and the estimated heads and fluxes, as well as the hydrologic parameters, are constant over time (Mary P. Anderson et al., 2015b). It is usually the first step in the transient flow model. According to Anderson et al. (2015), a steady-state simulation is sufficient to address many modeling goals, including calculating regional water table gradients, estimating average annual leakage from a losing stream, analyzing average groundwater flow patterns and flow rates, and simulating flow directions affected by long-term pumping. The consequences of time-averaged stress, such as expected long-term pumping or lengthy drought, can also be predicted using steady-state models, and it is also the first step in transient modeling (Anderson et al., 2015).

Implementing this numerical model assures the reliability of the hydrogeological conceptual model. It can be initial for the next transient integrated hydrological model (IHM). In conjunction with the hydrogeological conceptual model, the numerical model can partly be used to understand the groundwater situation and conclude aquifer characteristics. This will give the required information to apply prevention mechanisms and estimate the aquifer's potential for the study area.

1.2. Related works

Several studies have been conducted in the Zamra catchment (ZC) for different purposes, but only a few are related to groundwater. Some of the results from them have been used in this study. The paragraphs below show some of the work that has already been done on ZC that is somehow related to this work.

Hagos et al. (2015) have done the hydrogeology of the Tekeze river basin, where the ZC is one of the main tributaries. They tried to conceptualize the hydrodynamics and assess the area's potential for society's supply. They also identify a better scientific approach to determine the occurrence and movement of groundwater in the complex geology of the upper Tekeze basin (UTB). This was done with the help of published and unpublished geological and geophysical data, hydrogeological maps, spring discharge, and location data, pumping test data, and borehole logs for the study area.

Girmay et al. (2015) have developed the conceptual groundwater flow model of the Mekelle sedimentary outlier and northern Ethiopia by using dissolved ions and environmental isotopes (18O and 2H). They did fieldwork to prepare geological maps and cross-sections and collect water samples. Using these isotope tracers, they figured out the discharge and recharge areas of the upper Tekeze basin. They found the shallow, intermediate, and deep flow systems in the UTB by looking at geologic and hydrochemical settings and isotopes.

Gebremedhin et al. (2021) prepared daily rainfall data following the effective protocols (downscaling, bias correction, and validation) for three years (January 1, 2015–December 31, 2015) in the UTB. They validated the insitu data for two downscaled and bias-corrected satellite products (MPEG and CHIRPS). These validated satellite products combined geographically weighted regression (GWR) with in-situ data to improve accuracy and select the best-performing one. They concluded that MPEG performed slightly better than CHIRPS in the UTB. The steady-state numerical model in this study used the average of this precipitation of one hydrological year lasting from September 1, 2019 – August 31, 2020, as input.

Gebremedhin et al. (2022) derived the potential evapotranspiration (PET = ETo*Kc) by remote sensing by applying the FAO Penman-Monteith reference evapotranspiration (ETo) and crop coefficient (Kc). They validated and corrected the advection bias of the satellite derived daily ETo by comparing it with the insitu data computed using ETo. They convert this bias-corrected satellite-derived daily reference ETo into PET. The satellite-derived daily ETo has been validated using one-year in-situ data from the four ATMOS 41 weather stations. They validate PET using the wet season actual evapotranspiration from the FAO water productivity open access portal (WaPOR). Similar to precipitation the average potential evapotranspiration data of one hydrological year lasting from September 1, 2019 – August 31, 2020, was used as input for the steady-state numerical model of this study. In addition, some unpublished papers are used to cross-check model parameters and to have clues where there is no previous work in the study area. (Sima, 2018; Siyoum, 2020).

1.3. Problem statement

In Ethiopia, groundwater management and evaluation are poor. This is due to the cost-effectiveness of management and evaluation tasks, scarcity of in-situ soil and groundwater data, and the country's water policy (Mengistu et al., 2021). Sideways, groundwater demand intensifies. Ethiopia is primarily reliant on groundwater for drinking, cattle, and industry. Aquifers provide more than 80% of the total water supply for the country (Mengistu et al., 2021).

Due to the short rainy season and high rainfall variability, water scarcity remains a significant issue in the semi-arid region of the country, including the Zamra catchment. This results in recurrent droughts and a lack of potable water for society. Due to this recurrent drought and poor groundwater management, many groundwater wells are dry in the Zamra catchment. The operation of such wells needs a well-grounded evaluation of groundwater resources for sustainable management. However, most of the areas of Ethiopia, including the Zamra catchment, have not been explored in detail.

Few studies have been done in the Zamra catchment. Hagos et al. (2015) and Girmay et al. (2015) highlighted the regional hydrogeology of UTB where the Zamra catchment is under the domain. They even tried to address the groundwater flow and aquifer potential assessments regionally, but none of them did the conceptual and numerical model of the Zamra catchment.

1.4. Objective and research questions

1.4.1. Objectives

The main objective of this research is to build an effective hydrogeological conceptual model (HCM) of the Zamra catchment by integrating data from numerous scales and sources and convert it to a steady-state numerical model.

To achieve the main objective outlined above, the following specific objectives are formulated:

- Define the 3D model of the hydrostratigraphic units of ZC.
- Determine groundwater flow patterns and hydrogeological boundary conditions.
- Develop steady-state numerical modeling using Modflow 6.
- Calibrate the steady-state numerical model and test its sensitivity to evaluate the uncertainty of the conceptual model.
- Identify the water balance components of the Zamra catchment.

1.4.2. Research questions

The following are the research questions that can be addressed in this proposed research:

- How many hydrostratigraphic units are in the Zamra catchment, and what is their spatial extent and thickness?
- What is the groundwater flow direction in the Zamra catchment?
- What are the Zamra catchment water balance (Hydrologic) components?
- To which aquifer parameters the model of Zamra catchment is the most sensitive?

1.5. Hypothesis and assumptions

Hypothesis

- The Zamra River is hydraulically connected with the groundwater and drains the aquifer.

Assumptions

- The aquifer leakage across the bottom layer (towards basement rock) is negligible.
- The driving forces (*P* minus interception, *PET*) and state variables can be represented by their means.
- Due to a lack of recorded data and previous work, the geological structure's (faults and joints) impact is considered negligible and not included in the model (both conceptual and numerical).
- Due to a minor contribution to the overall water balance, the well-abstraction is considered negligible.
- A well-calibrated steady-state groundwater model can accurately quantify the groundwater balances and recharge of the ZC.

2. STUDY AREA DESCRIPTION

2.1. Location

The Zamra catchment is located in the UTB in northern Ethiopia. The study area is, on average, around 60 km away from Mekelle, the capital of the Tigray region, and Mekelle is around 925 km away from Addis Ababa, the capital of Ethiopia. The study area includes four distinct woredas: Amba Alaje, Enderta, Huntalo wejerat, and Seharti Samre. The Zamra catchment is located between latitudes of 12^0 38' 12" and 13^0 20' 16" N and longitudes of 38^0 59' 23" and 39^0 40' 05" E, in the upper Tekeze basin, Northern Ethiopia. The study area covers an area of about 1588 km^2.

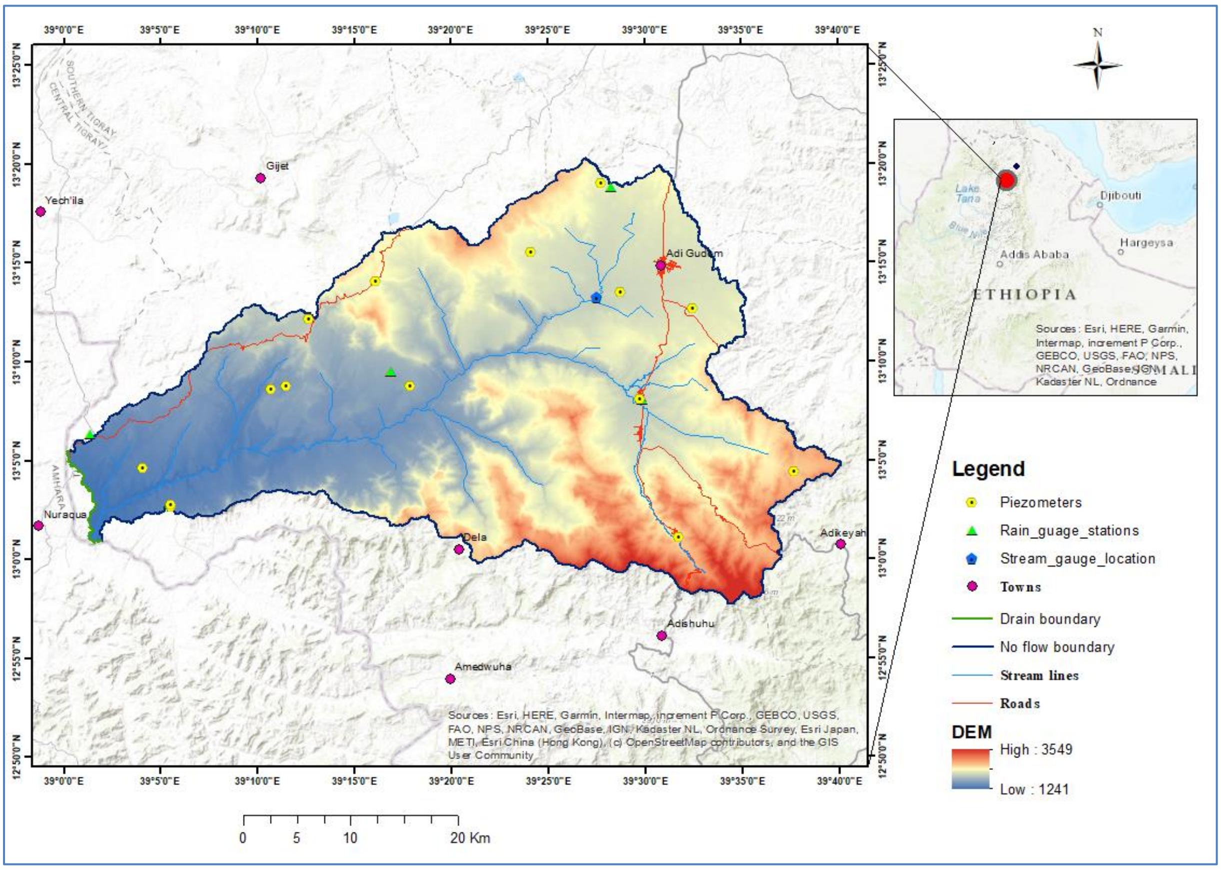

Figure 1: Location map of Zamra catchment

2.2. Climate

It is known that climate significantly varies spatially and temporally. The Atlantic and Indian Ocean monsoons impact the northern Ethiopian rainfall regime (Hagos et al., 2015). The Inter-Tropical Convergence Zone's seasonal migration controls the flow of monsoon precipitation to the area. The physiographic elements of the basin interact with the intertropical convergence zone to control the flow of monsoon precipitation in the highlands of northern Ethiopia (Hagos et al., 2015). The Zamra catchment has characterized by a semi-arid climate. It has an average temperature of 13^0C in the highlands and 35^0C in the lowlands (Girmay et al., 2015). The study area has average annual precipitation in the range of 450mm (in lowlands) and 970mm (in highland areas) (Girmay et al., 2015). In Ethiopia, as well as in the Zamra catchment, there is a bimodal rain season. The ZC receives a little rain in the Bega (winter) season and a lot of rain in the summer, as shown in Figure 2. The climate varies geographically and temporally due to the topographic and seasonal effects.

Drought frequently occurs in this area. Precipitation and temperature vary by location, which is associated with topography. The graph below represents the climatology of the study area and indicates the monthly average, temperature, and average monthly precipitation from 1991 to 2020. Due to climate change and recurrent droughts, the agricultural sector has been severely impacted, contributing to food insecurity in society. Similar to the other semi-arid and arid regions, the springs, and streams, including the groundwater level, drastically decrease from their levels in the dry season (Siyoum, 2020).

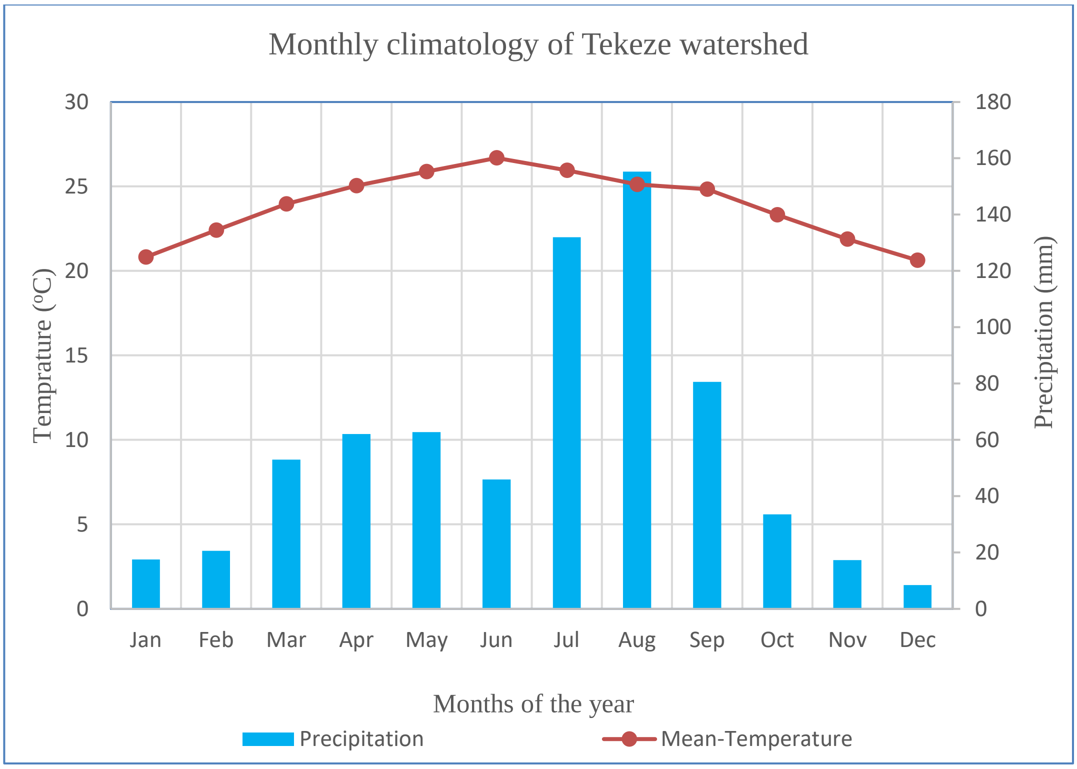

Figure 2: Monthly climatology presented as monthly average from year 1991-2020 (world bank climate portal)

2.3. Topography and drainage system

As indicated in Figure 1, the study area has a rugged topography with a high elevation difference. In addition to rugged topography, the study area has a rocky land surface outcrop. Based on topographic information from the ALOS PALSAR high resolution (12.5m) digital elevation model, the area's elevation ranges from flat to highland areas, from 1241 to 3549m above mean sea level. Due to the rugged morphology, the area is also characterized by high surface runoff. The lowest elevation is in the southwest direction, and the highest is in the study area's southeast. Some parts of the area have steep slopes (more than 30^0), and more than half of the study areas have 15–20^0 slopes.

The drainage pattern of the study shows a dendritic pattern, as indicated in Figure 1. This pattern is visible in every geological layer of the study area. The Zamra river sculpts, gorges and canyons with its sharply sloping river valleys. Many springs emerge along the contacts of the various rock units in these valleys, which serve as discharge places (Hagos et al., 2015). These regions are characterized by runoffs and have high surface drainage.

2.4. Land use land cover (*LULC*)

Land use is a constantly changing phenomenon that varies across time and space. This is due to anthropogenic factors. People can switch from crop to forest, forest to bare land, cropland to building, etc. Due to this dynamism, updated landcover information is necessary to monitor and evaluate the hydrology of the catchment (Calijuri et al., 2015). In any catchment, *LULC* has a considerable impact on hydrological processes. As indicated below in Figure 3, the Zamra catchment is highly covered with shrubs, followed by croplands. A tiny part of the study area is covered by dense vegetation. According to Seyoum (2020), the study area's popular trees are eucalyptus. The shrubs mainly cover the rugged area unsuitable for agricultural activities.

The *LULC* map of the study area is prepared from a sentinel-2 image of the year 2020, taken from the summer season, to identify the cultivated land correctly (https://scihub.copernicus.eu/dhus/#/home.). The training points are collected from the Google Earth image and interpreted based on the study area's knowledge. The classification has been done using five classes.

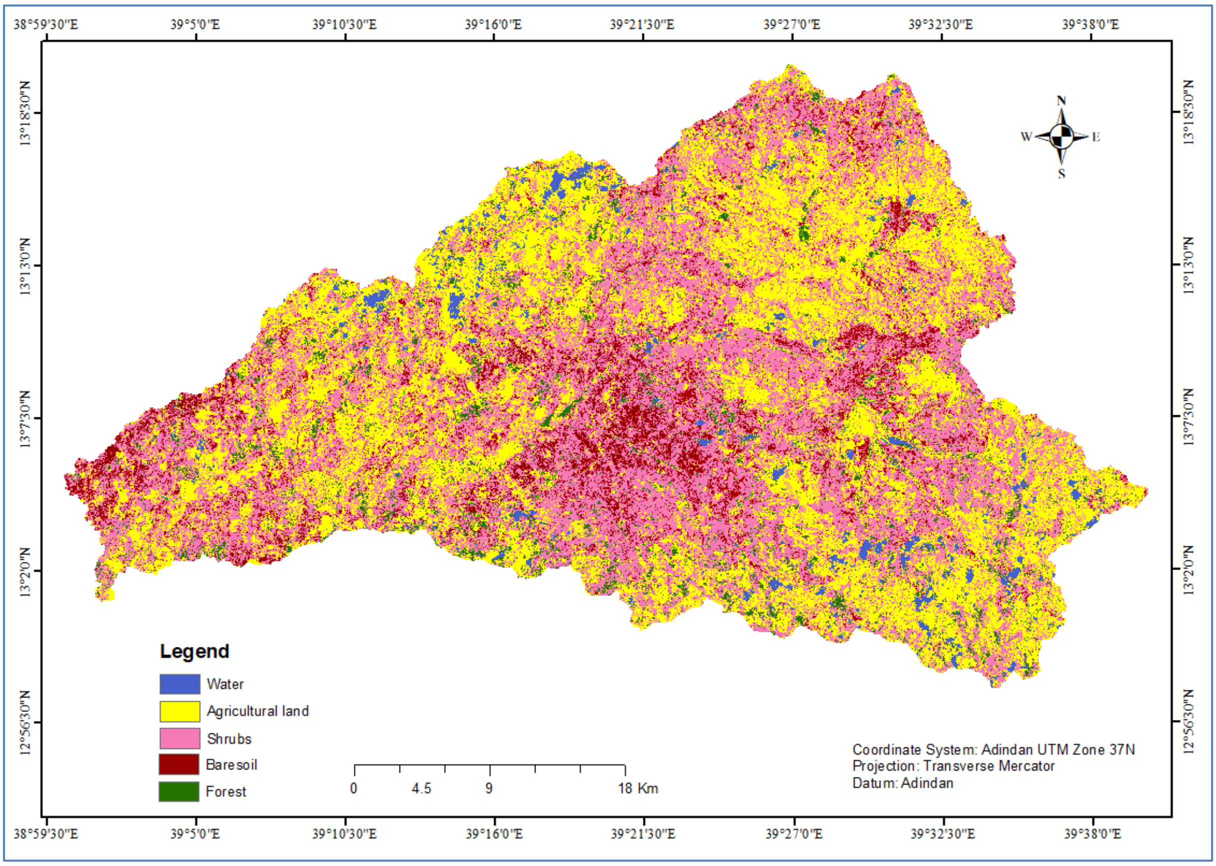

Figure 3: Landcover and land use map of Zamra Catchment

2.5. Soil

Most of the study area is covered by a variety of leptosols, as shown in the map in Figure 4. According to the Ethiopian ministry of water and irrigation study, leptosol has five varieties (Eutric, Dystric, lithic, Umbric, and Litic). Next to the leptosol, the cambisol covers a large area of the catchment. The varieties of vertisol cover small areas in the eastern and northwest regions of the area.

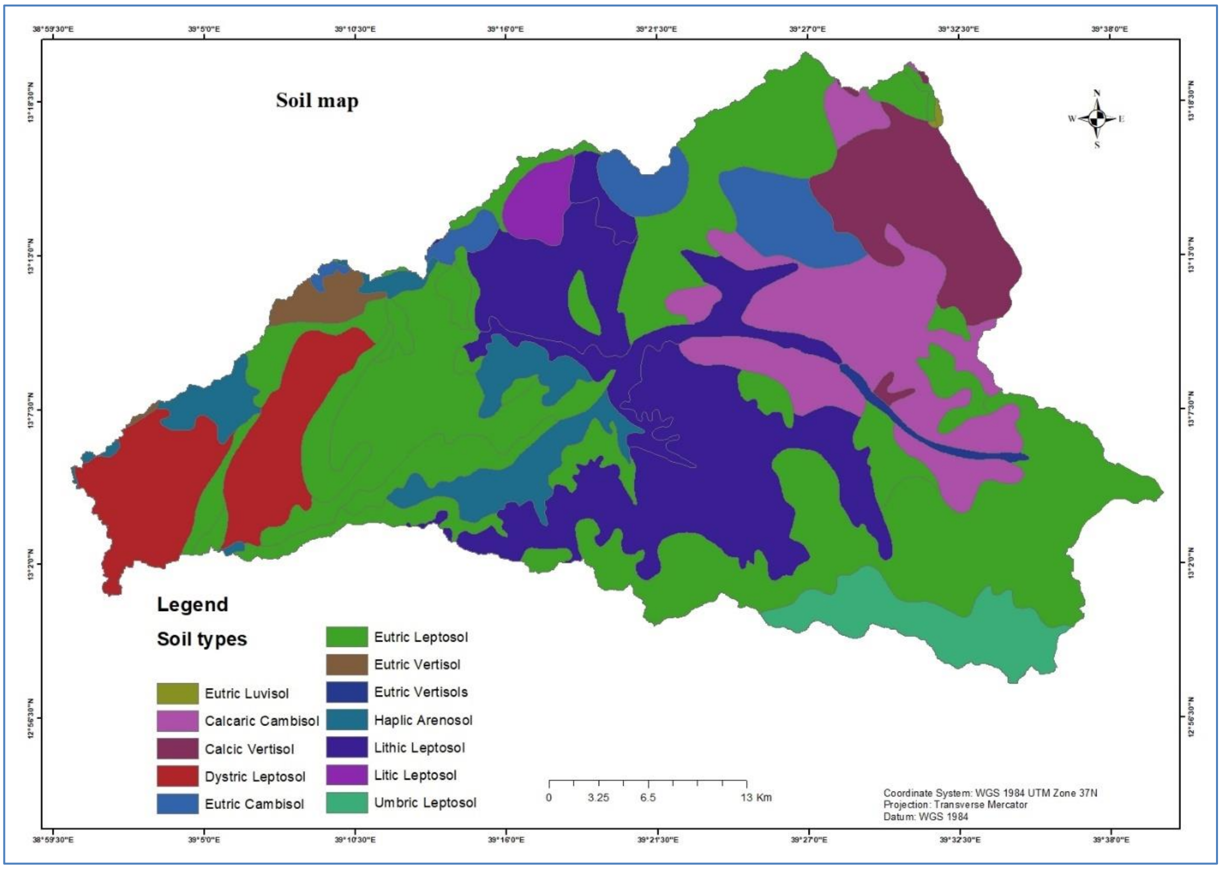

Figure 4: Soil types of the study area (by Ethiopian Ministry of Water and Irrigation)

2.6. General geology

The Paleozoic-Mesozoic sedimentary sequence, which is topped by tertiary volcanics, overlies an unconformably deposited Precambrian basement to characterize the study area's geology (Sembroni et al., 2017). The rock units are highly affected by different tectonic structures with varying ages from the Neoproterozoic to the present (Gebreyohannes et al., 2010). The geology of northern Ethiopia is complicated and highly diversified. The geology of northern Ethiopia, including Zamra, is classified based on the mode of formation and age (Beyth, 1972; Gebreyohannes et al., 2010; Sembroni et al., 2017, 2016; Wolela, 2008). Depending on this category, the geology of Northern Ethiopia has been classified as:

- Quaternary deposits (unconsolidated sediments)
- Tertiary volcanic and dolerite dikes and sills (flood basalts and equivalent intrusions)
- Mesozoic sedimentary rocks (Adigrat sandstone, Antalo limestone, and Agulae shale)
- Paleozoic sedimentary rocks (Enticho sandstone and Edaga Arbi tillites) and
- Precambrian basement rocks

2.6.1. Unconsolidated sediment (Quaternary deposits)

The unconsolidated sediment is recent in age (quaternary) from all formations in northern Ethiopia (Beyth, 1972). It covers extensive areas in the intermountain grabens eroded and transported from the hillside of mountainous areas. It includes residual soils, colluvial, talus, and alluvial deposits (Ayenew and Barbieri, 2005). They are soft sand, gravel, clay, and sandy sediments. Unconsolidated sediments are found along rivers, intermountain grabens, and low-lying areas. A matrix of silty clay soils surrounds the basaltic cobbles and gravel that make up these formations. There are large rocks and pebbles in the riverbeds of the unconsolidated sediment part. Large basalt blocks are frequently found in talus and friable, loose, weathered volcanic rock that fell from high cliffs of the basaltic terrain. A highly weathered rock primarily underlies residual soils and humus-rich found in northern Ethiopia (Ayenew and Barbieri, 2005).

Unconsolidated sediment deposits generally have good permeability, but compaction reduces the permeability of the sediments at depth (Sima, 2018). Hagos et al. (2015) states that unconsolidated sediment deposits with enough thickness have a very productive aquifer.

2.6.2. Flood basalts

Ethiopia's Tertiary Trap series, which includes most of Ethiopia, Eritrea, and Yemen, is linked to the Afar hotspot (Sleep, 1998). It is distinguished by several Late Eocene and Oligocene fissure basalts with approximately ~1000 m total thickness (Sembroni et al., 2017). They are mountainous and drain into low-lying areas. The flood basalt contains various minerals compositionally from mafic to felsic. The rock units have been highly affected by intense weathering and secondary porosity (Sima, 2018). The flood basalt formation's potential as an aquifer is based on how much it has weathered and how much it has jointed and faulted (Hagos et al., 2015).

2.6.3. Ambaradom formation

The Ambaradom formation is the youngest sandstone unit and unconformably overlays the Agulae shale formation. It comprises whitish to reddish sandstone, lenses of conglomerate, and lateritic paleosols (Coltorti et al., 2007). At its contact with the overlying flood basalts, the Ambaradom sandstone acts as an aquiclude, forming a spring line (Sima, 2018). The formation has poor jointing and no intergranular permeability. Groundwater movement from the Trap volcanic (flood basalt) to the Mesozoic formation is likely through a few penetrative fractures. According to Sima (2018), many springs discharge at the contact of this unit with the underlying Agulae shale in areas with high granular and fissural permeability.

2.6.4. Agulae shale formation

The Agulae shale formation is exposed on the surface unconformably overlying the Antalo limestone and reaches a maximum thickness of around 300 m.(Enkurie, 2010). It is formed by the regression processes of the Jurassic Seas formed in northern Ethiopia (Sembroni et al., 2017) and formed in lagoonal and tidal environments. It is the upper top formation of the Mesozoic sedimentary rocks. The Agulae shale includes cross-bedded, well-sorted, laminated mudstones, shale dolomite, and gypsum beds (Beyth, 1972). It has soft and powdery behavior and is hard and compact in other areas. Sima (2018) states that the soft Agulae shale has a lower infiltration rate than the hard shale. Agulae shale is intercalated with marl and limestone in most study areas. This intercalation gave the rock unit naming and shared property with limestone and marl, especially in the case of permeability. So, the shale unit with a higher limestone component has a higher permeability than the intercalated portion. The Agulae shale, in general, has poor permeability.

2.6.5. Antalo limestone formation

The Antalo limestone is the major stratigraphic succession of the Mesozoic sedimentary rocks. It has a thickness of up to 800 m. It is also a secondary stratigraphic unit covering many parts of the Zamra catchment next to the unconsolidated sediment. Gebreyohannes et al. (2010) state that the Antalo limestone has major facies depending on the lithological variation. This includes the limestone marl intercalation at the bottom, the marl-limestone intercalation at the middle, and the top shale-marl-limestone intercalation.

According to Sima (2018), the permeability of those facies of limestone varies depending on the amount of marl & shale content and the presence or absence of geological fractures.

2.6.6. Adigrat sandstone

The Adigrat sandstone is unconformably overlain on the basement rocks except in a few localities. In these exceptions, it's underlain by the upper Paleozoic sediments (Enticho sandstone) (Saxena & Assefa, 1983; Sembroni et al., 2017; Wolela, 2008). Continental clastic makes up most of the formation (Wolela, 2008). These continental clastics include sandstones, siltstones, conglomerates, gravely, carbonaceous materials, and mudstones. It is represented by a well-sorted, well-rounded, pinkish to white color, ripple pattern, and medium-grained size (Beyth, 1972; Dow et al., 1971). The Adigrat sandstone with a well-bedded and sorted adjustment has good permeability (Sima, 2018).

2.6.7. Enticho sandstone

The Enticho sandstone is one of the glacial facies in northern Ethiopia (Dow et al., 1971). It is unconformably overlaid on the basement rocks and consists of the eolian and glacial quartzites (Sembroni et al., 2017). According to Sima (2018), Enticho sandstone is a white, fine-to medium-grained sandstone with surface-leached calcareous cement. On average, the thickness of Enticho sandstone reaches more than 160 m (Dow et al., 1971). The sandstone's grain size, sorting, and cementation degree vary in different areas. The upper part of the sandstone is cross-bedded, and the lower part is primarily massive (Sima, 2018).

2.6.8. Basement rock

The Precambrian basement rock is the oldest in northern Ethiopia. It forms the transition zone between the high-grade metamorphic rocks of southeast African Orogen (Mozambique belt) and the low-grade metamorphic rocks of the northeast African (Arabian Nubian shield) (Miller et al., 2003; Sembroni et al., 2016). This basement rock has a variety of lithologies that vary in degree of metamorphism, weathering, and parent rock composition. The metavolcanic rock from the category of basement rock has been exposed in the southwest of the study area. Sima (2018) stated that it has poor permeability, especially in metavolcanics, metapelites, dolomites, and related metasediments.

Table 1: A simplified representation of the geological setting and stratigraphy of Northern Ethiopia (Beyth, 1972)

Lithology	**Formation, thickness, and age**	
Alkaline Basalts	Termaber Formation 800-1000 m (thickness) Oligocene - Miocene age	**Flood basalts**
Tholeiitic to sub alkaline basalt, tuff, ignimbrite, and rhyolite	Alaje Formation 100-500 m Oligocene	
Tholeiitic to sub alkaline basalt	Aiba Formation 600-800 m Oligocene	
Alkaline to sub alkaline basalt, basaltic agglomerate, and basanite	Ashenge Formation	
	600-800 m Oligocene	

Sandstone	Amba Aradom Formation 50-200 m Cretaceous	**Mekelle Outlier**
Shale, limestone, gypsum, dolomite	Agulae Formation 60-250 m Upper Jurassic	
Limestone, marl	Antalo Formation 750-900 m Upper Jurassic	
Sandstone	Adigrat Formation 300-600 m Lower Jurassic to Triassic	
Sandstone, tillite	Enticho & Edaga Arbi formation 150-300 m Paleozoic	
Metavolcanics, slate, dolomite, schist, marble, granite	basement ___ Neoproterozoic	**Basement rocks**

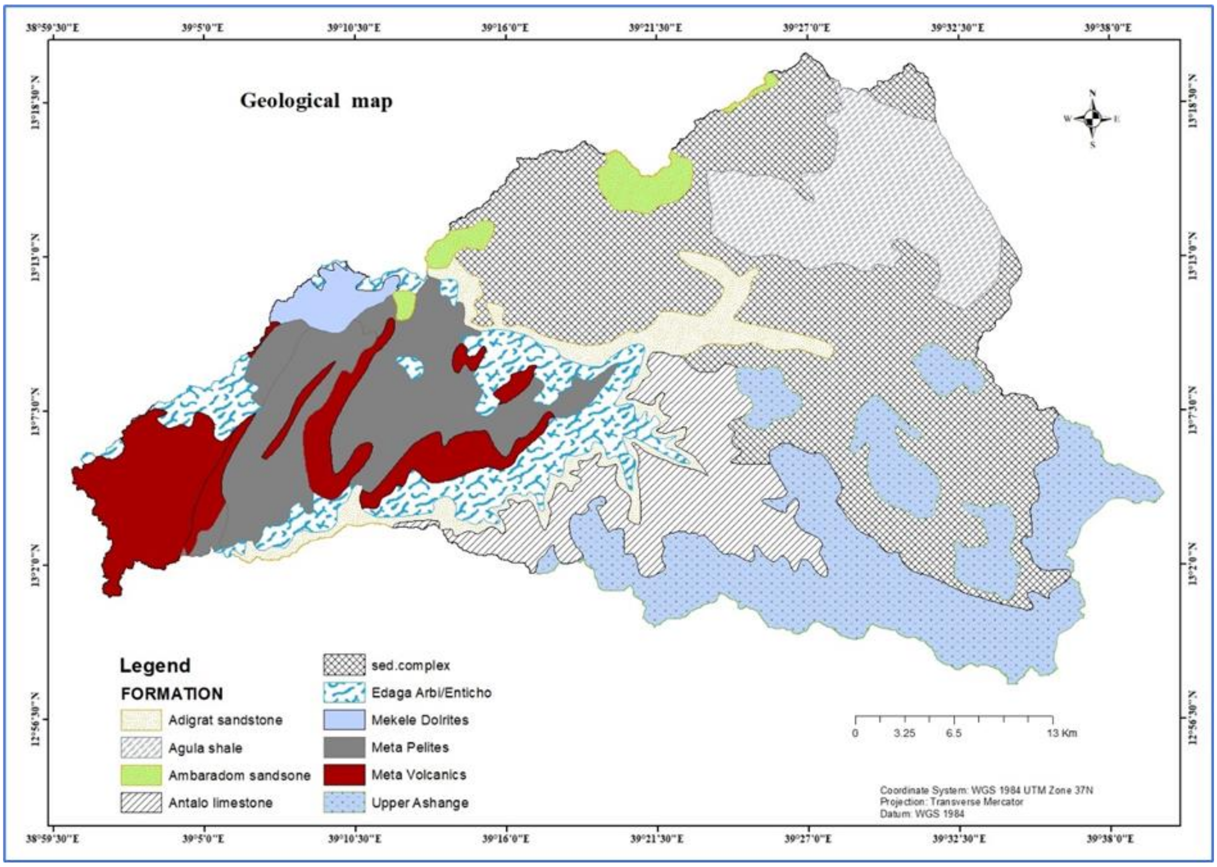

Figure 5: Geological map of ZC (by Ethiopian Ministry of Water and Irrigation)

2.7. Hydrogeology

Geological formations, geomorphology, and topography all influence the hydrogeology of the Zamra catchment. Depending on the grain size and composition of the materials, different lithologies affect the area's hydrogeology. The water bodies (surface and groundwater) found in the study area change their water level depending on the seasonal variation (Girmay et al., 2015). The hydrogeology of ZC consists of seven layers (Hagos et al., 2015; Girmay et al., 2015). According to the data collected from the ministry of water irrigation development, the layers in Zamra catchments are eight hydrostratigraphic units, as indicated in the map below Figure 6.

The study area is characterized by highlands in the east and lowlands in the west, with rivers flowing toward the western portion of the catchment. Hagos et al. (2015) stated that the catchment experiences the highest flow during the summertime because of overland flows, and there is ongoing base flow during the dry season. The study area is characterized by relatively shallow groundwater and numerous springs, especially in the summer. The highland plateaus' precipitation replenishes the shallow groundwater system and discharges to the surface through baseflow into rivers and springs.

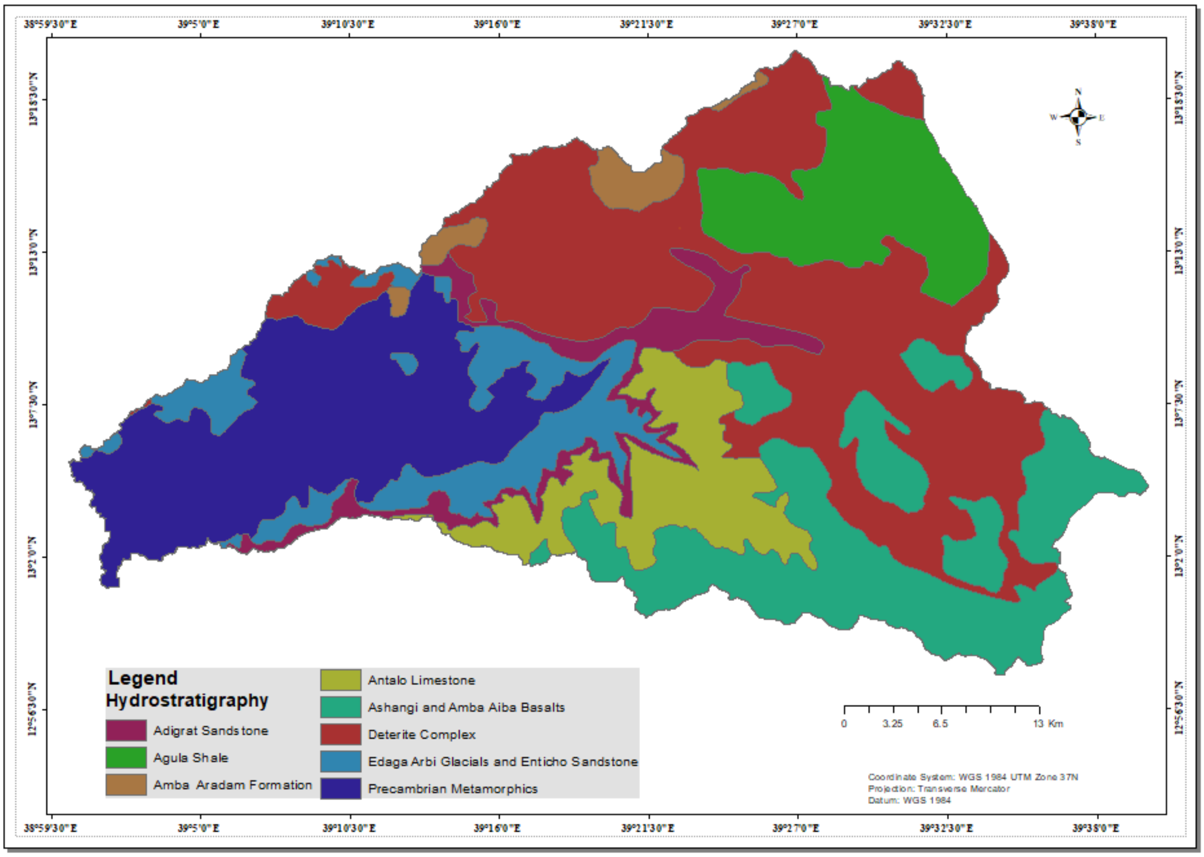

Figure 6: Hydrostratigraphic map of Zamra catchment (by Ethiopian ministry of water and irrigation)

2.7.1. Groundwater flow patterns

As Peeters et al. (2010) stated "the flow direction and gradient of an aquifer system and the depth of the water table in the case of an unconfined aquifer are all shown on the head contour map". Typically, the higher groundwater level coincides with the high surface elevation areas and the lower water level areas with lower surface elevations in the unconfined aquifers of ZC. Like the surface elevation, highlands define the study area in the east and decline in the west, where river water flows.

Intricate interactions between recharge and discharge occurring within local and regional groundwater flow systems make up the groundwater flow in the ZC. As Girmay et al. (2015) stated, the general groundwater flow direction of the catchment is from east to west by analyzing the seepage zones, springs, and shallow groundwater wells and using the existing geomorphological and geological maps.

2.7.2. Unsaturated zone

The unsaturated zone is one of the system's main zones (land surface & saturated and unsaturated zone). The driving force of the model is the primary input of the unsaturated zone in a groundwater model. The unsaturated zone thickness is the difference between the surface elevation and groundwater level. The water depth in the Zamra catchment lies between 5.81 and 24.09 m from the surface after interpolating the static water head records. The unsaturated zone thickness of ZC has a similar trend with surface morphology (thick around the mountain picks).

The variation of unsaturated zone thickness (UZT) results in the spatial variability of the recharge to the groundwater (Halford, 1997). Similarly, areas with thin UZT are more susceptible to groundwater evaporation and exfiltration to the surface than areas with thick UZT. This exchange happens through the unsaturated zone and infiltration processes.

2.7.3. Aquifers

Hagos et al. (2015) determine the aquifer types using relevant information from various sources, such as lithological logs, pumping test results, and geophysical survey findings. They determined that unconfined aquifers are the most prevalent aquifer type in the study area. In all types of rocks located in various physiographic zones, the unconfined aquifer is the shallowest and most popular aquifer (Hagos et al., 2015). Due to the diverse geological history, the study area has a complex hydrogeological environment, and many lithologies in the study area have low porosity and permeability. Even though it has low permeability, those lithology types are affected by high weathering and fracturing with the variable spatial distribution. As indicated in the above hydrological map (Figure 6), the study area does not have a regional aquifer due to the absence of the lithologic unit that extends over a large area.

Previous studies have confirmed that all the hydrogeological layers are mostly aquifers, and sometimes, some units become aquicludes (Girmay et al., 2015; Hagos et al., 2015; Sima, 2018). According to those previous works, the aquifers in metavolcanic rocks are mainly associated with geological weathering and are shallow and localized. They also determined the Antalo limestone and the Adigrat sandstone are exceptionally large semi-regional and most productive aquifers. These two principal aquifers are characterized by joint fractures, bedding, and dissolution cavities available for groundwater flow and accumulation. In contrast, the metavolcanic rocks, Paleozoic sediments, Agulae Shale, and Amba Aradom Sandstone are distinguished by shallow, local groundwater systems that essentially serve as recharge to the underlying layers.

A variety of joints, likewise the Antalo limestone, impact the Agulae shale formation. The rock blocks swell when saturated with infiltrating water because of their predominately clayey content, reducing secondary permeability (Hagos et al., 2015). Even though recharge rates can also be low, they concluded that the shale-dominated units should be regarded as horizons that replenish the Antalo limestone formation's underlying limestone and marl units. Semi-regional aquifers are located in intermountain depressions, river valleys, and lowland plains, which are filled with weathered and fractured volcanic rocks that generate raised plateaus, as well as alluvio-colluvial deposits (Hagos et al., 2015). Hagos et al. (2015) stated that volcanic rocks, particularly the Ashenge basalts, are important aquifers.

The aquifer in the quaternary deposits is inadequately productive except in some areas because of the thickness of the layer. According to Hagos et al. (2015), this layer is rich up to 42 m in the northern part of the upper Tekeze basin, but it is thin in most areas. However, it is thin; the unconsolidated sediment has much higher transmissivity and permeability than the other aquifers in the study area (Sima, 2018).

3. RESEARCH METHODOLOGY

3.1. Methodology

The proposed methodological flow chart has two main components; the left side was used for the conceptual model, and the right side of the flow chart was used for the steady-state numerical model.

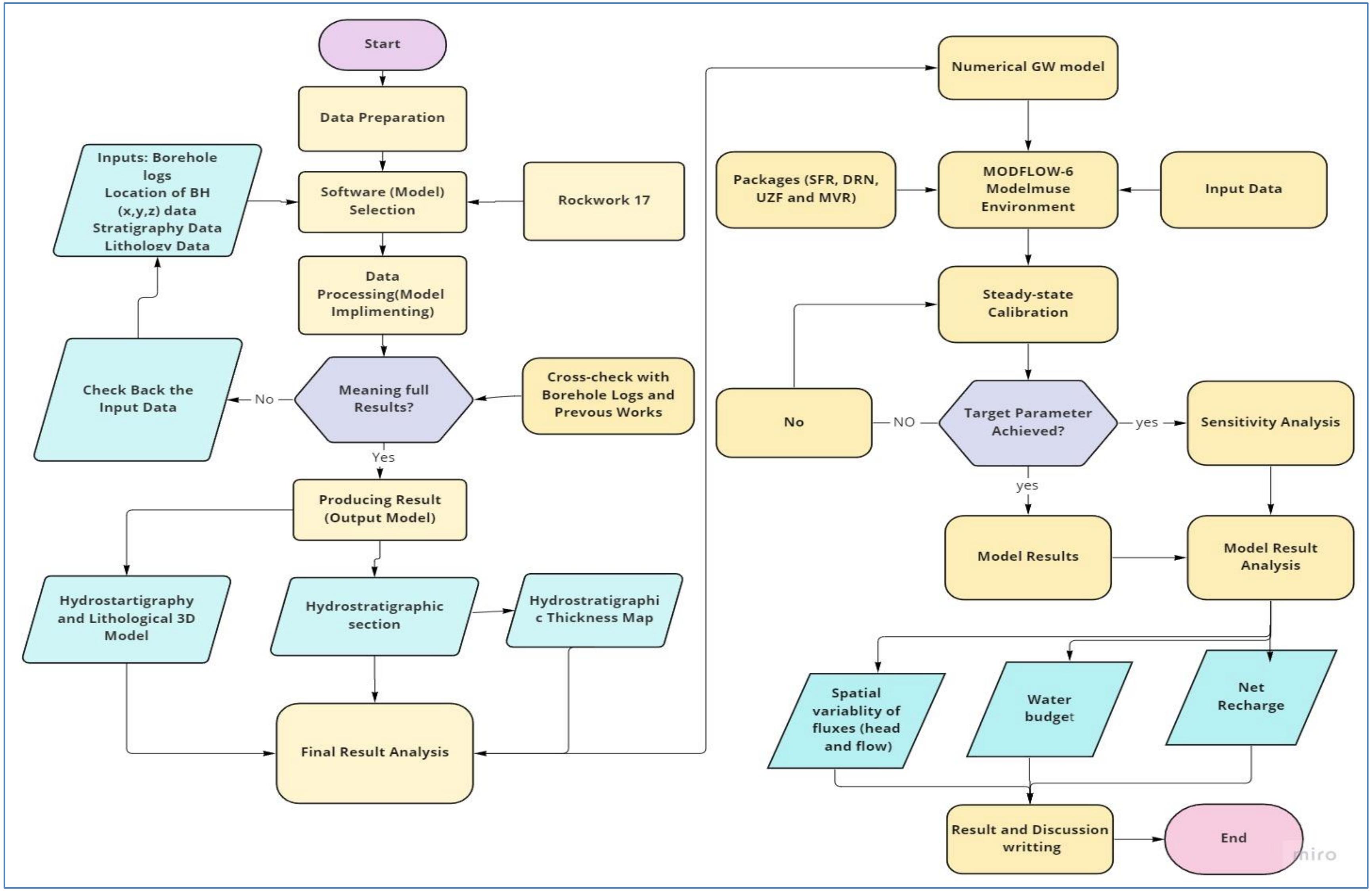

Figure 7: Methodology flow chart for conceptual model (left) and steady-state numerical model (right)

3.2. Data sources

The geological maps, hydrogeological reports, and geological information were collected from literature and other sources. Various online websites help to have an idea about the hydrogeology of the region. For example, Ethiopia's hydrogeology and hydrogeochemistry maps (http://gis.gse.gov.et/hg_maps/) and reports are included on this website. The available dataset used to do both the conceptual and steady-state numerical models are summarized below in Table 2.

Table 2: Summary of dataset description used to achieve the research objectives

No	Data type	Purpose	Source	Environment
1	DEM	To extract elevation of boreholes And input to the Numerical model	ALOS PALSAR	ArcGIS
	Sentinel 2	To do *LULC* map	European Space Agency (ESA)	Google Earth Engine
2	Borehole log data	To build a 3D hydrostratigraphic model, series of cross-sections, and determine the spatial distribution of hydrostratigraphic units.	Tigray region water office	Rockworks 17
	Spatio-temporal data (P and PET)	Input for steady-state model	(Gebremedhin et al., 2021)	MODFLOW 6
	State variables	To calibrate the model	Literatures	MODFLOW 6
3	System parametrization	Input for Numerical model	Literatures	MODFLOW 6
	Interception rate of land cover types	To calculate interception	Literatures	ArcGIS

3.3. Conceptual model

The methodology applied was summarized in the flowchart above, Figure 7, to address the study's first two objectives related to the conceptual model. Two primary data types were used to process the conceptual model's critical components. These data types are remote sensing data and borehole log data. The borehole log data includes the borehole's stratigraphy, lithology, location, and depth. Integrating those all-data types and adjusting different model parameters (checking the variographs and testing different modeling options within the rockworks), representative cross-sections, thickness maps of each layer, and a 3D hydrostratigraphic model were produced. At the same time, the ALOS PALSAR DEM data has been used to extract the elevation of each borehole log.

Rockworks 17 software was used for producing a 3D hydrostratigraphic model, 3D lithologic model, series of cross-sections, and data processing. Stratigraphy, lithology, downhole geochemistry, geotechnical measures, geophysics, fractures, aquifer data, and color intervals are just a few of the many types of data that Rockworks can analyze in both surface and subsurface data form.

Rockwork software is widely used in the hydrogeology, environmental, geotechnical, geophysics and mining industries to visualize subsurface data. Maps, logs, fence diagrams, solid models, and volumetric are some of the most used tools in this software.

Its main advantages are its ease to use and the ability to combine it with other GIS-type applications iteratively and supported by ArcGIS. ZC hydrostratigraphic units were better understood using the Rockworks code. Using a 3D hydrostratigraphic code in the rockworks is critical because it simplifies the combination of lithological, hydrogeological, and structural geological data with hydrostratigraphic data if any are available. Input data for the software was prepared in excel by collecting the paper-based borehole points recorded by Tigray water resource, mines, and energy office.

3.3.1. Hydrostratigraphic model development

The geology of northern Ethiopia is complicated and highly diversified. The geology of northern Ethiopia, including Zamra, is lithologically classified based on the mode of formation and age (Beyth, 1972; Gebreyohannes et al., 2010; Sembroni et al., 2017, 2016; Wolela, 2008). The study area contains about nine lithological units. The lithological units are more than nine, but this model is made based on the data of borehole logs. In the lithological model, due to data limitation, all the varieties of sandstone rock units (Enticho, Adigrat, and Ambaradom) have been taken as sandstone rock units.

According to previous studies in the upper Tekeze basin (Girmay et al., 2015; Hagos et al., 2015), there are seven hydrostratigraphic units in the study area. The stratigraphic units are unconsolidated sediment, flood basalt, Agulae shale, Antalo limestone, Adigrat sandstone, Enticho sandstone, and metavolcanic rock. Hagos et al. (2015) have determined aquifers in all types of stratigraphy located in various physiographic regions.

The method applied to answer the research question and achieve the objective related to hydrostratigraphic model development of ZC is done in five significant steps. These steps include data preparation, model selection, hydrostratigraphic or stratigraphic modeling, producing the result, and analysis.

In this study, first, the paper logs and descriptions of boreholes from the Tigray water resource office are screened and turned into Excel format. The borehole data available was found enough to model the 3D hydrostratigraphic model of the Zamra catchment. A total of 201 borehole logs, including the fictitious points (65 points), are used for model development after a detailed screening of the paper-based data. The selected borehole logs were arranged in a suitable (.xlsx) format for the input of the rockwork software, which includes the location in X, Y, Z, lithology, and stratigraphic sheets. The elevation for each borehole was extracted from the ALLOS PALSAR_TR1 at 12.5m resolution using ArcGIS. The ALOS PALSAR_TR1 data was downloaded from the website of the Alaska satellite facility at https://search.asf.alaska.edu/#/. Once the stratigraphic and lithological data are adequately arranged in a suitable format (excel), the stratigraphic data is imported into borehole manager utilities in rockwork software.

The hydrostratigraphic and lithologic models were built by interpolating the borehole log vertical intervals and surface layers. The borehole log data was imported into the software and interpolated using the kriging method. After many trials, a representative three-dimensional (3D) hydrostratigraphic model, lithologic model, and cross-sections were produced by adjusting the parameters. The 3D stratigraphic model is used to construct a conceptual model of the hydrogeological system, and it is necessary for understanding the flow of water based on the unit elevation and thickness.

This model is used to identify the spatial distribution and heterogeneity of the hydrostratigraphic units. It can also be used to detail the characterization of stratigraphy to identify the geometry of each lithological unit in the study area. A 3D attributed stratigraphic model's accuracy depends on an array of precisely documented borehole log data, distribution, and physical properties to properly visualize it.

Table 3: Hydrostratigraphic units of Zamra Catchment

Supergroup	**hydrostratigraphic unit**	**Lithology**	**Thickness and age in the ZC**
Quaternary deposits	Unconsolidated sediment	Alluvium, talus, colluvium lacustrine, and swamp deposits	0 – 27 m
			Quaternary - present
Flood basalts	Flood basalt	Alkaline Basalts	0 - 69 m (thickness)
		Thiolytic to sub alkaline basalt, tuff, ignimbrites, and rhyolite	
		Alkaline to sub alkaline basalt, basaltic agglomerate, and basanite	Oligocene - Miocene age
Mekelle Outlier	Agulae shale	Shale, limestone, gypsum, dolomite	0 - 58 m
			Upper Jurassic
	Antalo limestone	Limestone, marl	0 - 76 m
			Upper Jurassic
	Adigrat sandstone	Sandstone	0 - 49 m
			Lower Jurassic to Triassic
	Enticho sandstone	Sandstone, tillite	0 - 45 m
			Paleozoic
Basement rock	Metavolcanics	Metavolcanics	0 - 45 m
			Neoproterozoic

3.3.2. Flow system direction

The groundwater head surface is created using geostatistical approaches, including the statistical features of the measured data in the prediction process (Antonakos and Lambrakis, 2021). These algorithms can generate the spatial distribution of anticipated values and error or uncertainty spatial distributions and indicators, allowing you to assess how accurate the predictions are. The principle of regression kriging (RK) works; the predictions are made separately for the drift and residuals and then added back together. Girmay et al. (2015) have conceptualized regional (northern Ethiopia) groundwater flow using isotopes. But the flow system for this specific catchment has not been determined before. Therefore, the regression kriging interpolation method was used to determine the groundwater heads to interpolate the initial hydraulic heads and determine the flow system direction of the catchment.

Due to the well-known orographic effects on groundwater movement, surface elevation (DEM) is considered a predictor while implementing the RK interpolation method in ZC. The geostatistical approach uses auxiliary information to quantify spatial uncertainty and improve the water table mapping of the study area. This interpolation was done using 384 groundwater level recorded points and a digital elevation model (DEM) as a predictor grid input. The static water level of wells was measured by the Tigray water resource, mines, and energy bureau. Hydraulic head points are defined by subtracting the static water level depth from the surface elevation points. The surface elevation points were extracted from the ALOS PALSAR 12.5m DEM in ArcGIS. The RK interpolation was processed in the system for automated geoscience analysis (*SAGA*) software (Conrad et al., 2015). It was done following the steps indicated in Figure 8.

In this study, producing the potentiometric and groundwater head map is mainly used to determine the groundwater flow direction and the boundary condition of the system. Even if he doesn't quantify how much it fluctuates, Siyoum (2020) indicates the groundwater levels of the study area fluctuate according to seasonal changes, but at this time, it was done using only a single event record. After interpolating initial hydraulic heads using RK, the water level map was produced.

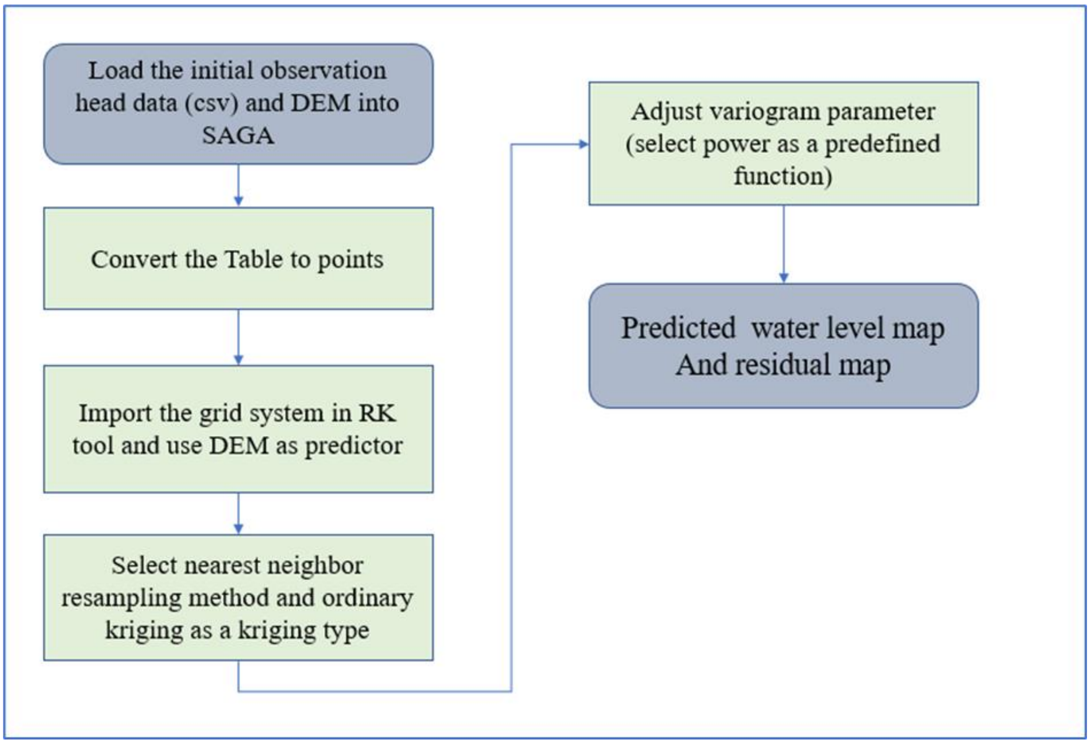

Figure 8: Steps to interpolate the groundwater level record in SAGA software (Conrad et al., 2015).

3.3.3. Boundary condition

The mathematical boundary condition of the numerical model is based on the boundary condition along the conceptual model (Anderson et al., 2015). The system boundary condition determines the flow in and out of the system (Taha, 2015). This study's boundary condition was determined primarily using the potentiometric lines produced from interpolated groundwater levels. In numerical modeling, boundary conditions are crucial since their boundaries highly affect the hydrologic components.

3.3.3.1. External boundary

The hydraulic boundary condition for the Zamra catchment was identified by delineating the streamlines, using the potentiometric maps produced from the recorded hydraulic heads during the drilling of boreholes, and using a 3D terrain model from ALOS POLSAR. According to Taha (2015), the divides of catchments can be used as a hydraulic boundary, forming no-flow boundaries. Depending on that information, the Zamra catchment external boundary condition has no flow boundary in the perimeter except the discharge area

3.3.3.2. internal boundary

According to Anderson et al. (2015b), the major surface water features, including the streams, lakes, and oceans, are considered internal boundaries. Surface water bodies directly connected to the groundwater system form formidable physical boundaries. The Zamra stream and its tributaries are considered internal boundary conditions in this study.

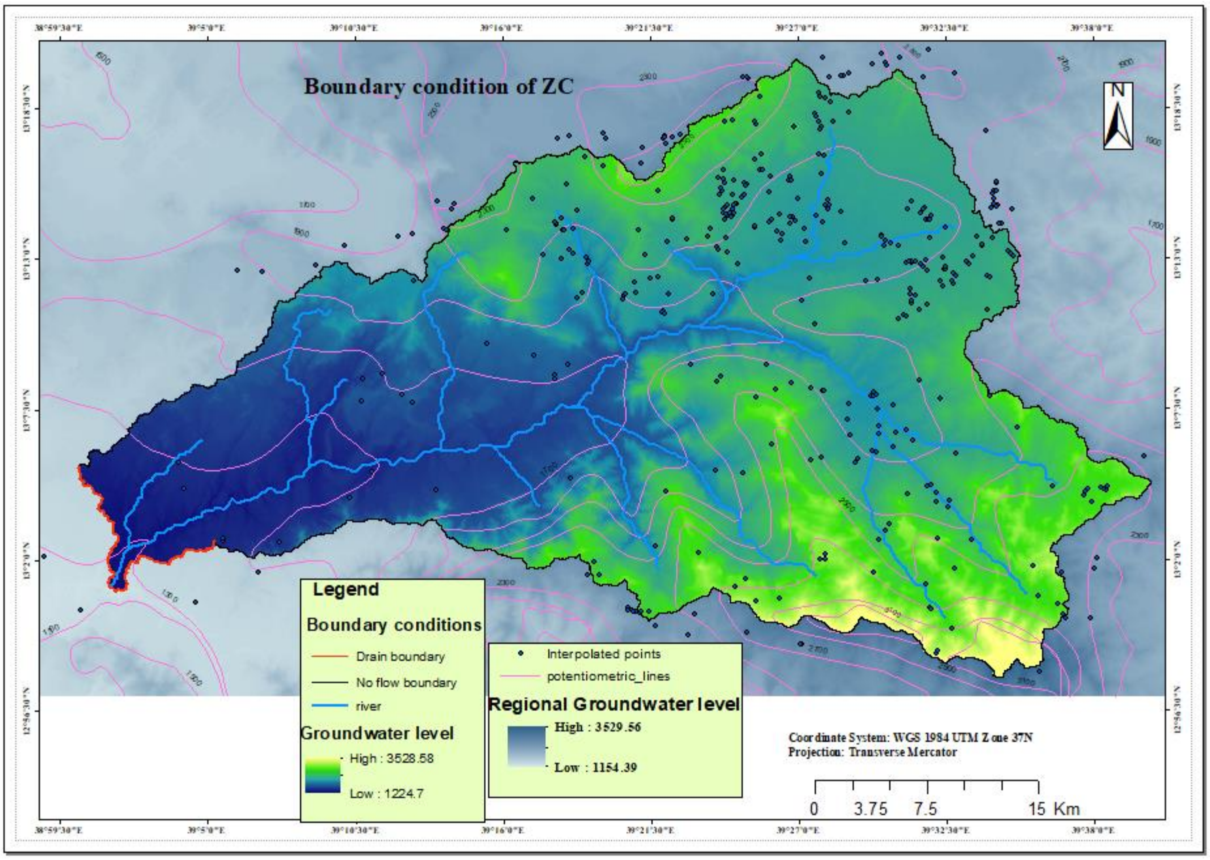

Figure 9: Map shows the boundary condition of ZC

3.3.4. Water balance

The inflow and outflow of the groundwater are provided by the groundwater budget components, which are the essential pieces of every groundwater model (Anderson et al., 2015). The only input to the system for ZC is precipitation. The main outputs are river discharge, groundwater evapotranspiration, and a minor amount of lateral groundwater discharge. The detail of the water balance has been discussed in the numerical model below in section 3.5.

3.3.5. Schematic conversion of conceptual to numerical model

The hydrostratigraphic and overall conceptual models are built by systematically integrating multiple data sets from diverse sources in the Zamra catchment and regionally from UTB. The initial step in setting up the model was defining the hydrostratigraphic units, which required a thorough understanding of the area's geology and hydrogeology. However, Hagos et al. (2015) have previously defined the hydrostratigraphic units in this case. In addition to the geological and hydrogeological data from borehole logs, groundwater levels were utilized to determine the conceptual model properly.

Once the conceptual model has been built based on the currently available geological and hydrological data, which are the borehole log data, water level data, and expert geological interpretation, schematic conversion of the conceptual model to the numerical model has been done. To construct the numerical model, the conceptual model is one of the critical background steps. As a result, the transition from the conceptual to the numerical model is carried out as efficiently as possible. The transition from the conceptual to the numerical model is not straightforward since it depends on the software packages and their interface specifications (Lekula et al., 2018).

In the case of the Zamra catchment, it is difficult to show all the layers on the schematic diagrams due to the geological complexity of the area. The strata of the area are not continuously covered, and in some areas, the layers are very thin. So, in the schematization, all layers are also included and not to scale. Due to the discontinuities of the units in ZC, finding the profile section that contains all lithologies is difficult. Therefore, the schematized diagram of the numerical model was done by taking a snapshot image of the more representative side of the 3D hydrostratigraphic units and by considering the spatial extent of the layers from the 3D model. The flow direction and aquifer system gradient information were taken from the head contour map.

3.4. Numerical model

This study is planned to do a steady-state numerical model of the Zamra catchment. According to Anderson et al. (2015), the governing equation of a steady-state model ($\partial h/\partial t$) is zero, and the estimated heads and fluxes, as well as the hydrologic parameters, are constant over time. Therefore, the steady-state solution is represented by the following formula:

$$\frac{\partial}{\partial x}\left[K_x\frac{\partial h}{\partial x}\right]+\frac{\partial}{\partial y}\left[K_y\frac{\partial h}{\partial x}\right]+\frac{\partial}{\partial z}\left[K_z\frac{\partial h}{\partial z}\right]+W=0 \qquad [1]$$

where:

K	hydraulic conductivity in x, y, and z direction	[L.T^{-1}]
X, y, z	Cartesian orthogonal coordinates	[L]
h	piezometer head	[L]
W	source or sink	[T^{-1}]

Therefore, this study has no change in the storage of the aquifers. By their very nature, groundwater systems are almost never in a steady state, yet for many issues, the modeling goal can be successfully met by looking at steady-state conditions (Anderson et al., 2015). The time-averaged steady-state model represents the averaged heads over that specified period.

3.4.1. Software selection and packages

The most recent MODFLOW version, MODFLOW 6, under the model muse environment was used in this research. The MODFLOW-Newton NWT's Raphson formulation option was activated to address the system nonlinearity. A model cell can be hydraulically connected to nearby cells because MODFLOW 6 supports Quadtree grids and the structured grid. The unstructured grid technique makes it easier to narrow the area of interest to the desired cell size.

The Node property flow package (NPF), observation utilities, and advanced stress packages simulate the steady-state numerical model. From the advanced stress packages unsaturated zone flow package (UZF 6), stream flow routing (SFR), drain and water mover package (MVR) were implemented. In MODFLOW 6, the NPF package determines the flow between neighboring cells. According to Langevin et al. (2017), the NPF Package adds Newton-Raphson terms to intercell flow equations in MODFLOW 6, computes intercell conductance values, and controls cell wetting and drying. Additionally, unlike the previous version of MODFLOW, the NPF package enables each cell to be independently designated convertible or nonconvertible.

The default option of the NPF package was accepted since the default is the most stable for typical groundwater problems (Langevin et al., 2017). The NPF package replaces the Block-Centered Flow (BCF), Upstream Weighting (UPW) Packages, and Layer Property Flow (LPF) from the previous MODFLOW versions. It computes vertical and horizontal hydraulic conductance as part of the groundwater flow model. Ghost-Node correction package (GNC) is automatically switched on when the gride type changes to DISV. The Ghost nodes in DISV models are specified using this GNC package.

3.4.2. General model setup

Aquifer parametrization, aquifer geometry design, boundary conditions, and other anclinatory information are all included in the overall numerical setup, together with the grid configuration, general model assumptions, and software selection.

The model was built using five hydrostratigraphic layers. The Antalo limestone and Agulae shale units were merged as a limestone-shale intercalation layer. The Enticho and Adigrat sandstone are merged into the sandstone units' layer when imported to the numerical model. In addition, the input parameters are prepared in the required format before the gride setup of the model.

3.4.3. Spatial discretization

The model was constructed using the structured (uniform) grid design of 0.5 km by 0.5 km at the beginning. The grid network has 83 rows and 144 columns with five layers and 18405 active cells (before applying a Quadtree, unstructured grid refinement). The model alignment was done using a projected coordinate system WGS84_UTM _zone_37N. The Quadtree refinement has been done around the vicinity of observation wells and streams. After the Quadtree refinement, the number of active cells increased to 231138, and the cell size ranged from 30 – 500 m.

The thickness of the five layers was processed in an ArcGIS environment and imported into the model. This layer thickness and model top elevation determine the vertical discretization. ALOS PALSAR DEM assigned the model top. The model takes each cell's average value of points extracted from DEM. This principle was applied to all geological layer thicknesses because all the layers were resampled to the resolution of ALOS PALSAR DEM during data processing. After importing all the layer thicknesses, the elevation of each layer was calculated using the following formula:

$$first\ layer\ bottom = Model\ top - thickness\ of\ the\ first\ layer \quad [2]$$

$$second\ \ layer\ bottom = first\ layer\ bottom - thickness\ of\ the\ second\ layer$$

Continues up to last and

$$fifth\ layer\ bottom = fourth\ layer\ bottom - thickness\ of\ the\ fifth\ layer$$

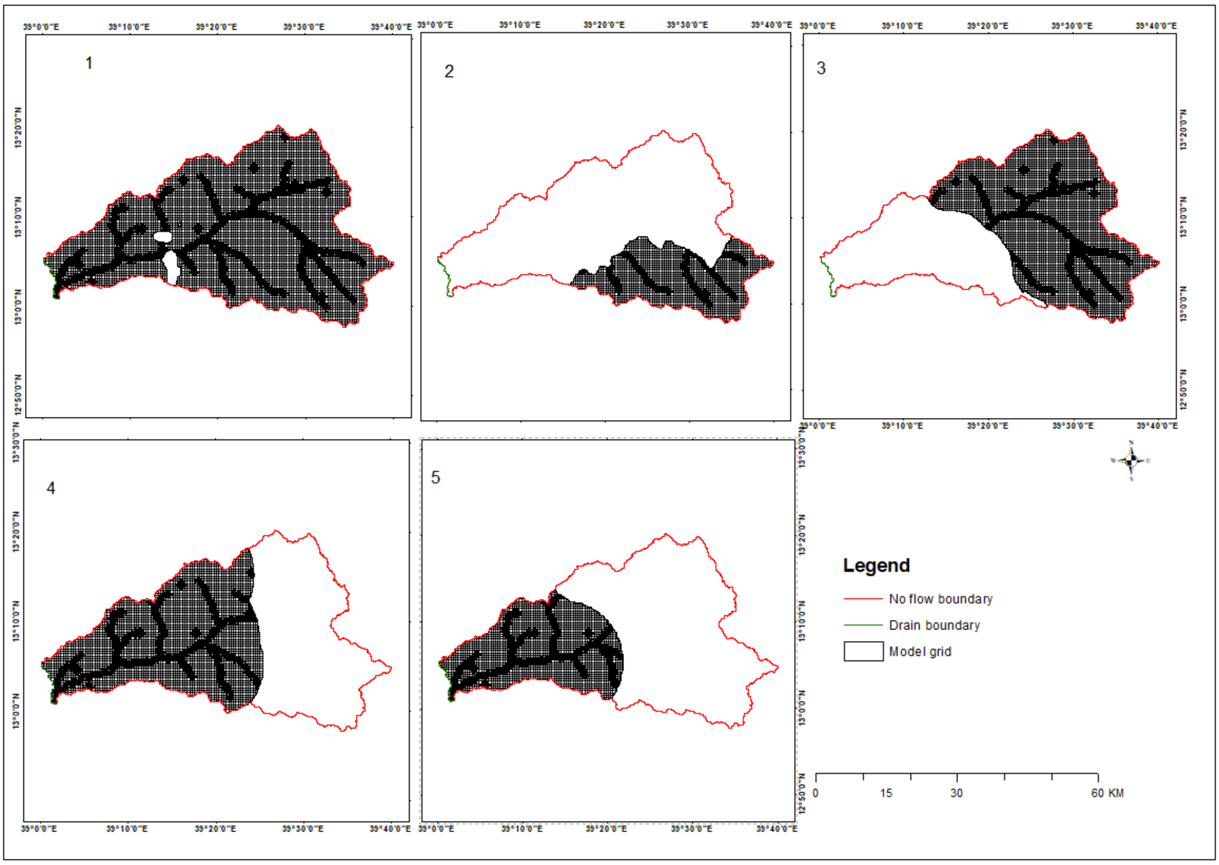

Figure 10: Model grid setup: Active cells of each layer from 1-5 sequentially

3.4.4. Driving forces

The primary input data for the numerical model consists of the driving forces, system parameters, and state variables. The driving forces in the specified model domain can vary in time and space, but in this case, there is no variation of driving forces in the time since the model is steady. The input of these driving forces also highly affects the model output, and these outputs vary spatially within the specified model domain. The three components of driving forces are precipitation (*P*), potential evapotranspiration (*PET*), and canopy interception (E_I), all determined with the help of remote sensing.

3.4.4.1. Precipitation

A bias-corrected daily MPEG precipitation processed by Gebremedhin et al. (2021) was used as an input to the numerical model. In particular, the daily mean of one hydrological year lasting from Sep 2019 to 31 Aug 2020 was used as discussed in section 1.2.

3.4.4.2. Potential evapotranspiration (PET)

Gebremedhin et al. (2022) processed the daily *PET* using the satellite-derived daily reference evapotranspiration derived from DMETREF, as discussed in section 1.2. That *PET* was used in this study (as driving force model input), taking the mean of daily *PET* for one hydrological year lasting from September 1, 2019 – August 31, 2020.

3.4.4.3. Interception (E_I)

Groundwater modeling requires the interception and rooting depth of various land use landcover (LULC) classes. The quantity of rainfall that remains on the vegetation canopy and is returned to the atmosphere via evaporation is known as an interception. The canopy size, the sparse gap between vegetation, and the climatic state of the area are all elements that influence the interception loss rate. This interception was calculated and subtracted from precipitation to find effective precipitation. The interception was calculated using the following equation:

$$E_I = P * I \qquad [3]$$

where:

EI = Canopy interception [mm day $^{-1}$]

P= Precipitation [mm day $^{-1}$]

I = Interception loss rate of each landcover class per pixel as indicated in Table 4 below and

The canopy interception was done by producing two land cover maps, one from the summer season by taking sentinel-2 images on 30-09-2021 and the other from winter on 21-04-2021. The above formula was applied to both landcover maps and produced two different rainfall interception values. Then, the average two-interception raster values were subtracted from average rainfall to get effective precipitation. This effective precipitation was calculated as follows:

$$P_e = P - E_I \qquad [4]$$

Table 4: Interception rate of different landcover types found in Zamra catchment

No	Landcover type	Area contribution (%)	I	Reference
1	Water bodies	2.26	0.00	(Gebremedhin et al., 2022)
2	Agricultural land	39.09	0.06	(Gebremedhin et al., 2022)
3	Bare soil	9.89	0.00	(Gebremedhin et al., 2022)
4	Shrubs	43.95	0.075	(Gebremedhin et al., 2022)
5	Forest	4.81	0.12	(Gebremedhin et al., 2022)

3.4.5. System parametrization

The NPF package was selected to simulate the groundwater flow between the adjacent cells by applying the default cell averaging mechanism (harmonic mean). This harmonic mean method of calculating inter-block transmissivity calculates the transmissivity of the aquifers in the horizontal direction. The parameters in the UZF package (surface depression depth, saturated vertical hydraulic conductivity, residual, saturated & initial water content, and Brooks Corey epsilon) are just given by estimating arbitrary values since there are not any previously tested models. The number of wave sets, and trailing waves is taken as the default values (40 and 7, respectively). The main parameters for any model are the transmissivity and the hydraulic conductivity of the aquifer. These parameters are roughly estimated in the study area regionally before (Hagos et al., 2015), as indicated in the table below in Table 5.

Table 5: System parameters (transmissivity and hydraulic conductivity) of the aquifers in the study area (Hagos et al., 2015)

Aquifers	Transmissivity (m^2 day ^{1})			K ($m.day^{-1}$)
	min	Max	Average	
Unconsolidated sediment	12	1005	482	0.42- 35
Flood basalt	1 - 6	32- 40	16- 20	0.15
Limestone-shale intercalation	7 - 110	20 - 146	14- 125	0.005 -17.6
Adigrat sandstone	196	261	229	0.08 - 3.14
Metavolcanics	3	57	20	0.02

3.4.6. Boundary condition

The boundary conditions were divided into internal and external. The external boundary determines how water flows into and out of the model, while the internal boundary is responsible for the flow between the system components. The advanced stress packages (Langevin et al., 2021) represent the internal boundary conditions in the numerical model. Therefore, from the advanced stress packages, the following are used as boundary conditions in this study.

3.4.6.1. Stream flow routing (SFR) package

To model the flow interaction between stream and groundwater, the Streamflow Routing (SFR) Package applies the continuity equation and the assumptions of piecewise uniform, constant density, and steady stream flow (Langevin et al., 2017). With no water being added to or removed from storage, streamflow is always channeled through a network of rectangular channels at the equal volumetric inflow and outflow rates. The SFR Package for MODFLOW 6 computes flow throughout the streambed using the stream depth estimated (active reaches) or specified (simple routing option reaches) at the midpoint of a rectangular cell.

This study uses the simple routing option reaches to simulate the stream flows. The required inputs for the SFR package are, reach width (rwid), stream top (stp), stream reach length (rlen), gradient (rgrd), hydraulic conductivity of the stream bed (rhk), and stream bed thickness (rbth). The reach width was assigned 5 m for the Zamra river and 2 m for the tributaries. The streambed top has been assigned using the function "InterpolatedVerteValue" for the main river and its tributaries. For the stream reach length, the software calculates the length from the imported shapefile, which has been processed from DEM in ArcGIS.

The stream gradient has been calculated in ArcGIS for each segment of streams and imported into the package manually. The hydraulic conductivity of the stream bed and stream bed thickness is assigned as 2.9 $m.day^{-1}$ and 0.2, respectively, at the beginning, and hydraulic conductivity was adjusted later during calibration. The connection between the stream segments was defined based on the elevation of the Zamra river and each of its tributaries. Each tributary was defined as upstream and had a higher elevation than the downstream segment.

The stream discharge (q) is equal to the sum of base flow (q_b), groundwater exfiltration (Exf_{gw}), and rejected infiltration (RI) from each active cell of the UZF packages and all stream segments.

$$q = RI^s + Exf_{gw}^s + q_B \quad [5]$$

$$q_b = q_{sg} - q_{gs} \quad [6]$$

while $q_{sg} = \frac{W_b * L_b * K_b}{b_b}(h_b - h_{aq})$ if $h_{aq} < h_b$

$g_{gs} = \frac{W_b * L_b * K_b}{b_b}(h_{aq} - h_b)$ if $h_{aq} > h_b$

where:

RI^s	Rejected infiltration routed to the stream	[$m^3.day^{-1}$]
Exf_{gw}^s	groundwater exfiltration routed to the stream	[$m^3.day^{-1}$]
q_B	Base flow	[$m^3.day^{-1}$]
q_{sg}	Stream reach leakage to groundwater	[$m^3.day^{-1}$]
q_{gs}	Groundwater leakage to the stream reaches	[$m^3.day^{-1}$]
W_b	Stream reach width	[m]
L_b	Length of stream reach	[m]
K_b	Stream reach bed hydraulic conductivity	[$m^2.day^{-1}$]
h_{aq}	Cell head that contains stream reach	[m]
h_b	Stage of stream reach	[m]
b_b	bed thickness of the stream reaches	[m]

3.4.6.2. Unsaturated zone (UZF) package

With the help of the unsaturated zone flow package, the aquifer is recharged by simulating the unsaturated zone flow. Part of infiltrated water may occasionally be rejected due to a specific high infiltration rate larger than the unsaturated zone's hydraulic conductivity. The water not allowed to penetrate the land's surface is redirected over it and immediately added to the features of other advanced stress packages (SFR, LAK, MAW, and UZF Packages). This addition of rejected water can be managed by another advanced stress package called water mover (MVR). The UZF package can serve as a provider and a receiver to the MVR package.

Negative pressure gradients are ignored in the UZF program, which is based on the kinematic wave approximation of Richards' equation. This is done to keep things as straightforward as possible (Langevin et al., 2017). To make the Richards equation easier to understand, these negative gradients have been left out, and the equation has been written in terms of length and time as follows:

$$\frac{\delta\theta}{\delta t} + \frac{\delta K(\theta)}{\delta z} + i_{ET} = 0 \quad [7]$$

Where:

θ	Volumetric water content in the vadose zone	[$L^3.L^{-3}$]

t	Time	[T]
$K(\theta)$	Vertical hydraulic conductivity as a function of water content	[L.T^{-1}]
i_{ET}	Unsaturated evaporation rate per unit depth (only in transient simulation)	[L.T^{-1}L^{-1}]
z	Vertical distance	[L]

The driving forces are the primary components that go into the UZF package. As was covered in section 3.4.4, two primary causes are driving this (effective precipitation and potential evapotranspiration). The term "infiltration rate" refers to the amount of water penetrating deeper into the ground over time and surface area. The Brooks-Corey equation included in the UZF package can be used to determine the relationship between the vertical hydraulic conductivity and the water content [eq. 8], and the infiltration rate can be converted into water content using the formula found below [eq. 9]. The amount of water that can penetrate the subsurface is restricted by a property known as vertical saturated hydraulic conductivity (K_{sat}). If the supplied infiltration rate is less than or equal to K_{sat}, the water content will be set to the saturated water content (θ_{sat}), which is the default value. If the given infiltration rate is higher than the K_{sat}, then the water content value will be the difference between the infiltration rate and the K_{sat}. The term "rejected infiltration" describes this distinction (*RI*). The amount of water rejected during this infiltration was converted to volume, multiplied by the cell's area, and then added to the SFR package (streams) through the MVR package.

$$K(\theta) = K_{sat} * \left[\frac{\theta-\theta_{resid}}{\theta_{sat}-\theta_{resid}}\right]^{\varepsilon} \quad [8]$$

$$\theta_{qa} = \left(\frac{q_a}{K_{sat}}\right)^{1/\varepsilon} (\theta_{sat} - \theta_{resid}) + \theta_{resid} \qquad 0 < q_a \leq K_{sat} \quad [9]$$

$$\theta_{qa} = \theta_{sat} \qquad q_a > K_{sat}$$

Where:

$Ksat$	Vertical saturated hydraulic conductivity	[L^3.T^{-1}]
θ_{resid}	Residual water content	[L^3.L^{-3}]
θ_{sat}	Saturated water content	[L^3 .L^{-3}]
θ_{qa}	Water content corresponding to a specified infiltration rate	[L^3 .L^{-3}]
q_a	Specified infiltration rate	[L.T^{-1}]
ε	Brooks Corey exponent	[-]

By removing water from the unsaturated zone, the UZF package meets potential evapotranspiration (*PET*) in such a circumstance. But if the water content drops to or equals the θresid, no water will be evacuated from the unsaturated zone. In steady state models (so also in this study), only groundwater evapotranspiration (ET_g) is simulated. Thus, all *PET* requirement is deducted from the saturated zone when it is not yet satisfied by the unsaturated zone's water content. The water table must be above the specified extinction depth (d_{ext}) to have ET_g. The groundwater exfiltration (Exf_{gw}) has also been simulated using the UZF package by defining surface depression depth (d_{surf}). The modeler allocated the (d_{surf}) according to how close to the land surface groundwater exfiltration begins. In this study, dsurf was assigned as 0.125 [m].

The extinction depth for each landcover class was done in ArcGIS. There were five landcover classes, and from those five landcover classes, a 0 m extinction depth was given to the water bodies, 7.5 m for the trees, 0.5m for bare soils, 1.5m for agricultural lands, and 2 m for shrubs based on literature as indicated in the map below Figure 11.

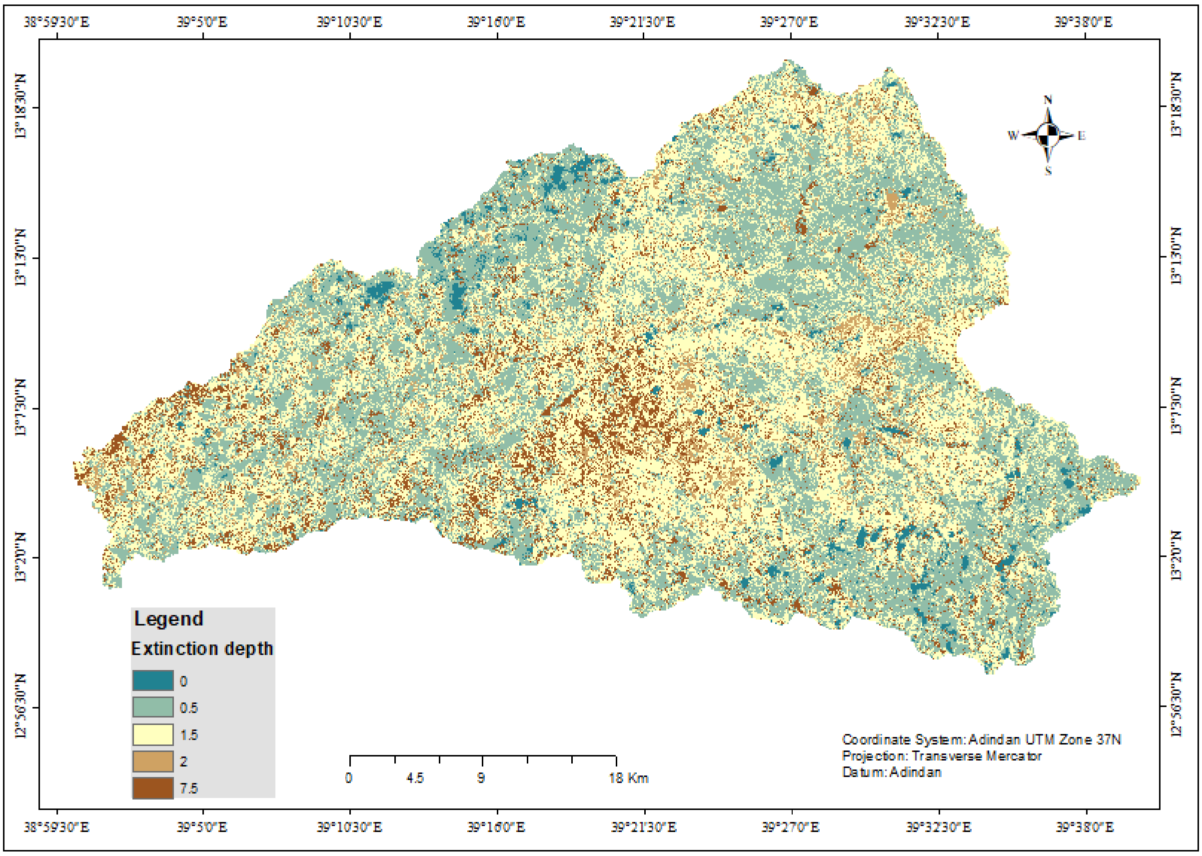

Figure 11: Extinction depth map for landcover class in ZC [m]

The following in the table are all the parameters used in the UZF package initially, and except ε all of them are adjusted later during calibration.

Table 6: Parameters used for the UZF package

Parameter		value	Unit
surfdep	Surface depression depth	0.125	[m]
vks	Vertical saturated hydraulic conductivity	=Kv	[$m^3.m^{-3}$]
θ_{resid}	Residual water content	0.05	[$m^3.m^{-3}$]
θ_{sat}	Saturated water content	0.35	[$m^3.m^{-3}$]
θ_{init}	Initial water content	0.3	[$m^3.m^{-3}$]
ε	Brooks Corley epsilon	3.5	[-]
extwc	Extinction water content	0.05	[$m^3.m^{-3}$]

3.4.6.3. Water mover package

Water can be transferred from specific "provider" characteristics of some packages (WEL, GHB, MAW, DRN, SFR, LAK, RIV, and UZF) to specific "receiver" features of more advanced packages (MAW, UZF, LAK, and SFR) using the MVR Package. It is a simple rule to quantify the amount of water moved from the provider to the receiver packages, and the provider and receiver packages can be set depending on the modeler's interest (Langevin et al., 2017).

According to Morway et al. (2021), by utilizing a generalized technique, MVR enables the movement of water between any arbitrary combination of simulated features (such as streams, drains, pumping wells, lakes, and so on) within a MODFLOW 6 simulation. These features include streams, drains, pumping wells, and lakes. The available water is moved from the provider package to the MVR package and subsequently from the MVR package to the receiver package; however, this is determined by the user's preferences. In this MVR package, any stress package (WEL, DRN, RIV, and GHB) and any advanced stress package (MAW, SFR, LAKE, and UZF) can act as a provider; however, the only packages that can act as receivers are the advanced stress packages that can solve the continuity equation (Daoud et al., 2022). These packages are listed in the previous sentence.

In this investigation, the MVR package is applied to measure the overland flow of groundwater exfiltration and rejected infiltration from the provider (UZF package) to the receiver (SFR package). Therefore, in this model of steady-state conditions, all of the rejected infiltration and exfiltration rates from the unsaturated cells in the UZF package are sent to the MVR package, which is subsequently provided to the SFR package. If the provider, which in this case includes all UZF cells, does not have any water available, there will be no flow of water from the provider to the MVR and the receiver. The factor option was used to calculate the flow rate through the receiver.

This factor has been specified by using the formula:

$$Q_R = \beta . Q_p \qquad [10]$$

where:

Q_R	The flow rate to the receiver	[m^3.day^{-1}]
β	Variable that transforms the supplier flow rate to the receiver flow rate	[-]
Q_p	The provider package's available flow rate	[m^3.day^{-1}]

The rejected infiltration (RI^s) and groundwater exfiltration (Exf_{gw}^s) are entirely routed to streams as the MVR factor (beta) having initial value of 1.0 was kept constant during calibration.

3.4.6.4. Drain (DRN) package

The external boundary condition of the system is set with no flow boundary condition in the study area except for the western part (river outlet), which is the drain boundary condition. The external boundary condition is discussed in detail in section 3.3.3.1 and Figure 9. Every model cell inside the outlet area is assigned as a drain cell. The drain (DRN) package allows the system to move water out of the system based on the elevation difference between the head and drain elevation and the conductance of the drain.

This relationship can be represented as follows:

$$Q_{out} = C_d * (h_{aq} - h_d) \quad when \ h_{aq} > h_d \qquad [11]$$

$$Q = 0 \quad if \ h_{aq} \leq h_d \qquad [12]$$

where:

Q_{out}	flow from the aquifer to out of the system	[m^3.day^{-1}]
C_d	Drain conductance	[m^2.day^{-1}]

which can be calculated as

$$C_d = K_d * A \perp / T_d \quad [13]$$

where:

K_d	is the hydraulic conductivity of the drain bed	[m.day^{-1}]
A	is the perpendicular area of the flow = cell width *cell thickness	[m^2]
T_d	is the drain bed thickness	[m]

The drain elevation was assigned as 10 m below the model top. The conductance was set as 20 [m^2.day^{-1}] at the beginning and adjusted later during calibration.

3.5. Water balance zone and components

The system is divided into two primary zones: saturated (groundwater) and unsaturated (vadose zone and surface) zone. Model input will include only effective precipitation, and output will consist of discharge to streams, total evaporation, and lateral groundwater flow *(q_g)*.

The water balance of the catchment can be represented in the following equation:

$$Inflow = outflow \quad [14]$$

Which is the same as:

$$P = ET + q_g + q \quad [15]$$

where:

P	Precipitation
ET	Total evapotranspiration
q	Total stream discharge at the catchment outlet
q_g	Lateral groundwater outflow at drain boundary

The total evapotranspiration in the Zamra catchment can be expressed as:

$$ET = ET_u + ET_g + E_I \quad [16]$$

where:

$ET_u = 0$	Evaporation from the unsaturated zone
ET_g	Evaporation from groundwater
E_I	Canopy interception

The total stream outflow from the Zamra river can be expressed in section 3.4.6.1

The unsaturated zone components and land surface components of the water budget can be expressed as:

$$P_e = RI^S + R_g + ET_u \quad [17]$$

$$P_e = P - E_I \quad [18]$$

where:

P_e	The effective precipitation

RI^s The rejected Infiltration routed to the stream
R_g The gross groundwater recharge

While the groundwater saturated zone for the catchment is expressed as:

$$R_g + q_{sg} = ET_g + q_g + q_{gs} + Exf_{gw}^s \quad [19]$$

where:
Exf_{gw}^s Groundwater exfiltration

Finally, the net groundwater recharge (R_n) is expressed as:

$$R_n = R_g - (ET_g + Exf_{gw}^s) \quad [20]$$

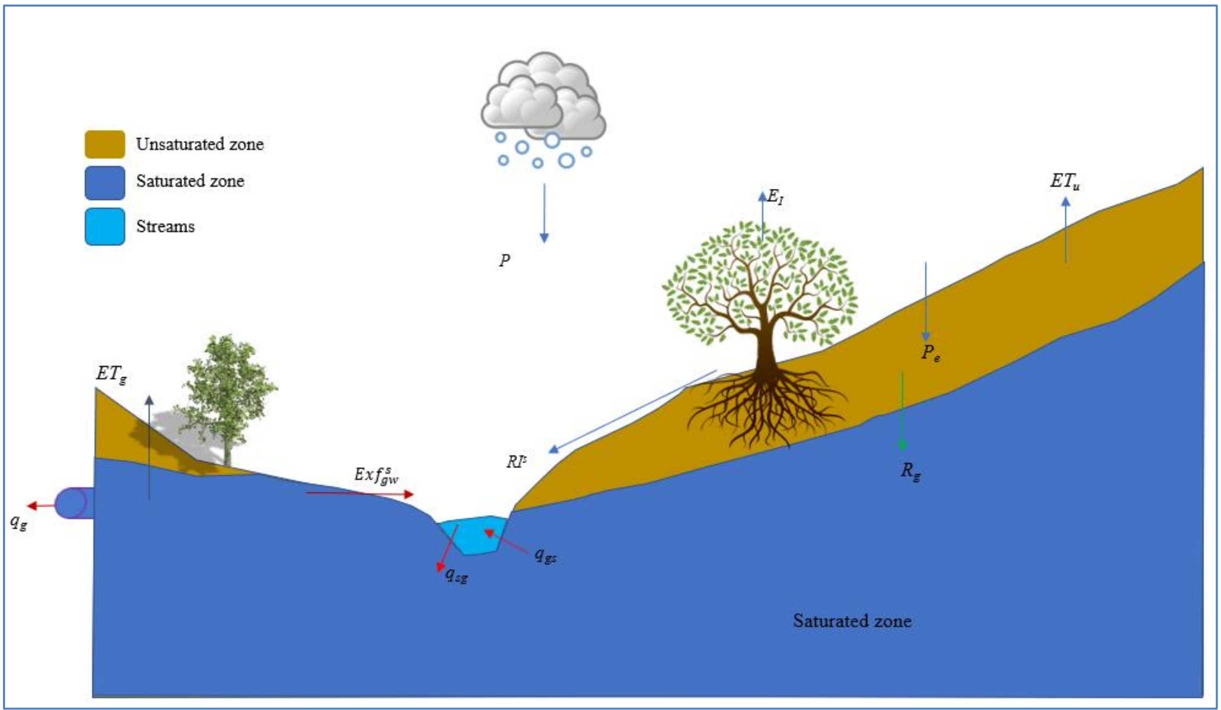

Figure 12: Schematic diagram of hydrological components and zones in Zamra catchment

3.6. State variables

In this study, the state variables are the groundwater observation heads. Only 15 well records have been used for the model as observation heads. There is a river gauge record from the Zamra, but the river flow could not be used during calibration because the data is not representative (the data is recorded only during the rainy season (summer).

3.7. Steady-state model calibration

The model calibration has always been done to find the best much between the observed head value and the simulated head. Model calibration, in general, has the following steps sequentially.

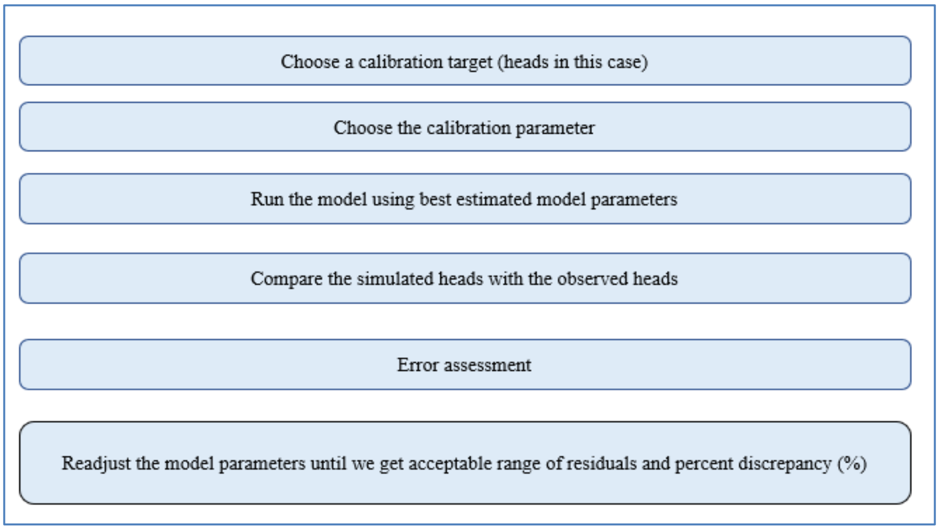

Figure 13: Steps used for steady-state model calibration

In this case, the calibration was done by a trial and error (manual) calibration mechanism. All the parameters in the solver are adjusted based on the acceptable value given in both linear and nonlinear conditions (U.S. Geological Survey, 2018). Obtaining the exact number during model calibration is unachievable due to the availability of uncertainties in every model. The model uncertainty will come from the conceptual model, model parameters, observation data, or from a boundary condition (Anderson et al., 2015). The calibration parameters are the hydraulic conductivity and the parameters used in the SFR, MVR, and UZF packages. However, all the parameters are not equally sensitive to the model, and in most cases, including this model, the hydraulic conductivity (K_V and K_h) are the main ones and susceptible to the model since these parameters have a significant effect on the model simulation. In general, this study selects the following parameters as calibration parameters.

Table 7: Model calibration parameters

Parameter		Dependency	Initial value	Unit	Model package
K_v	Vertical hydraulic conductivity		0.01	[m.day^{-1}]	NPF
K_h	Horizontal hydraulic conductivity		0.1	[m.day^{-1}]	NPF
K_b	Stream bed hydraulic conductivity	$= K_v$	0.01	[m.day^{-1}]	SFR
K_{sat}	Vertical saturated hydraulic conductivity	$= K_v$	0.01	[m.day^{-1}]	UZF
C_d	Drain conductance		20	[m^2.day^{-1}]	DRN
β	MVR factor		1.0	[-]	MVR
θ_{resid}	Residual water content		0.05	[m^3.m^{-3}]	UZF
θ_{sat}	Saturated water content		0.35	[m^3 .m^{-3}]	UZF
θ_i	Initial water content		0.3	[m^3 .m^{-3}]	UZF
θ_{ext}	Extinction water content		0.05	[m^3 .m^{-3}]	UZF
d_{surf}	Surface depression depth		0.25	[m]	UZF
ε	Brooks Corey epsilon		3.5	[-]	UZF

The root mean square error (*RMSE*), the mean error (*ME*), and the mean absolute error (*MAE*) have all been utilized to determine how reliable the calibrated model parameters are. The primary purpose of this statistics summary is to evaluate the accuracy of the head difference between the simulated and observed heads. The difference between the total amount of water entering and leaving the model was considered for the water balance analysis. According to M.P. Anderson et al. (2015), an inaccuracy between -1 and 1% in most groundwater models is acceptable.

$$RMSE = \sqrt{\frac{1}{n}\sum_{i=1}^{n}[H_{obs} - H_s]_i^{\,2}} \qquad [21]$$

$$ME = \frac{1}{n}\sum_{i=1}^{n}[H_{obs} - H_s]_i \qquad [22]$$

$$MAE = \frac{1}{n}\sum_{i=1}^{n}|H_{obs} - H_s|_i \qquad [23]$$

where:

H_{obs}	Observed head	[m]
H_s	Simulated head	[m]
n	Number of heads	[-]
RMSE	Root mean square error	[m]
ME	Mean Error	[m]
MAE	Mean absolute error	[m]

4. RESULT AND DISCUSSION

4.1. Hydrostratigraphic model

According to Hamdi et al. (2018), the three-dimensional hydrostratigraphic model is utilized for two distinct purposes: (1) Determining the geometry of the aquifers in the study area and computing aquifer storage. (2) The 3D hydrostratigraphic model allowed each hydrostratigraphic unit's location, spatial extent, and heterogeneity, especially in a geologically complex environment.

4.1.1. 3D lithological model

The groundwater flow model should be constructed using the most recent lithologic models available rather than presuming that the ground is composed of a homogenous two- or three-layer model. This technique also has the benefit of directly reflecting three-dimensional variability in the model. Complicated geology, containing about nine lithological units found in the study areas represented in Figure 14. The lithologies in the 3D lithological model can show the heterogeneity of the area and be used to estimate the aquifer parameters based on the variety. Lithologic models allow for the visualization of the subsurface in three dimensions. The 3D lithological model highlights the spatial correlations of the lithofacies between the boreholes and indicates the presence of lenses. In addition to demonstrating the complexity of the different rock units that govern groundwater flow and pollution transport, these models must take borehole data into account since the model depends on the interpolation of logs to fill the gap between them. Figure 14 shows the 3D lithological model of the study area with nine lithologies based on the borehole log records and clearly shows the dimension and heterogeneity of the lithologies in the study area.

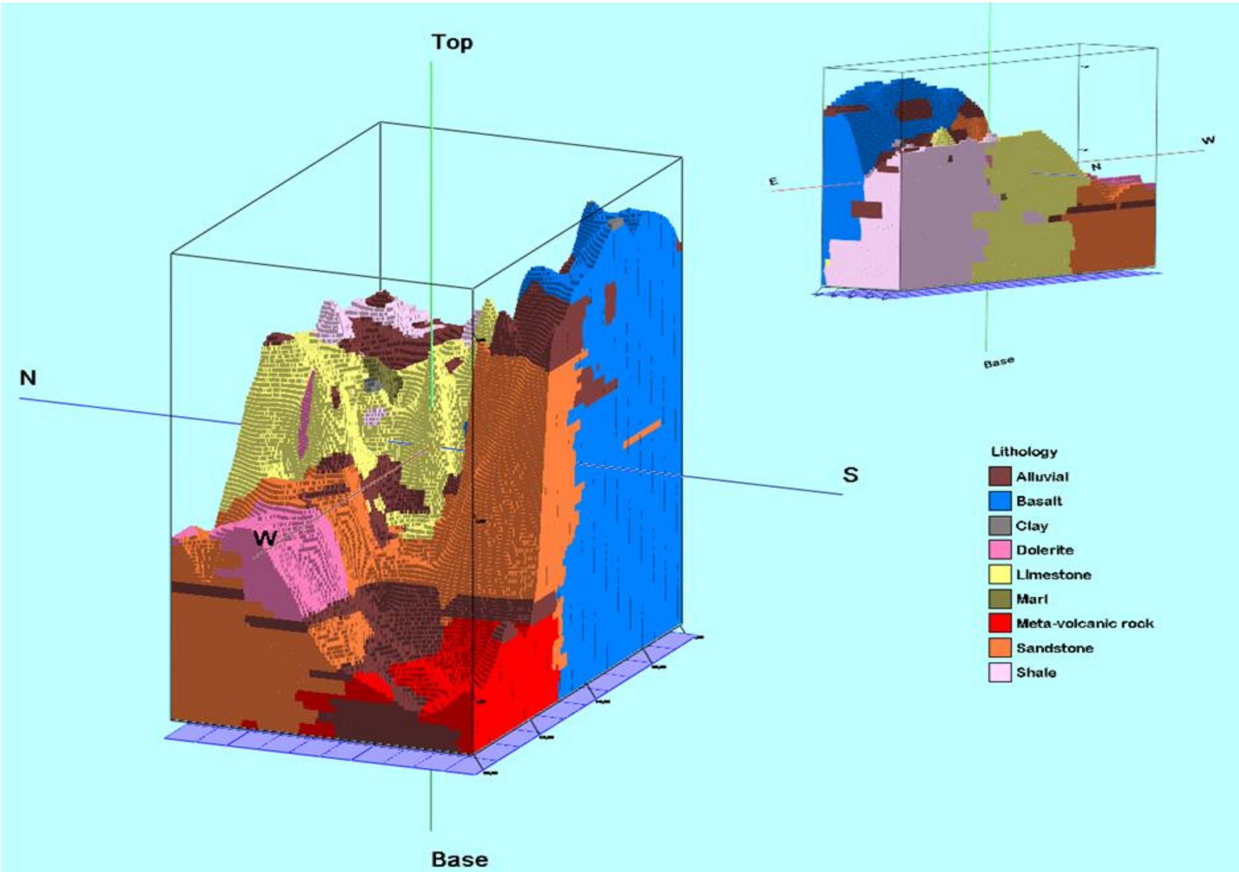

Figure 14: 3D lithological model of ZC

4.1.2. 3D hydrostratigraphic model

The solid 3D hydrostratigraphic model was produced using the kriging griding option of the surface interpolation algorithm, and it is used to illustrate the upper and lower surfaces of stratigraphic layers. The hydrostratigraphic model was done for the flow modeling at the catchment scale. An acceptable 3D hydrogeological model that matched up with the current understanding of the geology of the catchment and the existing borehole recordings was produced as the follow-up of the data preparation and interpolation approach utilized.

This 3D hydrostratigraphic model helps to determine the groundwater flow direction, estimate the groundwater, and surface water interaction, and make arbitrary guesses about the groundwater recharge. Generally, it gives the aquifers architecture. The hydrostratigraphic 3D models help better understand principal aquifers' distribution and connectivity in complicated geological environments. Additional local lithological units can be included within this model without deviating from the current conceptual model if additional data is available. This technique also keeps the conceptual knowledge about aquifers' distribution and connectivity.

Similar to the lithologic model, this model depends on the borehole logs. The software produces the result by interpolating three or more similar facies in different locations near each other. This 3D model was exported as an individual layer to determine each layer's spatial extent and thickness and used as input for the numerical model.

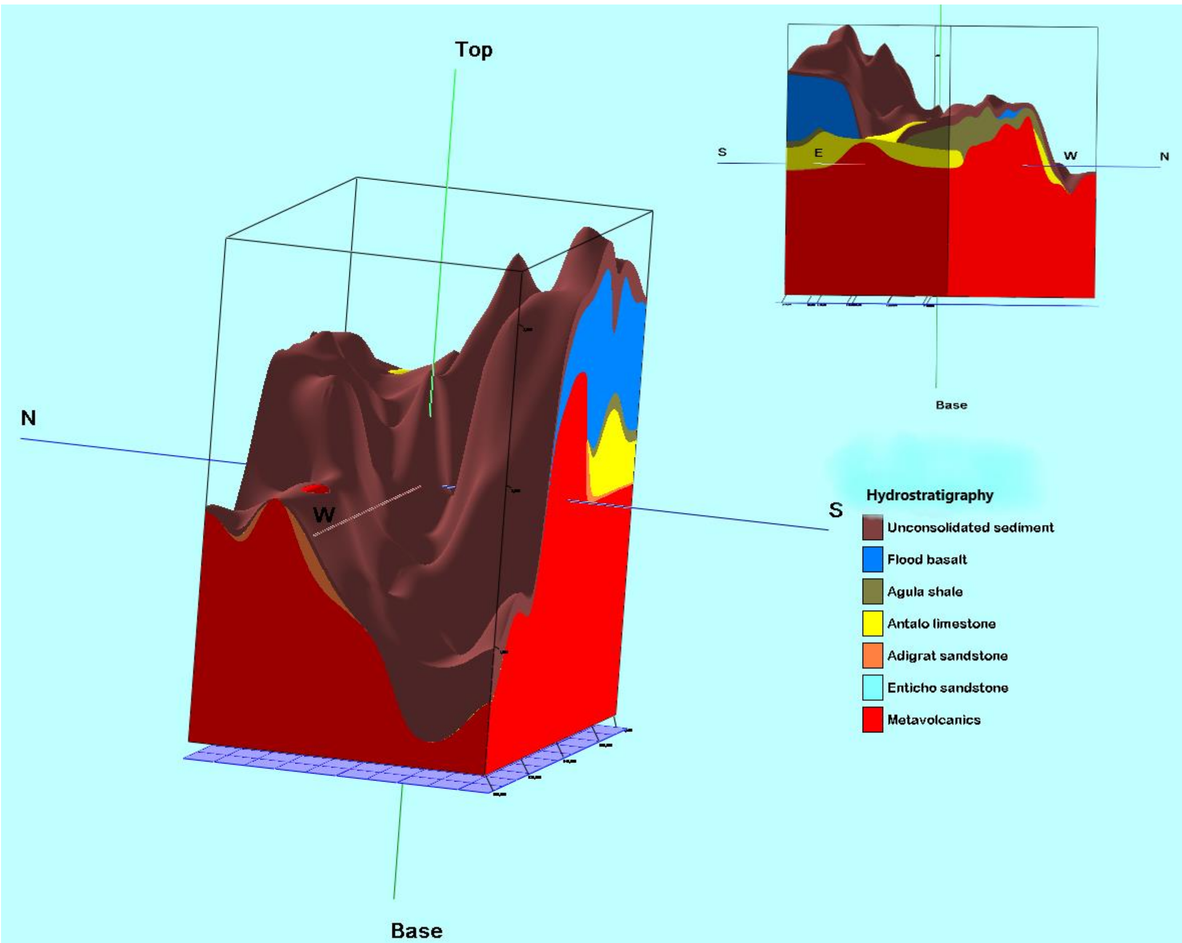

Figure 15: The 3D hydrostratigraphic model

4.1.3. Hydrostratigraphic cross-sections

Hydrostratigraphic cross-sections are presented below in Figure 16 and Figure 17. The hydrostratigraphic units are named based on the stratigraphic naming system given by Sembroni et al. (2017). The cross-section below was done using the cross-section lines in Figure 16A. From the cross-section below, we can adequately visualize the thickness and the correlation of hydrofacieses. In addition to this cross-section below is used to determine the geometry and inter-hydrostratigraphy relationship between the layers.

As indicated on the cross-sections, there are a large up and down on surface elevation that indicates the elevation difference within the catchment. Two cross-sections (D-D' and E-E') from east to west, three cross-sections from north to south (A-A,' B-B,' C-C'), and one cross-section from northeast to the south are presented as indicated in Figure 16A. The stratigraphic variations, geological background, and morphological availabilities (river gorges and grabens) were also considered during tracing cross-section lines.

The cross-sections below show the spatial variability of thickness and the subsurface contacts of each layer. The layers' superposition and complexity are also easily visualized in the cross-sections. All the cross-sections were done applying the vertical exaggeration factor (*VE*) of 30. This means the vertical axis is stretched by a factor of 30.

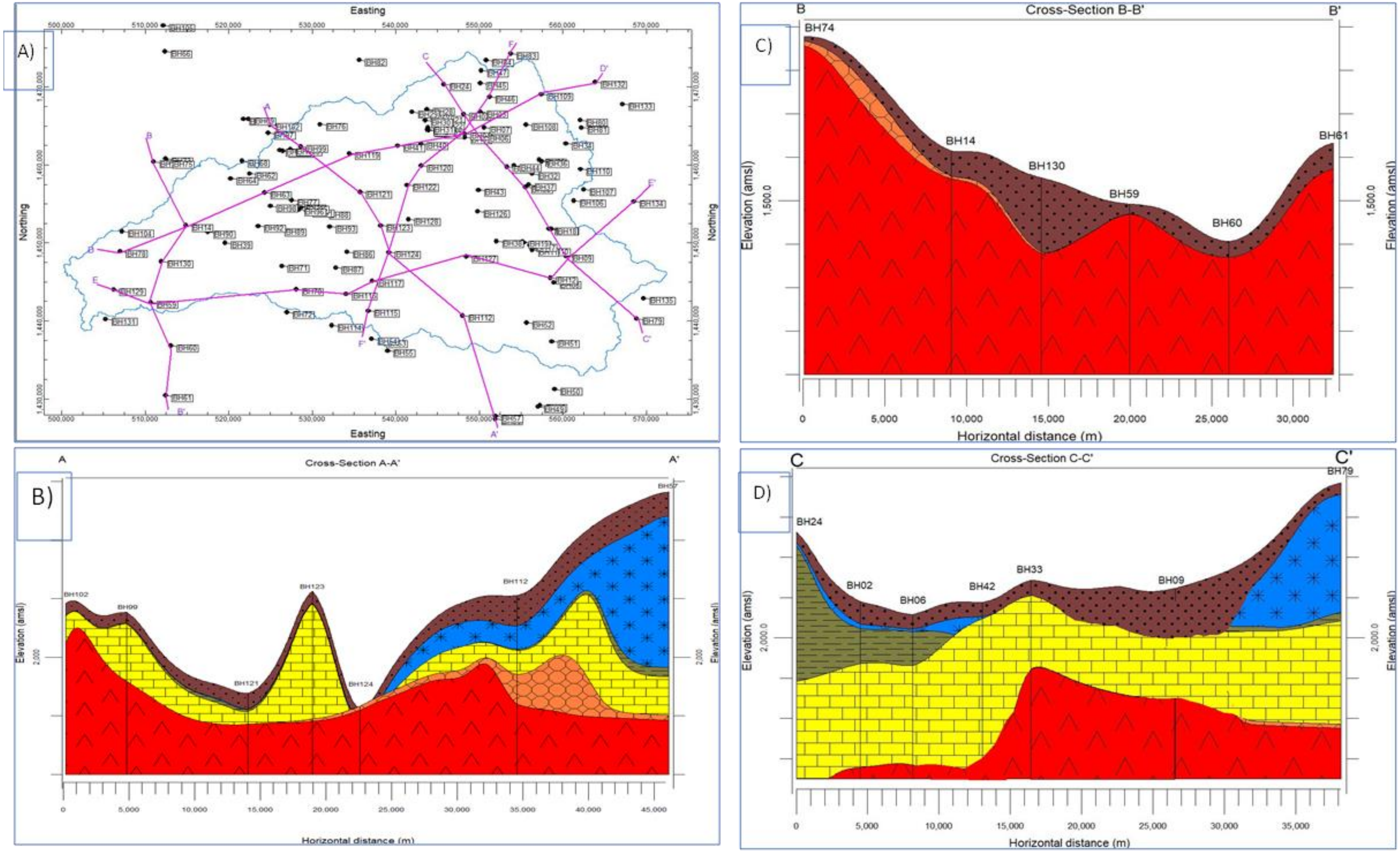

Figure 16: Represents; A) cross-section lines, B), C), and D) represents hydrostratigraphic cross-section through the line A-A', B-B', C-C' in the picture A

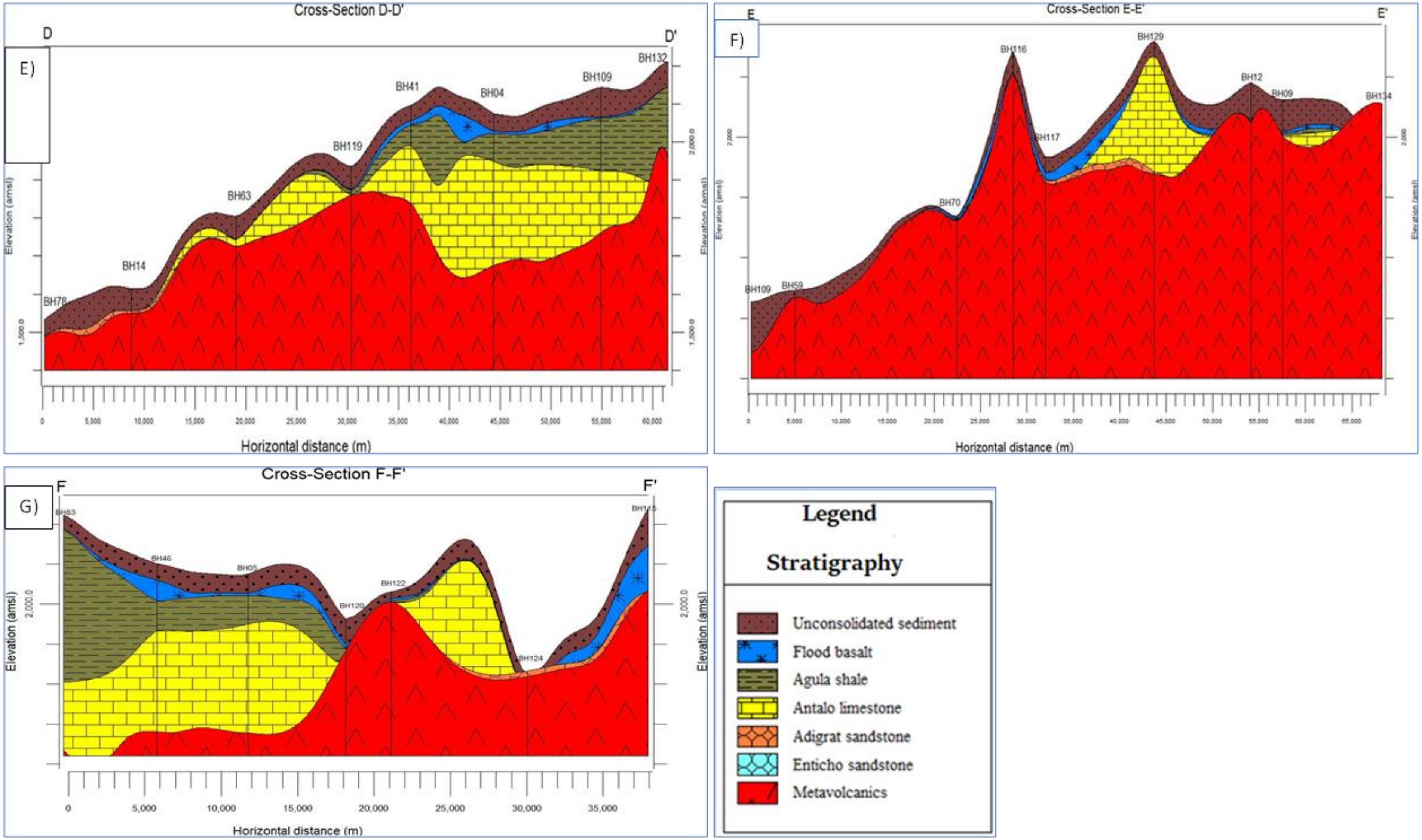

Figure 17: Hydrostratigraphic cross-section through the line E-E’, F-F' AND G-G' in the picture 18A

4.1.4. Thickness and spatial distribution of hydrostratigraphic units

Each layer's thickness and spatial distribution were determined by exporting the rockwork gridded thickness layers (isopach layers) in Esri shapefile format and further processing in the ArcGIS environment.

4.1.4.1. Unconsolidated sediment

The unconsolidated sediment is the product of erosional and weathering processes. It is made of relatively uniform sandy material that varies in thickness, color, content, and particle size. Mainly characterized by loss and poorly sorted with various colors in different areas. This layer has been removed in some areas susceptible to erosion, and the geology beneath has been exposed, as indicated in the thickness map in Figure 18. This layer has a valuable effect on groundwater recharge (percolation and infiltration) and evaporation simultaneously. The probability of groundwater recharge increases as the beds become thinner and the same as ET from both saturated and unsaturated zone. It is also a very productive aquifer in areas with enough thickness, especially in the graben of mountains and around the outlets of the river. In ZC, it covers a large area with a thickness ranging from 0-27 m.

4.1.4.2. Flood basalt

The flood basalt formed in the tertiary period and included the trap series and Mekelle dolerite. It is a succession of Late Eocene and Oligocene rift basalts. In the study area, it covers a small part of the catchment with thicknesses ranging from 0 m to 69 m. It is exposed on the surface in the southeast part of the study area.

4.1.4.3. Agulae shale

Agulae shale is evidence of the Jurassic sea's retreat from northern Ethiopia. It is exposed on the top of the Antalo limestone. From bottom to top, it is made up of well-sorted, laminated black shales and mudstones; cross-bedded fine quartz arenites (tidal bars), dolomites, gypsum beds, and oolitic limestones. It is exposed on the surface in the northern part of the study area. It has a thickness range of 0–76 m in ZC. In some areas of ZC, it is exposed intercalated with marl and limestone. It is a less productive aquifer as compared to limestone and sandstone units.

4.1.4.4. Antalo limestone

The Antalo limestone is a sedimentary deposit that dates back to the Mesozoic era. There are four distinct facies found within the Antalo limestone. These types of rock are known as facies and include the following: (1) a sandy oolite limestone with a few marls, a few chert layers, and coral, gastropod, and echinoid fauna; (2) marls and limestones interbedded with brachiopod, algal, and chert beds; (3) reef limestones with marls and stromatolites mixed; and (4) marls and black to grey microcrystalline limestones mixed in. Its thickness in ZC reaches 76 meters, and it is visible on the surface in the region that is central to the area under investigation. In certain parts of the study areas, this layer of limestone is sandwiched between shale and marl at various points. It is considered to be one of the more fruitful aquifers in ZC.

4.1.4.5. Adigrat sandstone

Friable, medium- to coarse-grained, cross-bedded white quartz sandstones make up Adigrat sandstone. It also contains well-distributed ferruginous silt lenses that exhibit turbidity structures. Sembroni et al. (2017) and Beyth (1972) interpret the sandstones as lacustrine-deltaic, estuarine, or continental deposits. It exposes the surface around the central parts of the study area. It relatively covers a large area next to unconsolidated sediment and Antalo limestone. The Adigrat sandstone has a thickness that reaches up to 49 m in this catchment. It is one of the most productive aquifers in the study area.

4.1.4.6. Enticho sandstone

The Enticho sandstone consists of eolian quartz arenites and lies unconformably overlying on Neo-Proterozoic basement rocks. Locally the Enticho sandstone is mixed and intercalated in some areas with the Edaga Arbi glacials; the formation has nearly the same age but different depositional processes. The Enticho sandstone has a relatively small spatial coverage and up to 45 m thickness around the central part of ZC. Similar to the Adigrat sandstone, it is a productive aquifer even though it covers only a tiny area.

4.1.4.7. Metavolcanics

The Metavolcanic rock is Precambrian and the oldest age-wise than those listed above. Metavolcanic rock is one of the northern East African Orogen's low-grade metamorphosed rocks (Sembroni et al., 2017). In the Zamra catchment, it is mainly exposed in the eastern part, and the thickness is spatially variable from 0 up to 45.5 m. but in the regional case, the thickness will go very deep beneath since the borehole records are very shallow in our study area. It is a very low-productive aquifer, and sometimes it serves as an aquitard.

4.1.4.8. Basement rock

The basement rock is Precambrian and the oldest age-wise. Basement rock is a transition zone between the southeast African Orogen's high-grade metamorphosed and deformed rocks and the northern East African Orogen's low-grade metamorphosed rocks (Sembroni et al., 2017). It is mainly characterized by the deformation process, plutonic activities, and metamorphism. It has regional coverage with very high thickness beneath the above layers. This basement rock includes different lithologies varying in the degree of metamorphism and its protolith. Basement rock in northern Ethiopia includes low grade (metasediments) and high grade (schist and gneisses) metamorphic rocks.

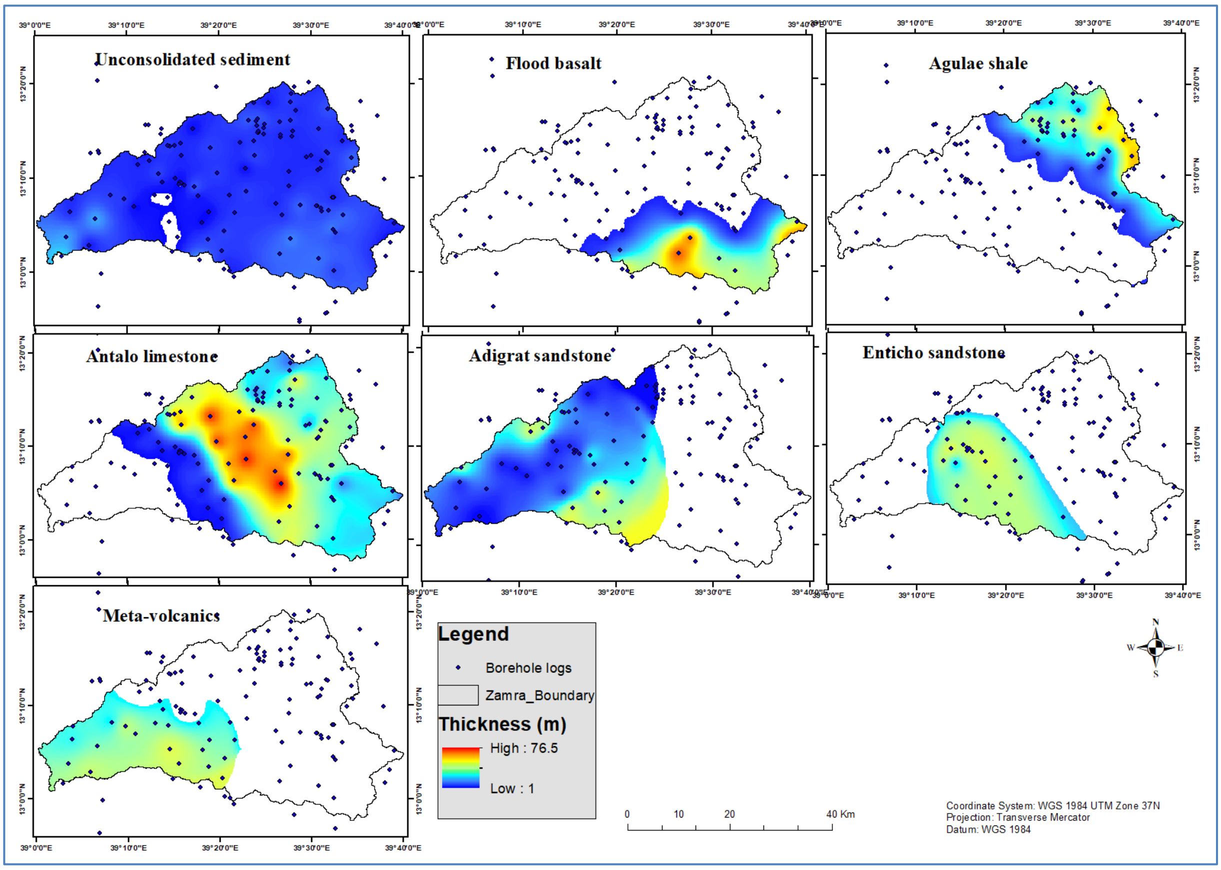

Figure 18: Spatial thickness distribution of hydrostratigraphic units at ZC

To have an adequate understanding of the occurrence and flow pattern of groundwater, a hydrogeological conceptual model is required. The building of conceptual models was based on the available geological and hydrological data, which are the borehole log data, water level data, and geological interpretation. The strata of the area are not continuously covered, and in some areas, the layers are fragile. As indicated in Figure 19, the unconsolidated sediment covers a large area of Zamra, but the thickness is shallow in most of the exposure. The Agulae shale and flood basalt cover a small amount. In the conceptual model below, the thickness of the layers is taken from one section of the 3D stratigraphic model that can show almost all stratigraphic units, and it is not to scale. The flow direction and aquifer system gradient information were taken from the head contour map determined by interpolating the hydraulic heads.

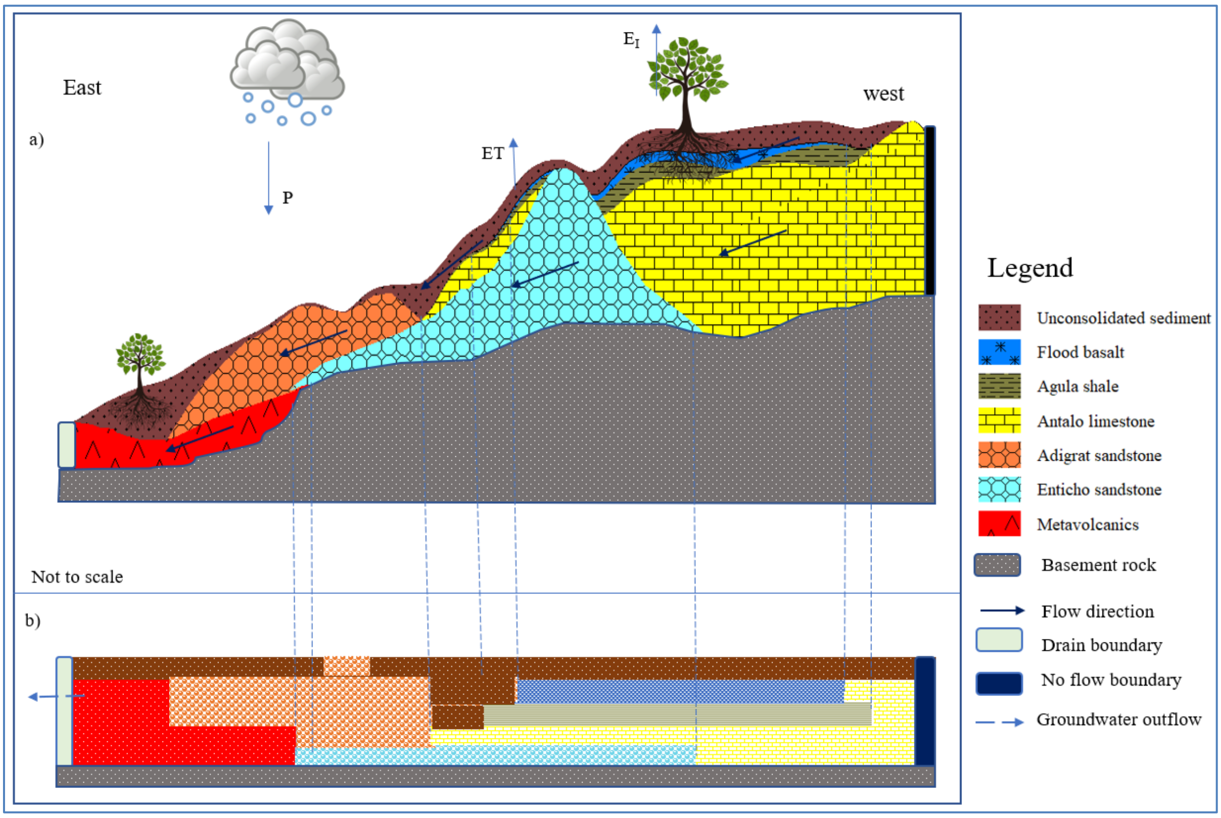

Figure 19: Schematic diagram of; a) hydrogeological conceptual model of the Zamra catchment, b) Schematic conversion of conceptual to the numerical model.

4.2. Interpolated hydraulic heads

The groundwater level in the Zamra catchment has been highly affected by the complex geology and morphology. The groundwater level in ZC shows a subdued replica of the surface morphology (follows a similar trend with the surface elevation). Like ground surface elevation, the groundwater heads are high in the eastern part and decrease in the western region.

In the Zamra catchment, the spatial distribution of initial hydraulic head fields observed is inconsistent due to the complex morphology. Even though there are sufficient static water level records, determining the groundwater heads was difficult in the Zamra catchment because the data set is usually scant regarding the geographical relief (lack of recorded data in the high relief parts). The static water level depth is shallow. There is also surface water (Zamra river) considered in my modeling system and has a direct leakage into the groundwater.

The result below shows groundwater heads, distribution, and movement in ZC. It is vital to know ZC groundwater potential to regularly track changes in static water heads for time series analysis. The groundwater heads at the river discharge area are very low relative to the western part of the catchment, as indicated in Figure 20. Similar to the surface elevation, there is also an extensive range of water level differences. Groundwater flow directions were deduced from the potentiometric-surface map. Typically, the higher hydraulic head coincides with the high surface elevation areas and the lower groundwater heads with lower surface elevations in the unconfined aquifer of ZC. The contour interval of 200 m contours the groundwater heads. As indicated in Figure 20, the general flow direction is from east to west. This interpolation result below shows only a single event record.

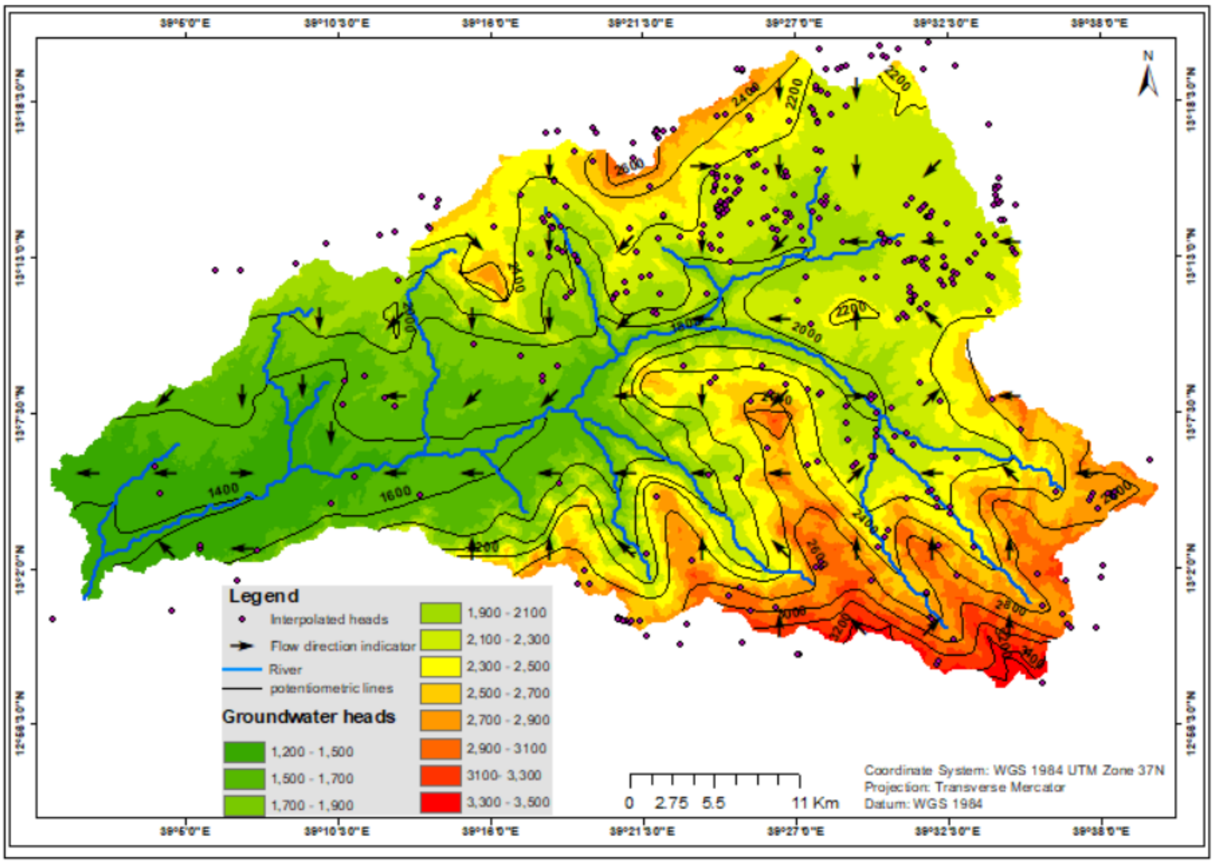

Figure 20: Interpolated by regression kriging groundwater heads [m].

4.3. Driving forces

The driving forces contain three components, as discussed in section 3.4.4. The average daily E_I is calculated using the method discussed in section 3.4.4.3 and then converted on yearly bases. To get this interception pixel base interception rate was used as shown below in the figure Figure 21. Using this interception rate and precipitation the interception of spatial distribution of ZC has been determined. As indicated in Figure 22, the annual mean interception of ZC ranges from 0 to 150 mm year^{-1}. The interception has a similar rainfall pattern since its calculation also depends on p.

Figure 23 shows the annual average *PET* spatial distribution (Gebremedhin et al., 2022). It is used for the model input, and as shown in Figure 24, it ranges from 410 to 1800 mm per year. The value of *PET* depends on the landcover types and altitude, and large values are observed in the low elevated areas. Low *PET* values are observed in the mountainous outcrop areas (high elevated).

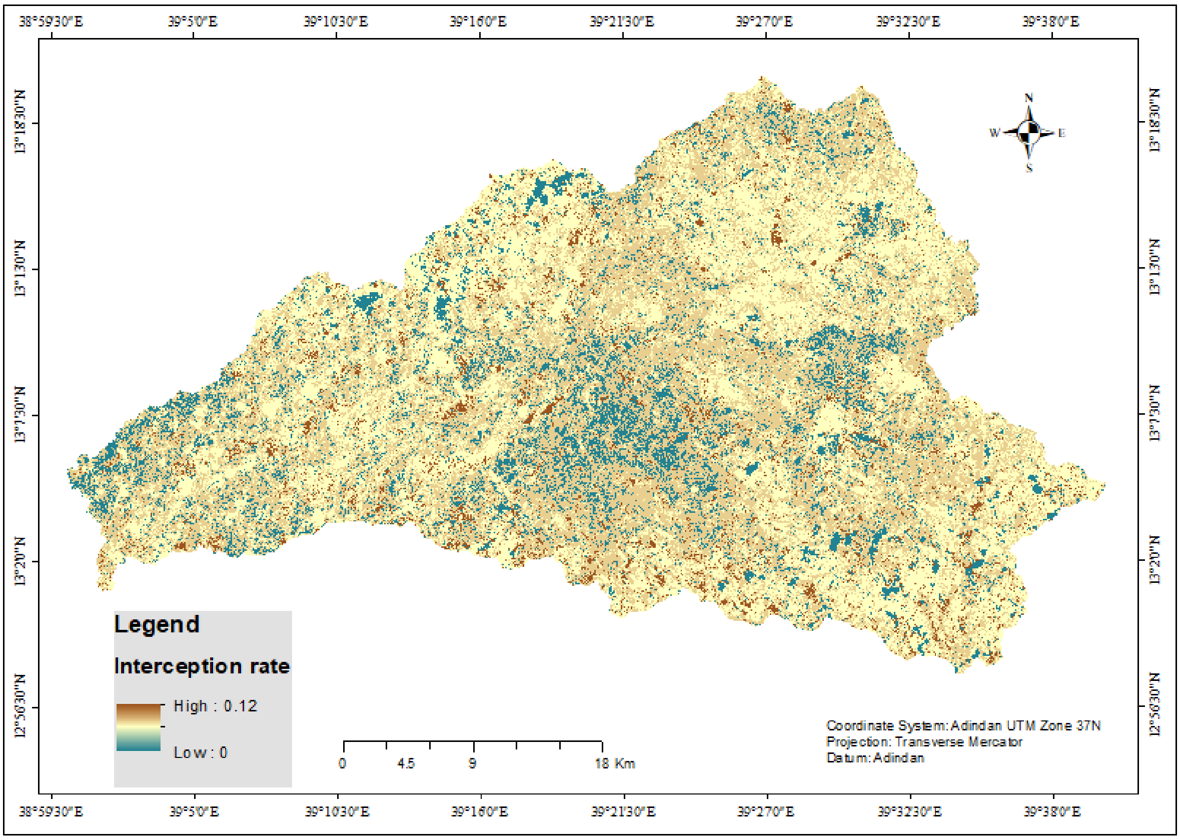

Figure 21: Pixel based interception rates of each land cover classes

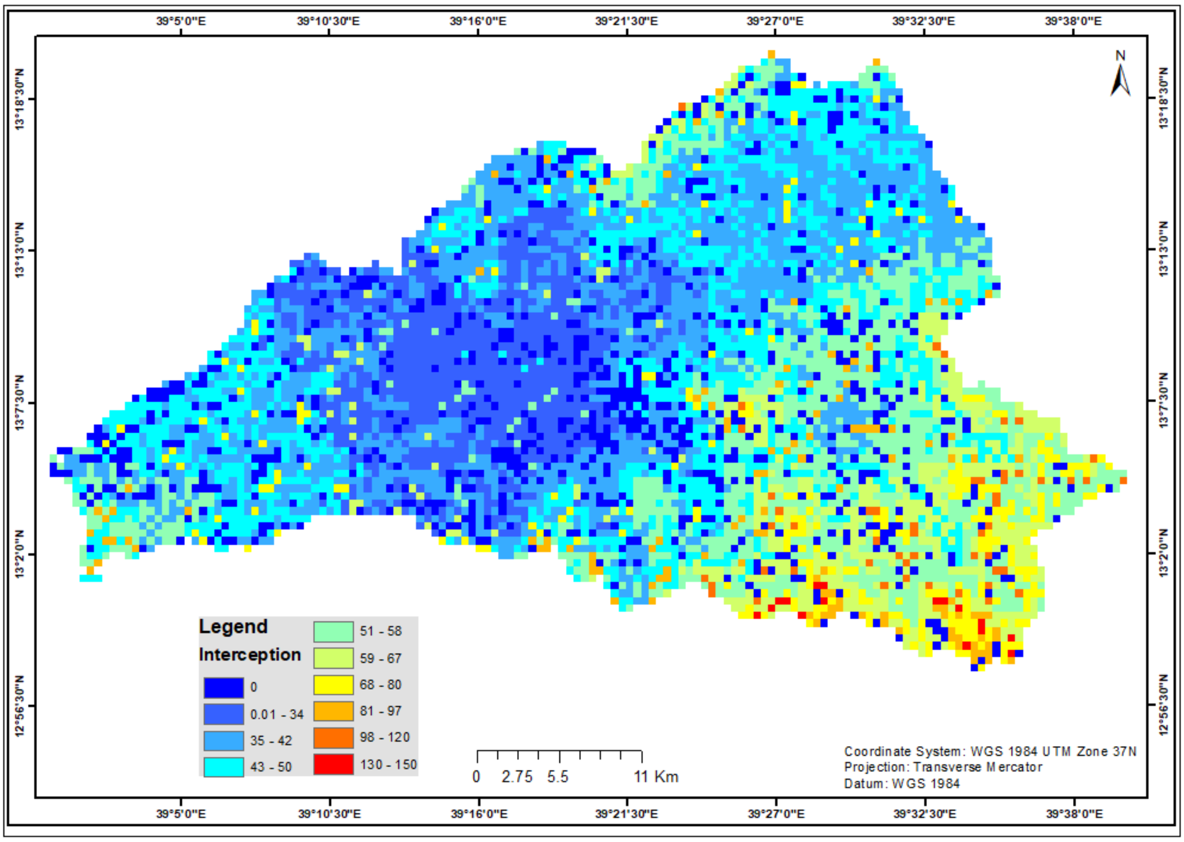

Figure 22: Spatial distribution of interception presented with 500 x 500 [m] model grid [mm. year $^{-1}$].

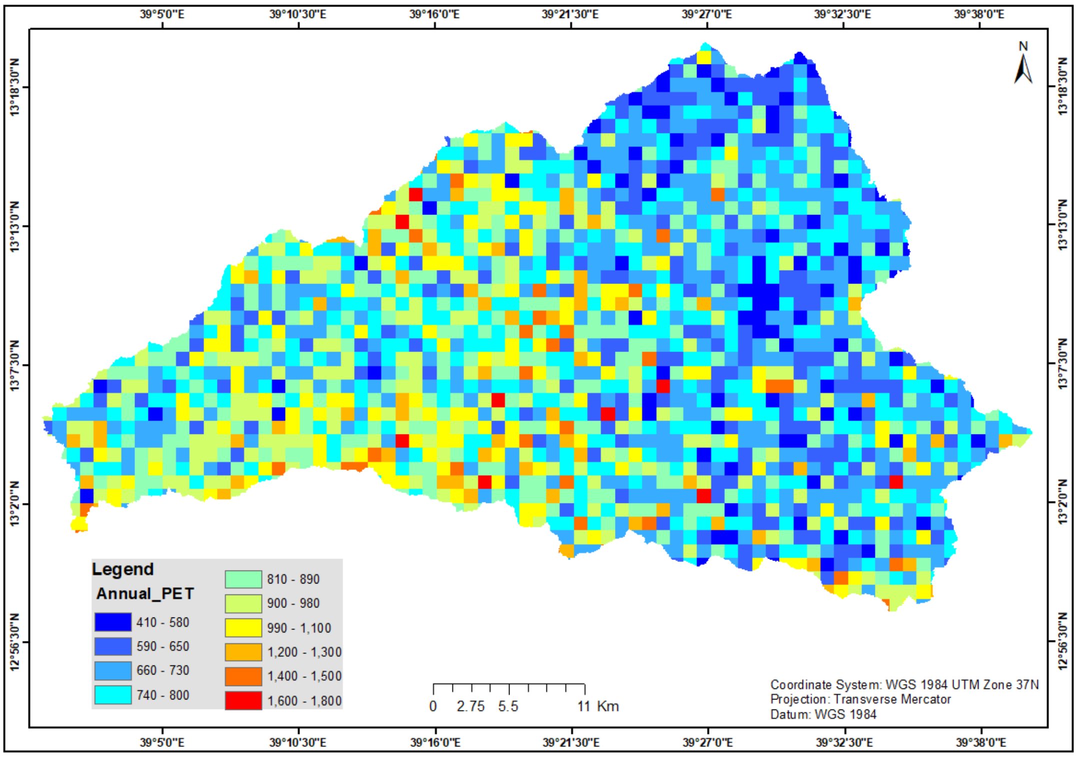

Figure 23: Spatial distribution of *PET* presented with 500 x 500 [m] model grid [mm. year $^{-1}$].

Figure 24 shows the spatial distribution of annual average rainfall in ZC (Gebremedhin et al., 2021). It is used for the model input, and as shown in Figure 24, the value ranges from 390 to 1300 mm year $^{-1}$. The southeastern catchment receives a large *P* per annum, while the central part receives the minimum value. This is due to the altitude difference similar to the *PET*.

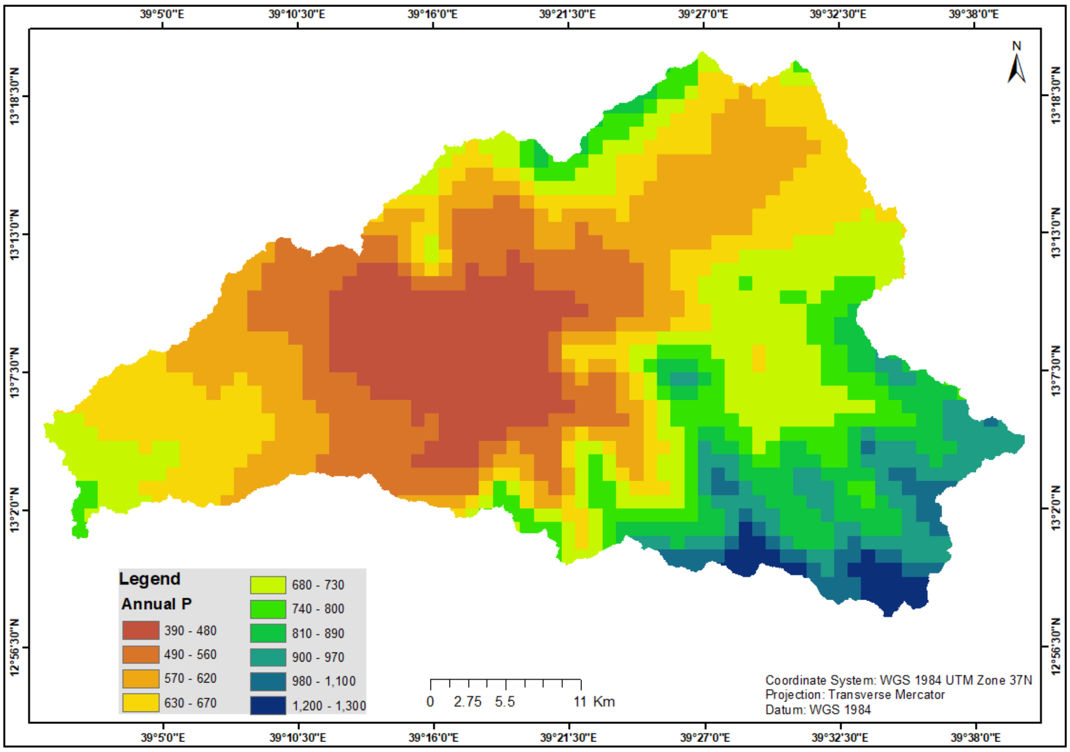

Figure 24: Spatial distribution of *P* presented with 500 x 500 [m] model grid [mm. year $^{-1}$].

4.4. Steady-state model calibration

This was addressed in the following parts. Namely: (1) calibrated parameters, 2) calibration error assessment (3) spatial variability of head and fluxes, (4) water budget, and (5) sensitivity analysis.

4.4.1. Calibrated parameters

Several parameters were involved during model calibration. Some show the model's spatial variation, while others are constant over the entire model after adjustment. As indicated in Table 8, most parameters have been adjusted for each layer or the whole layer and have a different range of values.

Table 8: Calibrated parameters

Parameter		Initial value	Calibrated value	Unit	Model package
K_v	Vertical hydraulic conductivity	0.01	0.001-4.8	[m.day^{-1}]	NPF
Kh	Horizontal hydraulic conductivity	0.1	0.01- 58	[m.day^{-1}]	NPF
K_b	Stream bed hydraulic conductivity	0.01	5 - 10	[m.day^{-1}]	SFR
K_{sat}	Vertical saturated hydraulic conductivity	0.01	0.015	[m.day^{-1}]	UZF
C_d	Drain conductance	20	260	[m^2·day^{-1}]	DRN
β	MVR factor	1.0	1.0	[-]	MVR
θ_{resid}	Residual water content	0.05	0.05	[m^3·m-3]	UZF
θ_{sat}	Saturated water content	0.35	0.45	[m^3 ·m^{-3}]	UZF
θ_i	Initial water content	0.3	0.15	[m^3 .m^{-3}]	UZF
θ_{ext}	Extinction water content	0.05	0.05	[m^3 .m^{-3}]	UZF
ε	Brooks Corley epsilon	3.5	3.5	[-]	UZF
d_{surf}	Surface depression depth	0.25	0.125	[m]	UZF

Low K_h and K_v values for the flood basalt and metavolcanic relative to other aquifers are expected from aquifers within hard rocks. The unconsolidated sediment and the sandstone have relatively high conductivity values. The flood basalt aquifer has a horizontal hydraulic conductivity ranging from 0.018 to 0.12 m/ day, and the metavolcanic aquifer has a K_h value ranging from 0.001 to 0.8 m/day. The values of K_h range from 0.01 - 58 m/day, and K_V ranges from 0.001 – 4.8 m/day. The hydraulic conductivity zones of K_h and K_v for each layer are presented in Figure 25 and Figure 26, respectively.

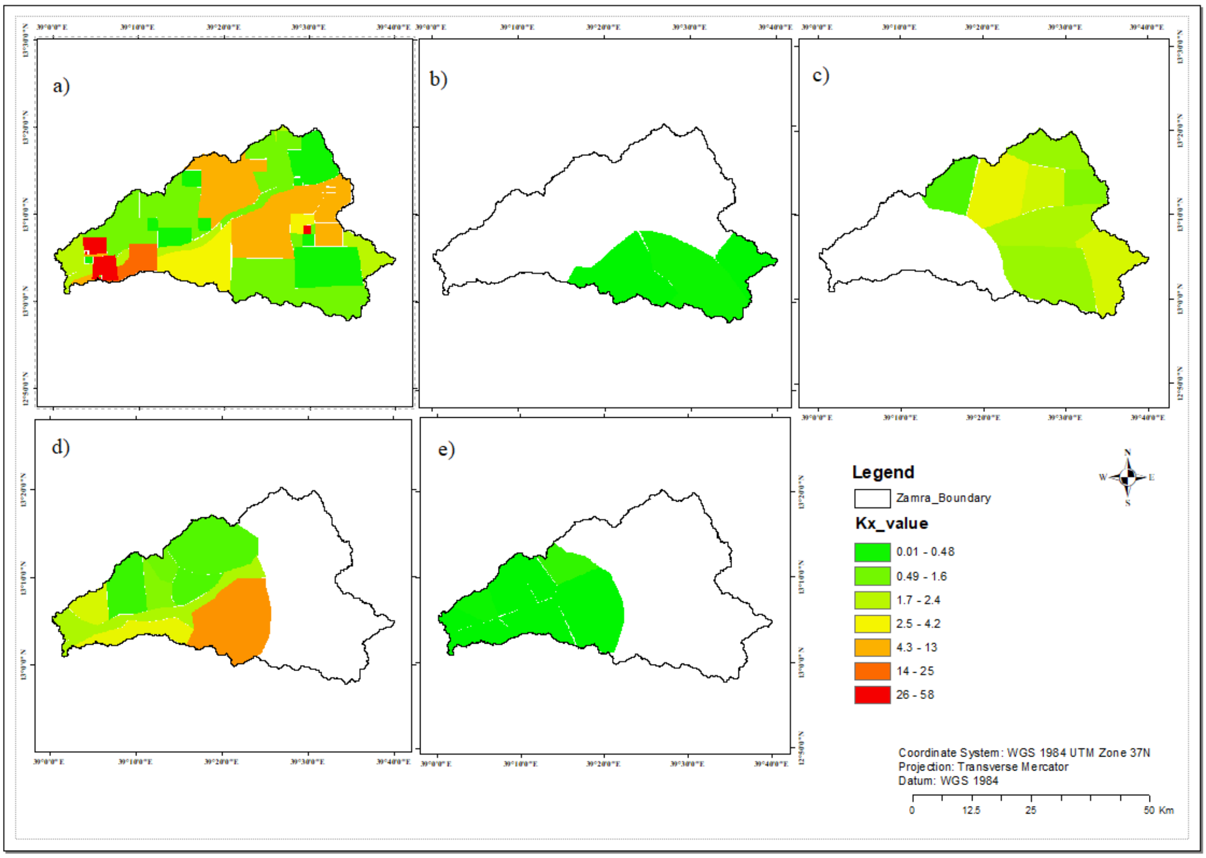

Figure 25: Spatial distribution of *Kh* per each layer

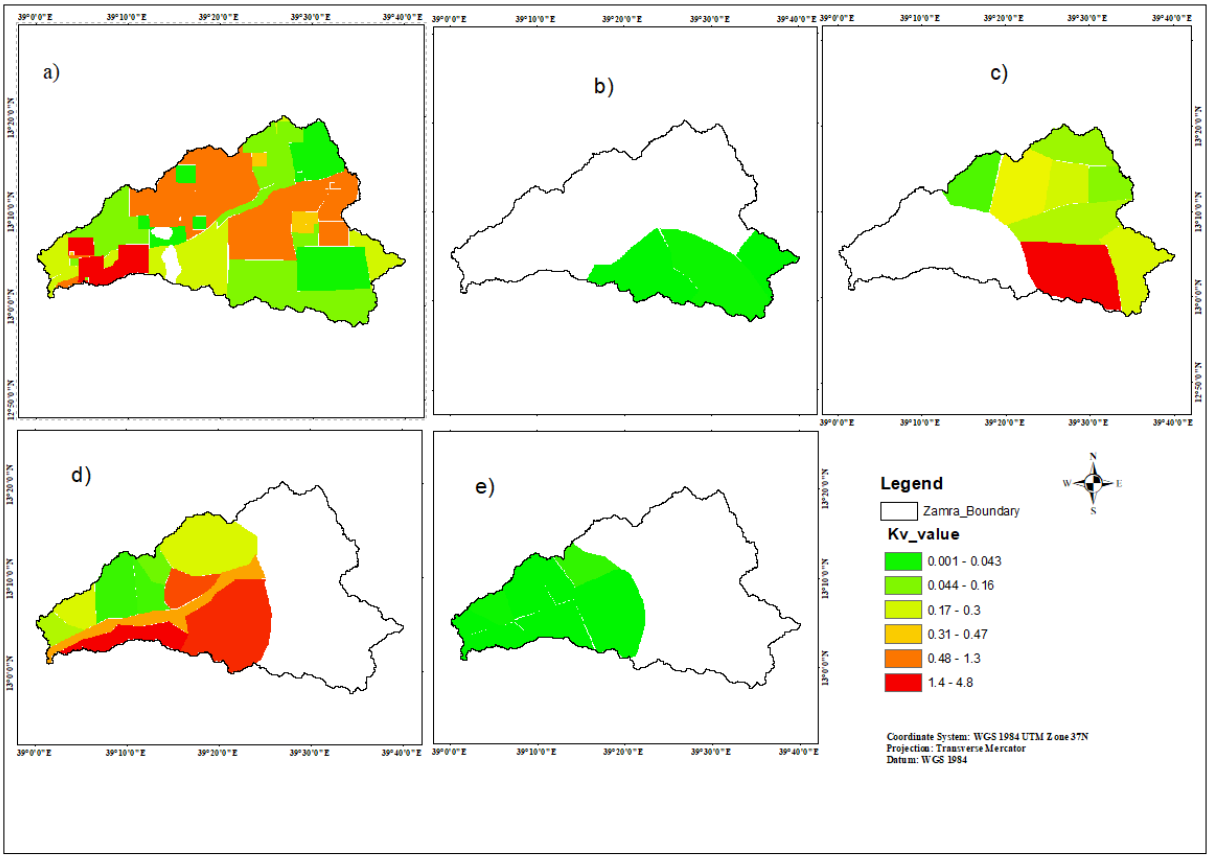

Figure 26: Spatial distribution of *Kv* per each layer

4.4.2. Calibration error assessment

It took some adjusting of the allocated hydraulic conductivity until the simulated head and observed heads matched. The mean absolute error (*MAE*), the mean error (*ME*), and the root mean square error (*RMSE)* were all computed to show the match between the observed and simulated heads. The values of these object functions are 0.19, -0.09, and 0.26, respectively, as indicated in Table 9. The simulated head varies from 1464.42 m to 2491.14 m, as shown in the table below. However, in the whole study area, the water table goes above this in the elevated areas (eastern part), and it goes below it in some areas in the western part of the catchment.

Table 9: Error assessment of heads after a steady-state calibration

Name	X	Y	Obs_heads (m)	Simulated heads (m)	Cell altitude applied [m.a.s.l]	Residual
Obs1	522905.8	1459595	1974.81	1974.56	1975	0.2466
Obs2	532340	1453323	1746.62	1746.55	1749	0.0685
Obs3	557371.2	1439242	2449.08	2449.35	2454	-0.2723
Obs4	558637	1460563	2116.22	2116.37	2118	-0.1513
Obs5	543572.1	1465831	2136.23	2136.19	2146	0.0403
Obs6	550137.5	1472256	2160.35	2160.36	2169	-0.0055
Obs7	529123.7	1463077	2227.40	2227.63	2230	-0.2287
Obs8	551897.9	1462134	2036.70	2036.44	2042	0.2581
Obs9	520765	1453392	1630.00	1630.60	1635	-0.5982
Obs10	507426	1445666	1474.00	1474.43	1485	-0.4298
Obs11	519400	1453048	1557.00	1556.99	1579	0.0094
Obs12	510051	1442073	1466.00	1465.97	1480	0.0315
Obs13	510029	1442272	1464.00	1464.42	1479	-0.4179
Obs14	568082.1	1445448	2491.12	2491.14	2495	-0.0168
Obs15	553780	1452096	1976.06	1975.92	1988	0.1446
				RMSE	0.26	
				ME	-0.09	
				MAE	0.19	

To show the performance and the correlation between the observed and simulated heads, the scatter plot of both heads was done as indicated in the graph below Figure 27. This shows the random distribution of points and the correlation between the simulated and observed heads. As indicated in the figure, the regression coefficient (R^2) is 1, reflecting the good model performance and match between the simulated and observed heads.

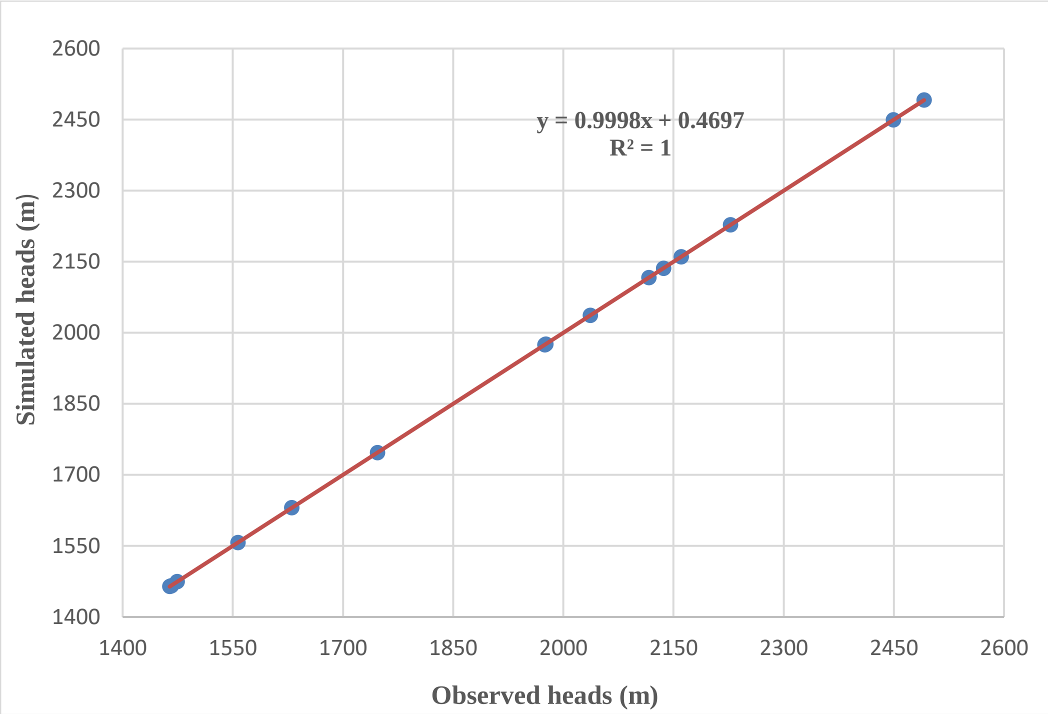

Figure 27: Scatter plots of observed and simulated heads after calibration.

4.4.3. Spatial variability of groundwater head and fluxes

The spatial variability of fluxes and heads was extracted from the steady-state model output only for a single hydrological year. The spatial variability of gross recharge depends on the amount of precipitation and property of the layers. In contrast, the spatial variability of Groundwater evapotranspiration is dependent on the spatial variability of the crop coefficient (K_c) and extinction depth.

Figure 28 indicates the gross groundwater recharge in the model. Groundwater evapotranspiration demand and the amount of water exfiltrated to the surface are subtracted from the groundwater recharge to get the net recharge [20]. The groundwater evapotranspiration occurs if the groundwater level is above the extinction depth determined in the model before simulation. The groundwater recharge is spatially distributed similarly to the mean precipitation used as an input to the model, except for some cells with shallow groundwater recharge and around refined grid cells. Because of the presence of streams and a groundwater table near the surface, the cells may be fully saturated, resulting in low recharge values. The saturated cells' infiltration rate (rejected infiltration, RI^s) was sent to the stream via an MVR package in the form of surface runoff with a total amount of 101.38 mm year^{-1}.

The R_g of the ZC varies from 0 mm year^{-1} to 889.5 mm year^{-1}. Generally, the catchment has a high R_g as compared to the P. The eastern parts of the catchment have high Rg relative to other regions of ZC.

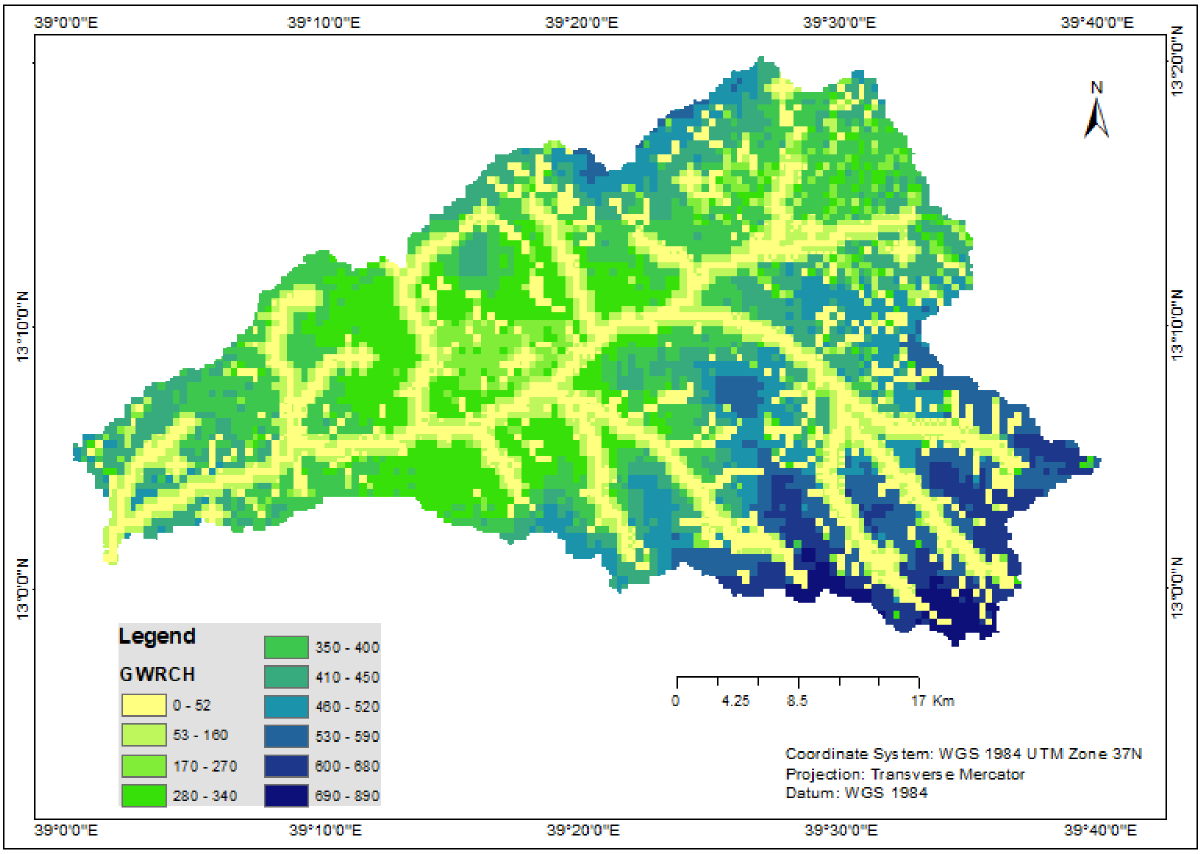

Figure 28: Gross groundwater recharge R_g after steady-state model calibration [mm. year^{-1}].

Figure 29 displays the groundwater evapotranspiration map. As shown on the map, most cells have zero value. This indicates that evapotranspiration does not take groundwater from those cells. In this investigation, the value of groundwater evapotranspiration varies from 0 to -790 mm year^{1}. The spatial variability of ET_g is due to spatial variable K_C and extinction depth.

Due to the absence of *ETu* in the steady state model simulation, the subsurface evapotranspiration (*ETss*) is represented by *ETg* (Niswonger et al., 2006). The negative indication shows that the water has been removed from the system. The groundwater evapotranspiration takes place from the groundwater above the extinction depth. If the groundwater level is below the extinction depth, there is no *ET*.

Figure 28 shows the spatial distribution of Exf_{gw}^{s}. It shows peak value in some cells at the flat area of the catchment. This is due to a shallow water table around those cells (possibly springs). The value ranges from 0 up to -813 mm year^{1}. But these large negative values are only observed in a few cells, as shown in the image below.

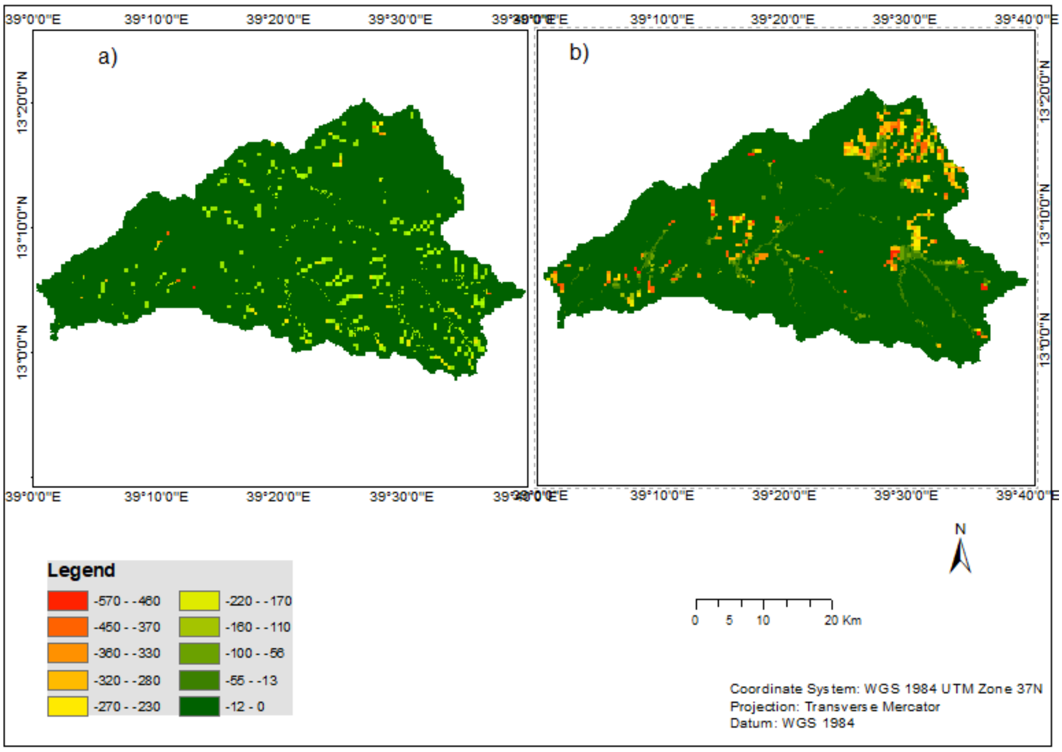

Figure 29: Spatial distribution of groundwater zone fluxes [mm. year^{-1}]: (a) ET_g, (b) Exf_{gw}^s

Figure 30 shows the net groundwater recharge can be calculated by subtracting the sum of ET_g, and Exf_{gw}^s from the R_g. Therefore, these three fluxes affect the spatial distribution of this net recharge. R_n has a negative value in the discharge area of the catchment (where Exf_{gw}^s and ET_g are very high relatively) and positive in recharge areas(those two components are relatively low).

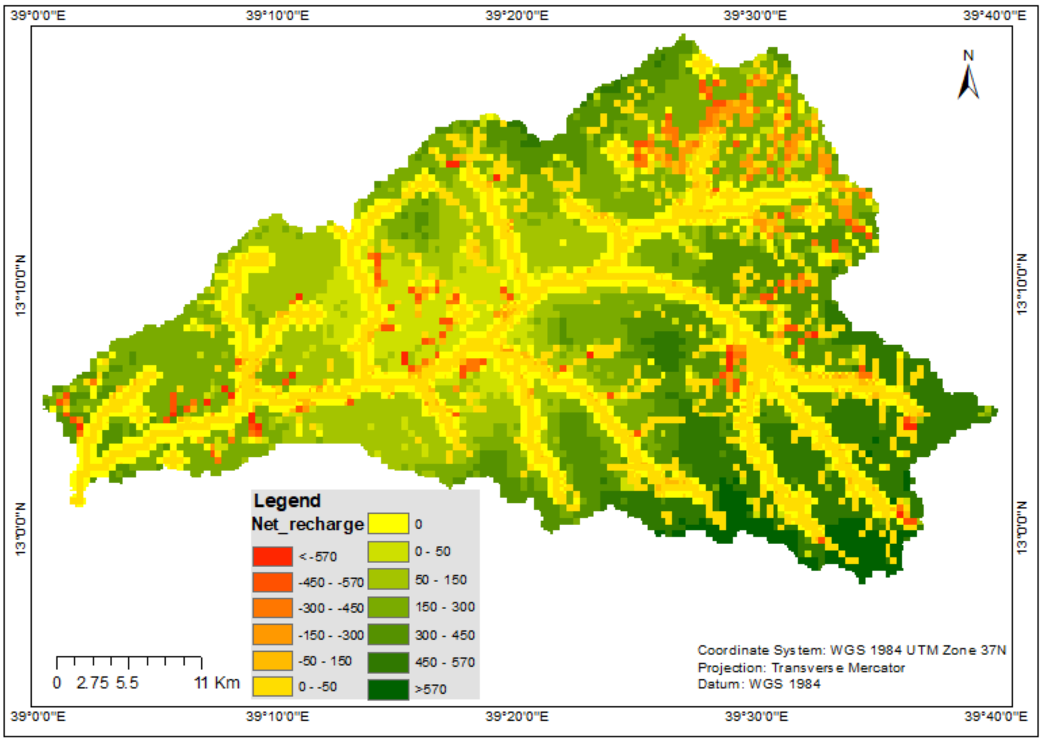

Figure 30: Spatial distribution of groundwater net recharge [mm. yr-1]

Figure 31 shows the groundwater level and potentiometric lines after the steady-state calibration of the model. This groundwater level trend has an almost similar pattern to the interpolated groundwater level in section 4.2. Even though they have similar trends, there is some head difference between the simulated and interpolated in some areas. This will be due to the following reasons.

1) Due to the lack of hydraulic head records in the mountainous areas of the catchment.
2) Due to the characteristics of the aquifers, especially on the second layer and fifth layer and in areas with thin coverage of the first layer have very low permeability, even though they are considered an aquifer in this investigation.
3) The main reason is that kriging does not consider any hydrological properties, while the steady-state model considers many hydrological properties and parameters.

Like the interpolated groundwater level, the higher groundwater level coincides with the high surface elevation areas and the lower water level areas with lower surface elevations in the unconfined aquifer of ZC after a steady-state model calibration. Similar to the surface elevation, highlands define the study area in the east and decline in the west, where the outlet of the rivers is assigned in the drain package.

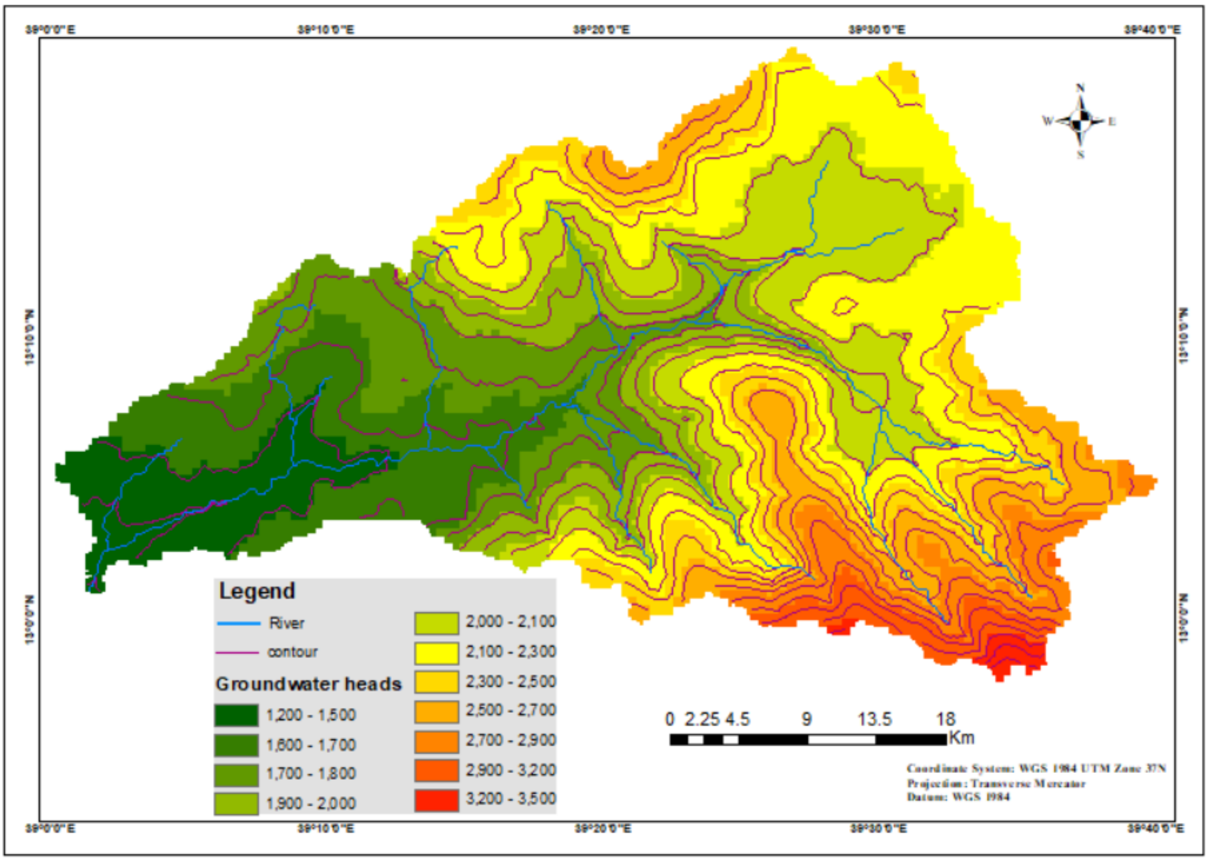

Figure 31: Spatial distribution of simulated hydraulic heads [m.a.s.l] after model calibration

4.4.4. Water budget

The daily rates of each hydrological component simulated by the MODFLOW 6 were converted to yearly rates. The total yearly water balance components of ZC are presented in Table 10. For the model simulation, the primary input is the P (660.28 mm year^{-1}), while the outputs are ET (38.64% of *P*), q_g is almost negligible (0.16% of *P*), and q covers the dominant outflow (61.19% of *P*). In this case, MODFLOW 6 only calculates the ET_g and considers $ET_u = 0$. This is due to the technical problem with the software. According to Niswonger et al. (2006), *ET* is not eliminated from the unsaturated zone during steady-state simulation due to a lack of storage. When the water table rises over the extinction depth, *ETg* from the groundwater becomes available.

As indicated above, the main output of the catchment was *q*, which was more significant than ET_g. This was acceptable because the stream flows perennially. *ET* is comprised of two components, both from the surface and subsurface. The surface component is E_I (16.21% of *ET*), and the subsurface component and main contributor is ET_g (83.79% of *ET*). The *q* is the sum of RI^s (25.09% of *q*), Exf_{gw}^s (66.78% of *q*), and q_B (8.12% of *q*). Here the sum of RI^s and Exf_{gw}^s is the total overland flow which covers 91.87 % of *q*.

In the case of the land surface and the unsaturated zone, the primary input is P_e (94.73% of *P*), while the outputs are R_g (83.62% of P_e)and RI^s (16.38% of P_e). The presence of higher P_e was expected due to the area being sparsely vegetated, and the dominant landcover type is shrubs, followed by agricultural lands and bare soils. So, the amount of *P* intercepted by the area's canopy is low, as discussed in section 4.3.

In the case of the groundwater zone, the primary inputs are R_g (78.38% of *P*) and q_{sg} (3.75% of *P*). R_g is the significant input component of the groundwater zone. This is mainly due to the thin unsaturated zone. The outputs are ET_g (41.31% of R_g), q_{gs} (11.13% of R_g), q_g (0.21% of R_g), and Exf_{gw}^s (52.13% of R_g). Exf_{gw}^s contributes a significant amount of the R_g for two main reasons; (1) The total Exf_{gw} is routed to the stream assuming Zero Exf_{gw}^e. (2) due to the shallow groundwater table at the graben parts of the study area and the side of mountains. This shallow groundwater is more susceptible to easily exfiltrating to the surface and gives a fast response to rainfall (which needs to be checked by applying a transient model).

The net recharge (R_n) is low as compared to the R_g. This is due to high Exf_{gw}^s and a significant ET_g loss at the groundwater zone. The presence of small R_n is because: (1) due to the thin unsaturated zone, (2) The other probable reason is zero ET_u due to the technical problem of MODFLOW 6.

Table 10, the water budget of ZC, depicts the total yearly inflows and outflows from the region under study. As shown in the table below, each of the depicted fluxes falls within the permissible range of percent discrepancy (between ±1%).

Table 10: The water budget of ZC after steady-state simulation (the year 2020) in [mm $year^{-1}$].

Hydrological components	P	E_I	P_e	ET	ET_g	RI^S	Exf_{gw}^s	q	q_B	q_{gs}	q_{sg}	q_g	R_g	R_n	IN	OUT	IN - OUT	PD (%)
Surface and unsaturated zone (UZF) budget		41.35	618.88			101.38							517.54		618.88	618.92	-0.04	0.00
Groundwater zone budget (GWZ)					213.80		269.84		32.82	57.62	24.81	1.06	517.54	33.90	542.35	542.33	0.02	0.00
Total water budget	660.28	41.35	618.88	255.15	213.80			404.04				1.06			660.28	660.25	0.03	0.00

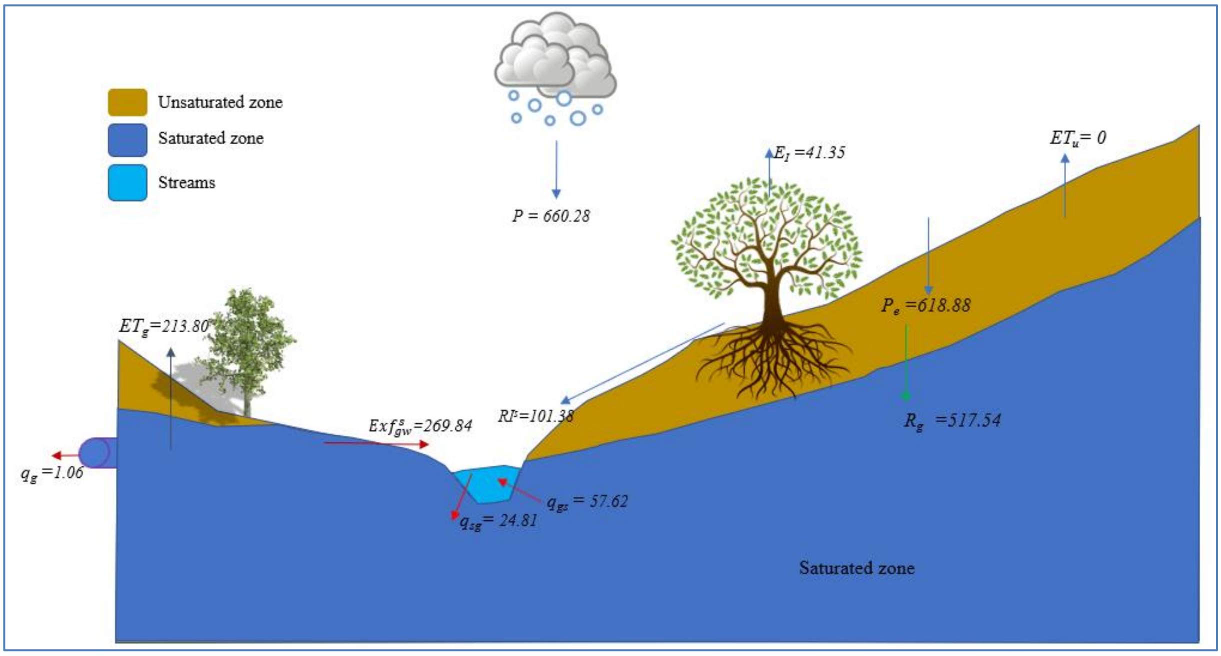

Figure 32: Represents the water balance of the entire catchment after the steady-state simulation [mm year^{-1}].

4.4.5. Sensitivity analysis

The purpose of the sensitivity analysis that was carried out was to investigate how the simulated head responded to variations in the horizontal hydraulic conductivity (Kh) as well as the vertical hydraulic conductivity (K_v), residual water content (θ_{resid}), riverbed conductance (K_b), drain conductance (C_d), and extinction water content (*extwc*).

But from the Examined parameters, the *RMSE* shows significant change while changing the three parameters only. The sensitivity analysis's findings were restricted to the model's statistical calibration results and how altering the model's parameters affected the simulated heads' total root-mean-square error (*RMSE*).

As indicated below in the graphs, the hydraulic conductivity (both K_h and K_v) is more sensitive in this study. The residual water content (θ_{resid}), extinction water content (*extwc*), and drain conductance (C_d) are less sensitive to changing the simulated heads. Instead, these parameters significantly affect the entire model's water budget. The 50% increase in K_h, K_x, and K_b change the *RMSE* to 8.93, 5.02, and 0.19 increase in the *RMSE* of the heads. This shows that hydraulic conductivity is an extremely sensitive parameter.

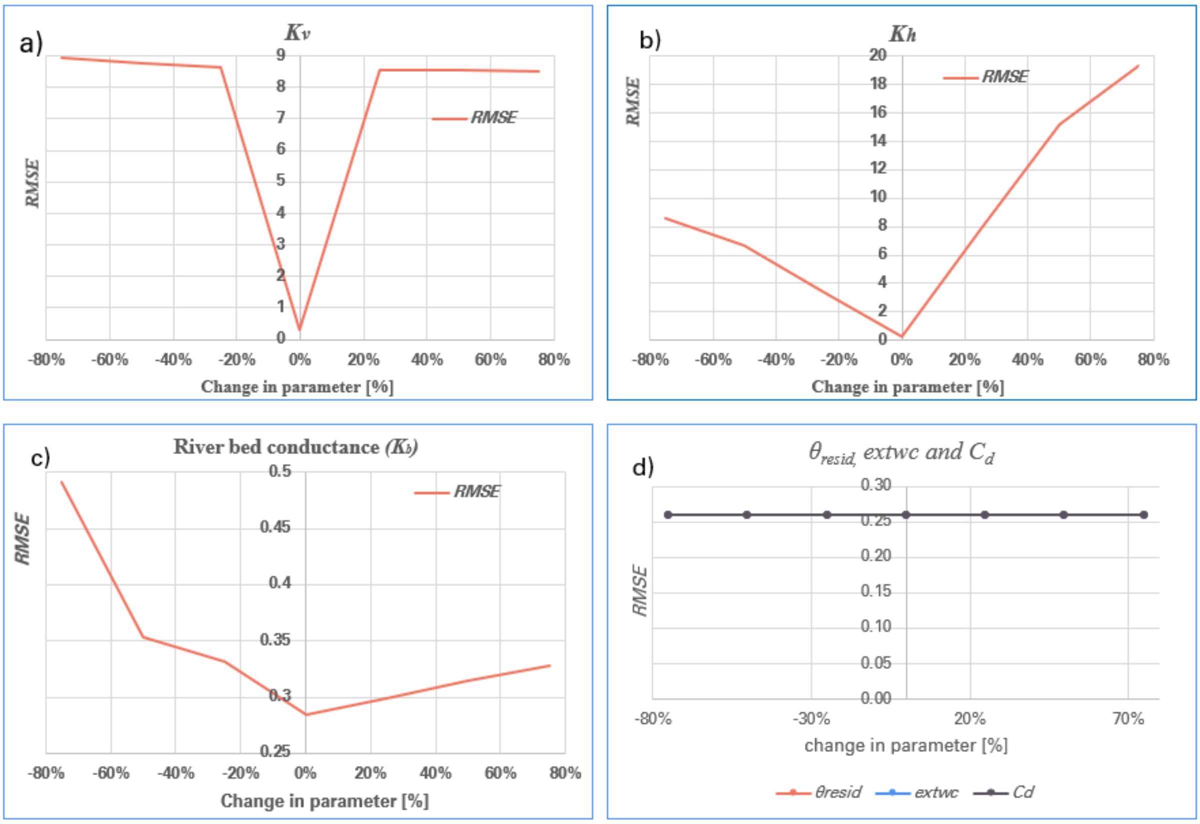

Figure 33: Sensitivity analysis of the model parameters a) *Kh,* b) *Kv,* c) *Kb*, and d*) θresid, extwc & Cd*

5. CONCLUSION AND RECOMMENDATION

5.1. Conclusion

The Zamra catchment is geologically and morphologically complex, with more than nine lithological units and seven hydrostratigraphic units. It has a dense drainage system with an elevation difference of 3229 m (defined using a 12.5 m resolution DEM). To evaluate the groundwater resources of such a complex area, proper conceptual models, and integrated hydrological numerical models (IHM) are mandatory.

A conceptual model requires understanding the hydrologic system's lithology, stratigraphy, hydrostratigraphy, and geometry. In addition, determining the flow direction and groundwater level of the catchment to be modelled, helps to determine the boundary condition of ZC. The hydraulic heads and flow direction were determined by interpolating the borehole records. There is a record of more than 380 static water levels within and outside the study area, and these static water levels were converted into hydraulic heads. A regression kriging interpolation method was applied to interpolate the Zamra catchment's groundwater level properly, i.e., taking into account topographic variability of the catchment.

The 3D lithological model and hydrostratigraphic model for the first two objectives of this study were done for flow modeling at the catchment scale. This hydrostratigraphic model determined the thickness, volume, and spatial extension of all hydrostratigraphic layers. The seven hydrostratigraphic units were determined during the conceptual model. These were unconsolidated sediment on top, flood basalts, Agulae shale, Antalo limestone, Adigrat sandstone, Enticho sandstone, and metavolcanics overlying the impermeable basement. Later, for the steady-state numerical model, the seven layers were merged into five hydrostratigraphic layers where the two sandstone units, Adigrat and Enticho, were merged as one sandstone layer, and Agulae shale and Antalo limestone merged as one limestone-shale layer due to the similarity in the geological properties of those layers.

The Rockworks 17 software was used for building proper 3D lithological and hydrostratigraphic models. The Rockworks software allowed to test different options by adjusting parameters to get representative 3D models and cross-sections. The software was very adaptable and allowed to produce a series of cross-sections that very well portray the horizontal and vertical variations of the strata. This cross-section helps define the shape of the layers so that they can be combined and fed into the numerical model.

The steady-state numerical model was set up using MODFLOW 6 with different advanced stress packages to represent the system and zones of the model properly. The UZF package was used to simulate the unsaturated zone flows appropriately. The SFR package simulates flow of the mainstream and its tributaries. The MVR package was used to route the groundwater exfiltration and rejected infiltration into the streams. The Drain package quantifies the amount of water moving out of the groundwater zone.

The model was simulated based on data covering an average of one year (01 September 2019 to 31 August 2020). The model calibration was done by using trial and error. The spatial distributions of groundwater fluxes, ET_g, R_g, Exf_{gw}^s, and R_n were determined from the calibrated model. The *RMSE, ME* and *MAE* of the residuals were assessed from the difference between observed and simulated groundwater heads. After the steady-state model calibration, the *RMSE, ME*, and *MAE* values were 0.26, -0.09, and 0.19, respectively.

The water budget demonstrated the annual mean ET (38.65 % of P), the annual mean total stream discharge q (61.20 % of P), and a very small amount of lateral groundwater outflow qg (0.16 % of P). The P_e was the primary input from the surface and unsaturated zone, and R_g (78.38% of P) was the main output. While from the groundwater zone, R_g is the primary input, and Exf_{gw^s} (52.13% of R_g) is the main output. ET_g (83.79% of ET) was the main contributor to ET in the entire catchment.

The sensitivity analysis of the model for a different parameter was tested, and the result indicates the model is most sensitive to changes K_h, K_v and K_b, while less sensitive to the changes in residual water content (θ_{resid}), extinction water content (*extwc*), and drain bed conductance (C_d), while the water balance was changing during the altering of these parameters.

5.2. Recommendations

There were not enough deep borehole head records (the borehole logs used in this study were shallow), and the data from the borehole logs was not arranged correctly during recording. The inclusion of the deep borehole logs provides also proof of the thickness and extent of each stratum. This makes the conceptual model and hydrostratigraphic layers more trustworthy for input to the numerical model. I would recommend adding some deep borehole logs to make the results more credible since there is no prior research to compare with this finding.

Data from monitoring points, particularly measurements of river discharge and groundwater levels, is scarce in this study. A more accurate model is simulated by considering the river discharge's calibration. As a result, I advise setting up gauges to assess the current groundwater level and an appropriate river discharge. For the model to be calibrated correctly, spatially representative observation heads are also essential.

The integrated hydrological model (IHM) is required to understand the interaction between surface water and groundwater fully. In the transient IHM model, all steady-state technical difficulties and aquifer parameters like specific storage and yield may be accurately specified and understood. Based on aquifer storage parameters, shape, and transmissivity, the transient IHM model may determine which aquifer system is more productive and which is less productive. Furthermore, IHM increases our understanding of the resource and will allow us to estimate a water budget more accurately. Therefore, I recommend running the IHM transient model.

Aghazadeh, N., Chitsazan, • M, Golestan, • Y, 2017. Hydrochemistry and quality assessment of groundwater in the Ardabil area, Iran. Appl. Water Sci. 7, 3599–3616. https://doi.org/10.1007/s13201-016-0498-9
Anderson, M.P., Woessner, W.W., 1992. The role of the post-audit in model validation. Adv. Water Resour. 15, 167–173. https://doi.org/10.1016/0309-1708(92)90021-S
Anderson, M.P., Woessner, W.W., Hunt, R.J., 2015. Applied Simulation of Flow and Advective Transport. Elsevier.
Anderson, M.P., Woessner, W.W., Hunt, R.J., 2015. Modeling Purpose and Conceptual Model, Applied Groundwater Modeling. https://doi.org/10.1016/b978-0-08-091638-5.00002-x
Anderson, M.P., Woessner, W.W., Hunt, R.J., 2015. Steady-State and Transient Simulations. Appl. Groundw. Model. 303–327. https://doi.org/10.1016/b978-0-08-091638-5.00007-9
Anderson, M.P., Woessner, W.W., Hunt, R.J., 2015. Forecasting and Uncertainty Analysis, Applied Groundwater Modeling. https://doi.org/10.1016/b978-0-08-091638-5.00010-9
Anderson, M.P., Woessner, W.W., Hunt, R.J., 2015. Model Calibration: Assessing Performance, Groundwater Modeling - Simulation of Flow and Advective Transport (2nd Edition).
Antonakos, A., Lambrakis, N., 2021. Spatial Interpolation for the Distribution of Groundwater Level in an Area of Complex Geology Using Widely Available GIS Tools. Environ. Process. 8, 993–1026. https://doi.org/10.1007/s40710-021-00529-9
Ayenew, T., Barbieri, G., 2005. Inventory of landslides and susceptibility mapping in the Dessie area, northern Ethiopia. Eng. Geol. 77, 1–15. https://doi.org/10.1016/j.enggeo.2004.07.002
Beyth, M., 1972. Paleozoic-Mesozoic Sedimentary Basin of Mekele Outlier, Northern Ethiopia. Am. Assoc. Pet. Geol. Bull. 56, 2426–2439.
Boukhemacha, M.A., Gogu, C.R., Serpescu, I., Gaitanaru, D., Bica, I., 2015. A hydrogeological conceptual approach to study urban groundwater flow in Bucharest, Romania. Hydrogeol. J. 23, 437–450. https://doi.org/10.1007/s10040-014-1220-3
Calijuri, M.L., Castro, J. de S., Costa, L.S., Assemany, P.P., Alves, J.E.M., 2015. Impact of land use/land cover changes on water quality and hydrological behavior of an agricultural subwatershed. Environ. Earth Sci. 74, 5373–5382. https://doi.org/10.1007/s12665-015-4550-0
Coltorti, M., Bonadiman, C., Faccini, B., Grégoire, M., O'Reilly, S.Y., Powell, W., 2007. Amphiboles from supra subduction and intraplate lithospheric mantle. Lithos 99, 68–84. https://doi.org/10.1016/j.lithos.2007.05.009
Conrad, O., Bechtel, B., Bock, M., Dietrich, H., Fischer, E., Gerlitz, L., Wehberg, J., Wichmann, V., Böhner, J., 2015. System for Automated Geoscientific Analyses (SAGA) v. 2.1.4. Geosci. Model Dev. 8, 1991–2007. https://doi.org/10.5194/gmd-8-1991-2015
Daoud, M.G., Lubczynski, M.W., Vekerdy, Z., Francés, A.P., 2022. Application of a novel cascade-routing and infiltration concept with a Voronoi unstructured grid in MODFLOW 6 to assess surface-water/groundwater interactions in a hard-rock catchment (Sardon, Spain). Hydrogeol. J. 30, 899–925. https://doi.org/10.1007/s10040-021-02430-z
Dassargues, A., 2019. Hydrogeology: Groundwater Science and Engineering, Groundwater.
Diana M. Allen, Nadine Schuurman, A.D.J.S., 2007. Data integration and standardization in cross-border hydrogeological studies: a novel approach to hydrostratigraphic model development. Environ. Geol. 1441–1453. https://doi.org/10.1007/s00254-007-0753-3
Dow, D.B., Beyth, M., Hailu, T., 1971. Paleozoic glacial rocks were recently discovered in northern Ethiopia. Geol. Mag. 108, 53–60. https://doi.org/10.1017/S0016756800050962
Enemark, T., Peeters, L.J.M., Mallants, D., Batelaan, O., 2019. Hydrogeological conceptual model building and testing: A review. J. Hydrol. 569, 310–329. https://doi.org/10.1016/j.jhydrol.2018.12.007
Enkurie, D.L., 2010. Adigrat Sandstone in Northern and Central Ethiopia: Stratigraphy, Facies, Depositional Environments and Palynology 166.
Everett, L.G., 2006. Ground Water Resources of the World and Their Use. National Ground Water Association.
Figuères, C.M., Tortajada, C., Rockström, J., 2012. Rethinking water management: Innovative approaches to contemporary issues. Water Manag. Innov. Approaches to Contemp. Issues 1–242. https://doi.org/10.4324/9781849772402
Gebremedhin, M. A., Lubczynski, M., Maathuis, B., 2022. Rainfall interception variability from earth

observation satellite, Upper Tekeze Basin, Northern Ethiopia. Unpublished Manuscript.
Gebremedhin, M.A., Lubczynski, M.W., Maathuis, B.H.P., Teka, D., 2022. Deriving potential evapotranspiration from satellite-based reference evapotranspiration, Upper Tekeze Basin, Northern Ethiopia. J. Hydrol. Reg. Stud. 41, 101059. https://doi.org/10.1016/j.ejrh.2022.101059
Gebremedhin, M.A., Lubczynski, M.W., Maathuis, B.H.P., Teka, D., 2021. A novel approach to integrate daily satellite rainfall with in-situ rainfall, Upper Tekeze Basin, Ethiopia. Atmos. Res. 248, 105135. https://doi.org/10.1016/j.atmosres.2020.105135
Gebreyohannes, T., Smedt, F. De, Hagos, M., Gebresilassie, S., Amare, K., Kabeto, K., Hussein, A., Nyssen, J., Bauer, H., Moeyersons, J., Deckers, J., Haile, M., Taha, N., 2010. Large-Scale Geological mapping of the Geba basin, Northern Ethiopia, Program.
Girmay, E., Ayenew, T., Kebede, S., Alene, M., Wohnlich, S., Wisotzky, F., 2015. Conceptual groundwater flow model of the Mekelle Paleozoic–Mesozoic sedimentary outlier and surroundings (northern Ethiopia) using environmental isotopes and dissolved ions Ermias. Hydrogeol. J. 23, 649–672. https://doi.org/10.1007/s10040-015-1243-4
Hagos, E., Ayenew, T., Kebede, S., Alene, M., 2015. Review of Hydrogeology of Tekeze River Basin: Implications for Rural and Urban Water Supply in the Region. SINET Ethiop. J. Sci 38, 91–110.
Halford, K.J., 1997. Effects of the unsaturated zone on aquifer test analysis in a shallow-aquifer system. Ground Water. https://doi.org/10.1111/j.1745-6584.1997.tb00112.x
Hamdi, M., Zagrarni, M.F., Djamai, N., Jerbi, H., Goita, K., Tarhouni, J., 2018. 3D geological modeling for complex aquifer system conception and groundwater storage assessment: Case of Sisseb El Alem Nadhour Saouaf basin, northeastern Tunisia. J. African Earth Sci. 143, 178–186. https://doi.org/10.1016/j.jafrearsci.2018.03.017
Hassan, S.M.T., Ghimire, C.P., Lubczynski, M.W., 2017. Remote sensing upscaling of interception loss from isolated oaks: Sardon catchment case study, Spain. J. Hydrol. 555, 489–505. https://doi.org/10.1016/j.jhydrol.2017.08.016
Hassen, I., Gibson, H., Hamzaoui-Azaza, F., Negro, F., Rachid, K., Bouhlila, R., 2016. 3D geological modeling of the Kasserine Aquifer System, Central Tunisia: New insights into aquifer-geometry and interconnections to better assess groundwater resources. J. Hydrol. 539, 223–236. https://doi.org/10.1016/j.jhydrol.2016.05.034
Karlovi, I., Markovi, T., 2021. Development of a Hydrogeological Conceptual Model of the Varaždin Alluvial Aquifer. https://doi.org/https://doi.org/10.3390/hydrology8010019
Langevin, C.D., Hughes, J.D., Banta, E.R., Niswonger, R.G., Panday, S., Provost, A.M., 2017. Documentation for the MODFLOW 6 Groundwater Flow Model: U.S. Geological Survey Techniques and Methods. B. 6, Model. Tech. 197.
Langevin, C.D., Hughes, J.D., Banta, E.R., Provost, A.M., Niswonger, R.G., Panday, S., 2021. MODFLOW 6 Modular Hydrologic Model version 6.2.1: U.S. Geological Survey Software Release 200 p.
Lekula, M., Lubczynski, M.W., 2019. Use of remote sensing and long-term in-situ time-series data in an integrated hydrological model of the Central Kalahari Basin, Southern Africa. Hydrogeol. J. 27, 1541–1562. https://doi.org/10.1007/s10040-019-01954-9
Lekula, M., Lubczynski, M.W., Shemang, E.M., 2018. Hydrogeological conceptual model of large and complex sedimentary aquifer systems – Central Kalahari Basin. Phys. Chem. Earth 106, 47–62. https://doi.org/10.1016/j.pce.2018.05.006
Mengistu, T.D., Chung, I.M., Chang, S.W., Yifru, B.A., Kim, M.G., Lee, J., Ware, H.H., Kim, I.H., 2021. Challenges and prospects of advancing groundwater research in Ethiopia aquifers: A review. Sustain. 13, 1–15. https://doi.org/10.3390/su132011500
Miller, N.R., Alene, M., Sacchi, R., Stern, R.J., Conti, A., Kröner, A., Zuppi, G., 2003. Significance of the Tambien Group (Tigrai, N. Ethiopia) for Snowball Earth events in the Arabian-Nubian Shield. Precambrian Res. 121, 263–283. https://doi.org/10.1016/S0301-9268(03)00014-7
Morway, E.D., Langevin, C.D., Hughes, J.D., 2021. Use the MODFLOW 6 Water Mover Package to Represent Natural and Managed Hydrologic Connections. Groundwater 59, 913–924. https://doi.org/10.1111/gwat.13117
Niswonger, R.G., Prudic, D.E., Regan, R.S., 2006. Documentation of the Unsaturated-Zone Flow (UZF1) Package for Modeling Unsaturated Flow Between the Land Surface and the Water Table with MODFLOW-2005: U.S. Geological Survey Techniques and Methods 6-A19 62 p.
Peeters, L., Fasbender, D., Batelaan, O., Dassargues, A., 2010. Bayesian data fusion for water table interpolation: Incorporating a hydrogeological conceptual model in kriging. Water Resour. Res. 46,

1–11. https://doi.org/10.1029/2009WR008353
Royse, K.R., 2010. Combining numerical and cognitive 3D modeling approaches to determine the structure of the Chalk in the London Basin. Comput. Geosci. 36, 500–511. https://doi.org/10.1016/j.cageo.2009.10.001
Saxena & Assefa, 1983. New evidence on the age of the glacial rocks of northern Ethiopia Summary. A fossil siphonophorid is described from the Palaeozoic rocks of the Enticho area in Tigrai, northern Ethiopia. This is the first fauna to be described from these rocks and the. Geol. journals 120, 549–554.
Sembroni, A., Faccenna, C., Becker, T.W., Molin, P., Abebe, B., 2016. Long-term, deep-mantle support of the Ethiopia-Yemen Plateau. Tectonics 35, 469–488. https://doi.org/10.1002/2015TC004000
Sembroni, A., Molin, P., Dramis, F., Abebe, B., 2017. Geology of the Tekeze River basin (Northern. J. map 5647. https://doi.org/10.1080/17445647.2017.1351907
Sima, J., 2018. Hydrogeological and Hydrochemical Maps of Nazret NC 37 – 15 Sheet Explanatory Notes.
Siyoum, M.H., 2020. Investigation of Water Quality and Evaluation of its suitability for Irrigation and Drinking purposes, Zamra Catchment, Northern Ethiopia. Unpubl. Work.
Sleep, C.J.E., and N.H., 1998. Cenozoic magmatism throughout east Africa resulted from the impact of a single plume. Nature 395, 788–791.
Taha, A., 2015. I . The numerical model. Groundw. Model. - Simul. Flow Advective Transp. (2nd Ed. 1–20.
U.S. Geological Survey, 2018. MODFLOW 6 – Description of Input and Output. MODFLOW 6 Doc. 200 p.
Wolela, A., 2008. Sedimentation of the Triassic-Jurassic Adigrat Sandstone Formation, Blue Nile (Abay) Basin, Ethiopia. J. African Earth Sci. 52, 30–42. https://doi.org/10.1016/j.jafrearsci.2008.04.001